ANALYSIS AND VERIFICATION OF A PROPOSED ANTENNA DESIGN FOR AN IMPLANTABLE RFID TAG AT 915 MHz

By

RAHUL BAKORE

Bachelor of Engineering in Electronics and Communication

University Of Rajasthan

Jaipur, Rajasthan, India

2008

Submitted to the Faculty of the
Graduate College of the
Oklahoma State University
in partial fulfillment of
the requirements for
the Degree of
MASTER OF SCIENCE
December, 2012

ANALYSIS AND VERIFICATION OF A PROPOSED

ANTENNA DESIGN FOR AN IMPLANTABLE

RFID TAG AT 915 MHz

Thesis Approved:

Dr. James C. West

Thesis Adviser

Dr. Chris Hutchens

Dr. Charles F. Bunting

ACKNOWLEDGEMENTS

I would like to thank my thesis advisor, Dr. James C. West, for giving me the opportunity to work under him for my thesis. Without his guidance and persistent help this thesis would not have been possible.

In Addition, I would like to thank my committee members, Dr. Chris Hutchens and Dr. Charles F. Bunting, for all the help and support provided during my thesis work.

Also, I would like to thank Rehan Ahmed for his help and support during my thesis work.

Name: RAHUL BAKORE

Date of Degree: DECEMBER, 2012

Title of Study: ANALYSIS AND VERIFCATION OF A PROPOSED ANTENNA DESIGN FOR AN IMPLANTABLE RFID TAG AT 915 MHz

Major Field: ELECTRICAL ENGINEERING

ABSTRACT: This work focused on design and analysis of an antenna to be used with an RFID tag that is implanted in human brain tissue. The goal is to maximize the power transferred between the external RFID measurement system and the implanted RFID tag while minimizing the power dissipated within the surrounding tissue. The commercial computational electromagnetics software package COMSOL, based on finite element method (FEM) has been used for design process. The COMSOL models have been validated against additional simulations using the FEKO commercial package based on method of moments (MOM) as well as against measurement of test antenna structures radiating in bulk homogeneous medium. The proposed antenna geometry is compatible with the human tissue and viable for use in implantable RFID Tag.

The proposed antenna is a planar folded dipole made from a gold conductor that acts as a biocompatible material. The metal thickness is 1 μm and the overall antenna dimensions are 22 mm × 3.5 mm. The antenna structure also includes a dielectric substrate and an acrylic coating. The antenna impedance is 28+j201.5 Ω at 915 MHz. The inductive reactance is high enough to compensate the capacitive reactance of RFID tag and the antenna resistance is close to effective chip resistance providing a conjugate match. This antenna fulfills the criteria for minimizing the power dissipation within the human tissue. Also, a radiation efficiency of 87% is achieved with this antenna at 915 MHz. The quality factor of greater than 10 is achieved which is sufficient to turn on the diodes in the electronic circuit of the RFID tag due to the high D.C voltage obtained.

TABLE OF CONTENTS

LIST OF TABLES

LIST OF FIGURES

CHAPTER 1

INTRODUCTION

Implanting radio frequency identification (RFID) tags into human tissue will aid doctors in determining patient symptoms. One application of implanted RFID tags is a brain machine interface that is useful for performing neural recording in human brain tissue [5]. Another application is wirelessly monitoring pressure in ocular tissue of glaucoma patients [1]. A biosensor made from gold and silk that is used to receive a tiny signal from proteins and chemicals in the body has been developed at Tufts University [2]. This biosensor is a biocompatible material that acts as an implanted antenna.

However, an implanted device must be powered by a source outside the living tissue. The minimum power required in order to operate the device is 35 μW [39]. Wirelessly powering implanted devices is therefore a prominent area of research in clinical application. It has been reported in [5] that the temperature rise due to power dissipation in an implantable device itself is much more significant than the temperature rise due to electromagnetic power absorption in human tissue. More temperature rise leads to the destruction of cells in human tissue. Hence, the FDA restricts the temperature rise to 1^0C. So, it has been proposed that communication with an implanted device via RFID may be a possible way to minimize the power dissipation from the implanted chip.

RFID is a technique for identification and tracking of objects using electromagnetic fields. This technology uses two pieces of hardware, an RFID reader and an RFID tag. A RFID tag contains three components, an antenna, a semiconductor chip and the encapsulation material. RFID tags may be passive or active. Active RFID tags require a small battery for sending the information to the RFID reader whereas passive RFID is powered by the electromagnetic field from RFID reader, so does not require a battery. Since an active RFID tag requires a battery which has a limited lifetime, frequent surgery may be required to replace battery in the tag device. Hence, for medical application, it is preferable to use a passive RFID tag which does not require battery. Since a medical device has to be implanted inside human tissue, an implantable device must be small.

There are two approaches for transferring power from the RFID reader to RFID tag, near-field (inductive) coupling and far-field (radiating) coupling. In near field coupling, an induced magnetic field generated in the tag coil due to the magnetic field from the reader coil using faraday's principle. In far field coupling, the RFID tag device captures radiated electromagnetic (EM) power from the reader then transmits data back to the reader. In the far field region, reactive power (power due to stored energy) in the electromagnetic field is negligible and only the radiated power is considered. The electromagnetic field in this region is in the form of plane wave. The inductive coupling can be used for short range communication as reported in [29] and requires Low frequency (LF) band, so low bandwidth is available. Far-field coupling operates in the UHF band [6], which allows a higher data rate. Hence, far-field coupling for communication with an implanted device is an appropriate approach for higher data rates.

Recent technology shows that electronic components and thereby the electronic chip size can be reduced to micron scale. However, very small antennas have poor radiation efficiency [3]. One way to improve the efficiency is to operate the antenna at higher frequency so that its length

increases in terms of wavelength. However, tissue losses increase with increase with frequency resulting in increasing temperature of human tissue and a lower signal to noise ratio. Specific absorption rate (SAR) is defined as the amount of absorption of the electromagnetic radiation per unit kilogram. FCC limits the SAR averaged over 1 gram of tissue to be not more than 1.6 W/Kg [4]. Thus, a lower frequency of operation is desired. For these reasons, the design of an RFID antenna that is compatible with use in human tissue or any other biological tissue is a current challenge.

1.1 Research objective:

The resonant frequency of an antenna reduces when it is surrounded by a lossless dielectric medium compared to that in free space. This results in increasing the antenna quality factor (Q). When the surrounding medium is replaced by a lossy dielectric medium, then the Q of the antenna will be increased due to increase in the dielectric constant and decreases with increase in the electrical conductivity or loss tangent of the medium [27]. Since the dielectric constant and electrical conductivity of human tissue varies with the frequency of operation, the determination of the antenna characteristics very challenging. Currently, numerical techniques are available which can take the advantage of high speed digital computers to solve the complicated problems in electromagnetics. Using such modern tools, an antenna has been designed for use with an implanted RFID tag.

The commercial software packages COMSOL Multiphysics version 4.2 (based on finite element method numerical technique) [13], [18] and FEKO (based on Method of Moments numerical technique) [30] has been used in the antenna design process. Measurement of sample antennas has been performed at the Mixed Signal VLSI Design Laboratory at Oklahoma State University. The objective of this research is to first verify the measured results using the COMSOL package. Once the results are in good agreement, the next objective is to design an antenna structure that maximizes the power transfer from the antenna to the electronic chip circuit

in the RFID tag while meeting physical constraints imposed by the need to implant the device in human tissue. It has been found that the simulation results and measurement shows good agreement. A radiation efficiency of around 87% is achieved with the proposed antenna design when radiating in a saline solution medium that simulates human tissue. FEKO is used in this research to verify the COMSOL simulation model with the antenna radiating in homogeneous medium, giving additional confidence in the results.

1.2. Thesis organization:

Chapter 2 gives an overview of the computational electromagnetics techniques and the design consideration for the antenna geometry applicable for the RFID tag. Chapter 3 gives a description of the COMSOL package and brief overview of the FEKO package. The analysis of a monopole antenna along with different excitation techniques are performed using COMSOL and FEKO package in Chapter 4. In Chapter 5, the input impedance of a folded dipole strip antenna is used as a first test case for comparing both the COMSOL and FEKO simulation results. FEKO and COMSOL results are also compared with the locally written Method of Moments code at Oklahoma State University. In Chapter 6, COMSOL simulations of four test antennas are considered when radiating in to both free space and a saline media. The FEKO package is used to validate the COMSOL model. Then, the COMSOL simulation results are compared with the measured input impedance for the antennas in Chapter 7. A proposed antenna geometry is introduced in Chapter 8 which is compatible with human tissue for use with the RFID tag. Last chapter is the summary and the conclusion.

CHAPTER 2

BACKGROUND

In this chapter, an overview of the available computational numerical techniques used in antenna simulations is given. Techniques for providing the excitation of source to the antenna structure for radiating into the surrounding medium are also reviewed. Criteria for the choice of the numerical techniques used in this work are explained. Effects of antenna geometry on antenna parameter such as its input impedance, efficiency, etc. are also discussed.

2.1 Overview of numerical techniques in electromagnetics:

All computational electromagnetic techniques discretize the computational domain into several small subdomains. Maxwell's equations are solved in each subdomain. These numerical techniques have advantages when designing complex antenna structures and can analyze arbitrary structures. Analytical methods cannot analyze complex antenna structures. Maxwell's equations in differential, time-dependent form are given as follows:

$$\nabla \times \mathbf{H} = \mathrm{J} + \frac{\partial \mathbf{D}}{\partial \mathrm{t}} \ , \tag{2.1}$$

$$\nabla \times \mathbf{E} = -\frac{\partial \mathbf{B}}{\partial \mathrm{t}} \ , \tag{2.2}$$

$$\nabla . \mathbf{D} = \rho \ , \tag{2.3}$$

$$\nabla . \mathbf{B} = 0 \ , \tag{2.4}$$

where E is the electric field, B is the magnetic flux density, D is electric flux density, H is magnetic field, J is surface current density and ρ is electric charge density. Currently, most simulation software is based on one of the following methods:

1. Finite difference time domain method (FDTD)
2. Finite element method (FEM)
3. Method of Moments (MOM)

FDTD [10], [11], [21], [24] is the most convenient numerical technique for antenna simulation. FDTD is based on solving partial differential equation. This tool requires the discretization of both the antenna structure as well as the medium surrounding the antenna. An antenna radiates electromagnetic field outward to large distance. Due to finite computational resources, the computational domain needs to be truncated into a finite volume. The boundary of the computational region must be treated to prevent reflections that yield inaccurate results. This can be accomplished using an effective perfectly matched layer (PML) or absorbing boundary condition [21]. The advantage of this method is that it is simple to implement. Also it does not require a matrix solution so can be more efficient than other approaches. The drawback in FDTD is that it is very difficult to discretize complex geometries such as complicated antennas or thin dielectric media. The discretization size must be very small which gives a large number of discretized elements. This leads to large computer memory requirements and long computational time.

FEM [10], [11] is more complicated to implement than FDTD. Like FDTD, FEM also solves a partial differential equation. This tool allows an unstructured mesh and can effectively mesh or discretized complex antenna geometries and the surroundings of the antenna. However, this method requires the inversion of a large sparse interaction matrix. This can be solved efficiently using advanced solving techniques. This method also requires the truncation of the

open region where the antenna radiates using an absorbing boundary condition, PML or a combination of both [8], [9].

The method of moments (MOM) [10], [11], [35] is the oldest computational electromagnetic method used to analyze antenna performance. It solves an integral equation derived from Maxwell's equations. The Sommerfeld radiation boundary condition [8], [9] is used, so the open region problem is solved. Thus, it does not require discretizing the medium surrounded by antenna; only the antenna structure itself must be discretized. Hence, the solution obtained can be more accurate than FDTD or FEM. The disadvantage of MOM is that it is typically implemented only for the simulation of metallic antennas radiating into bulk homogeneous media. Its solution requires the inversion of large dense matrix which increases the computational time.

2.2 Antenna design consideration:

Figure 2.1 shows the RF front end of the RFID tag obtained from [39] which contains the antenna, matching network, RF-DC converter and low drop out regulator (LDO). In this work, only the antenna and matching network that are used to supply the DC voltage to turn on electronic circuits are considered. Figure 2.2 shows the equivalent circuit of the antenna connected with a load representing the RFID chip circuit in receiving mode. V_T is the voltage induced at antenna terminal due to electromagnetic field impinging on the antenna structure. Maximum power transfer is possible when the antenna impedance Z_A is equal to complex conjugate of impedance of the RFID chip circuit load Z_T [15]:

$$Z_A = {Z_T}^* , \tag{2.5}$$

where ${Z_T}^*$ is the complex conjugate of load impedance Z_T ,

$$Z_A = R_A + jX_A , \tag{2.6}$$

$$R_A = R_r + R_L , \tag{2.7}$$

and

$$Z_T = R_T + jX_T \, . \tag{2.8}$$

Using (2.5), it can be shown that $R_A = R_T$ and $X_A = -X_T$ for maximum power transfer from antenna to chip circuit. Use as a medical device puts a number of constraints on the geometry of antenna. Since antenna must be implanted within human tissue, it is easier to insert if the geometry is thin and slender. The antenna impedance is the same whether transmitting or receiving due to the reciprocity theorem [15], [32]. So, input impedance of antenna surrounded by tissue medium for usable geometries has been analyzed in this work.

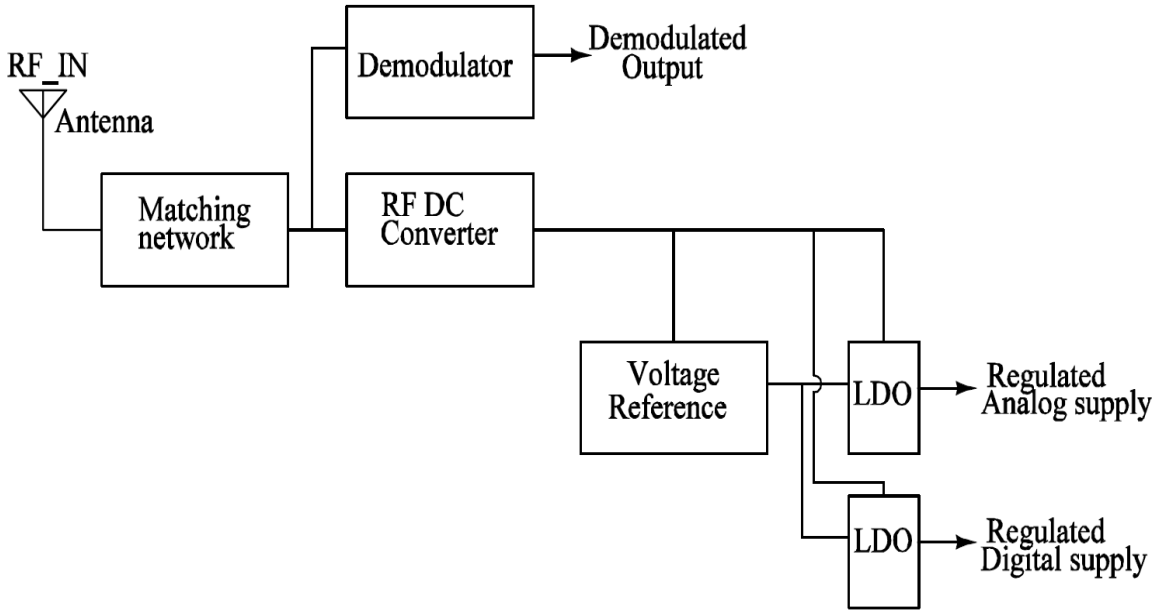

Figure: 2.1 RF front end of the RFID tag [39]

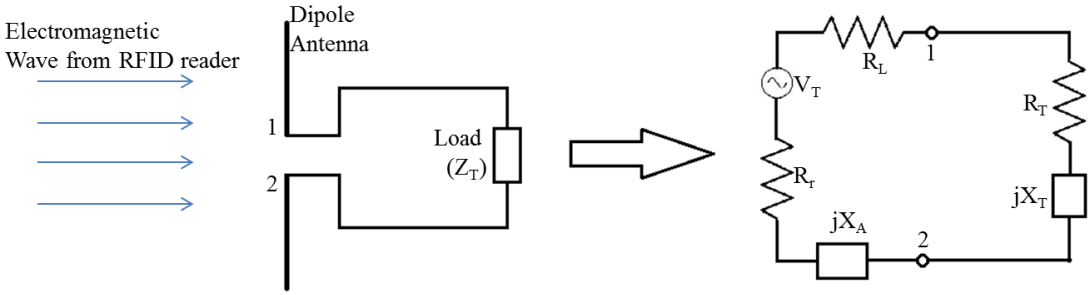

(a) Antenna in receiving mode (b) Thevenin equivalent

Figure 2.2: Antenna terminated with load and its equivalent circuit in receiving mode.

The frequency ranges for available RFID systems operating in the ultra-high frequency (UHF) band are 902-928 MHz and 2-2.483 GHz [6]. The input impedance and efficiency performance of implantable antennas are affected by the surrounding medium and by size constraint. The commercial RFID tag IC given in [7] for UHF band operating in frequency range of 860-960 MHz has equivalent circuit shown in figure 2.3. The impedance is a parallel combination resistance 1500 Ω and capacitance 0.85pF.This results in 27.4-j200.9 Ω at 915 MHz. The antenna impedance should be the complex conjugate of the RFID tag IC impedance for maximum power transfer. This show that the antenna designed should have a high inductive reactance that compensates the capacitive reactance of the RFID tag IC. High inductive reactance is possible with a rectangular loop planar antenna or planar folded dipole antenna for small geometry.

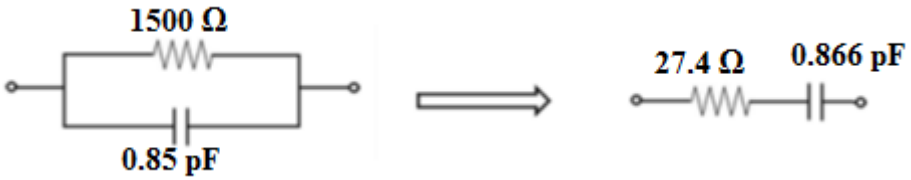

(a) (b)

Figure 2.3 (a) RFID tag IC impedance with parallel combination [7] (b) RFID tag IC with series combination

The geometries of several test antennas are shown in Figure 2.4. Samples of these geometries were built at the University of Texas at Dallas and were tested at the Mixed Signal VLSI Design Laboratory at Oklahoma State University. The testing was done by connecting those antenna configurations with the commercial RFID tag [7] and recording the response of RFID tag at a distance of approximately 30 cm from the RFID Reader. The testing was done first in a free space environment and then was repeated when the RFID tag was sandwiched between two saline bags of thickness 1.5 cm with 0.9% salt concentration. Among the five antenna geometries shown in Figure 2.4, the antenna configuration shown in Figure 2.4 (c) shows the best

response when connected with the commercial RFID tag in both the test configurations. The antenna configuration shown in Figure 2.4 (e) did not respond when used with the commercial RFID tag.

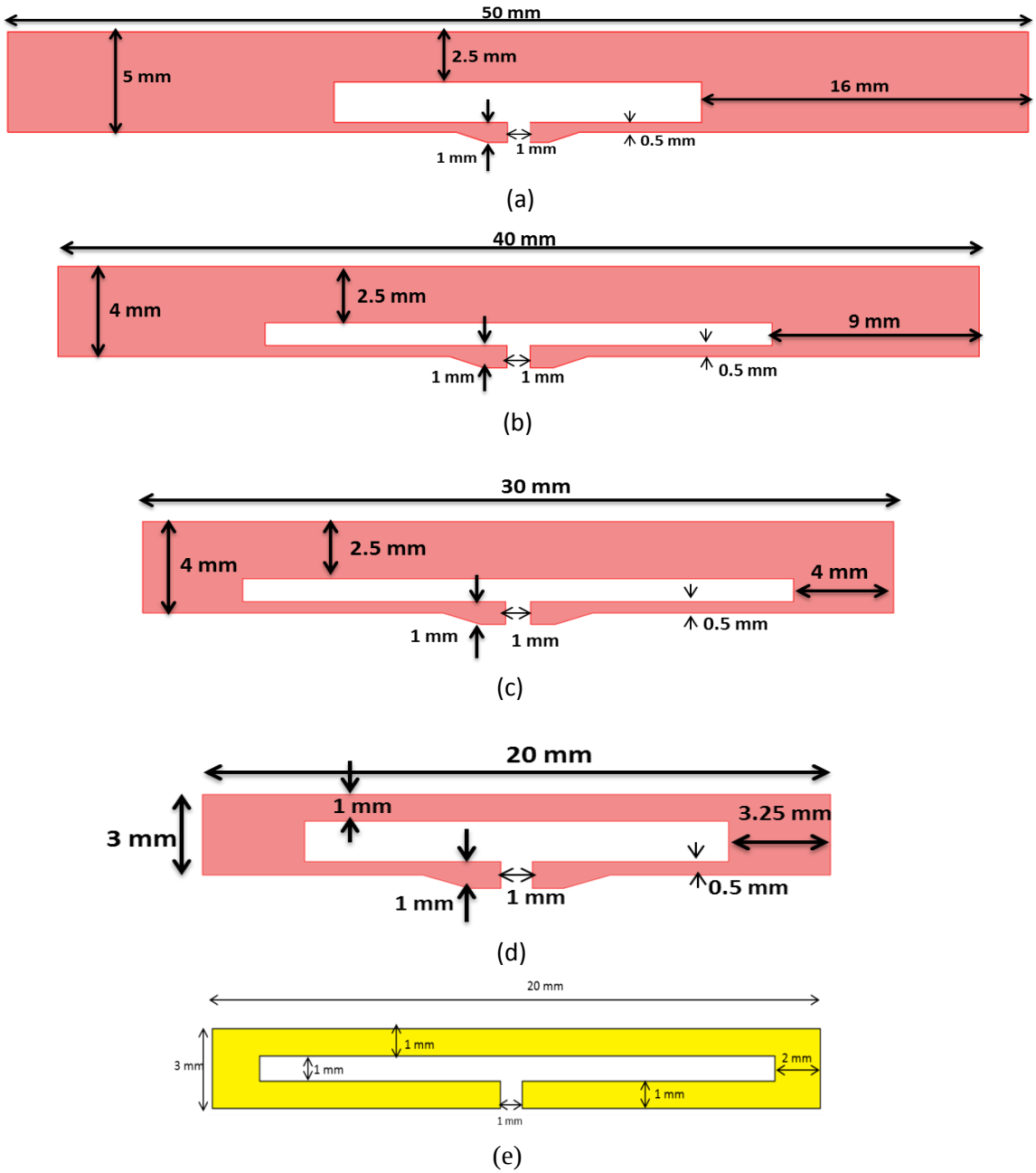

Figure 2.4: Geometry of designed antennas at Mixed Signal VLSI Design Laboratory, Oklahoma State University, Stillwater, OK

Then, the measurement of antenna impedance was performed in Mixed Signal VLSI Design Laboratory at Oklahoma State University using Hewlett Packard 8720D 50 MHz - 20 GHz network analyzer. The measured impedance was compared with the impedance of commercial RFID tag at 915 MHz. Among all antenna configurations, antenna in Figure 2.4 (c) resulted in higher inductive reactance. However, it was not high enough to compensate the capacitive reactance in commercial RFID tag chip in order for maximum power transfer. In this work, simulations of these test antennas are performed using COMSOL to verify the measured antenna impedance.

In Chapter 7, COMSOL simulation results are compared with the measured results for the antenna geometries shown in Figure 2.4 (a) thru (d). However, the antenna geometry in Figure 2.4 (e) is not considered for comparison with the measured results since the RFID tag did not respond when connected to this antenna. In Chapter 5, the antenna geometry in Figure 2.4 (e) is used as a first test case to validate the COMSOL simulation results using both FEKO simulation results and a method of moments code locally written at Oklahoma State University.

From [40], it can be shown that the inductive reactance and the resistance of a flat strip type in Figure 2.5 increases with decreasing strip width and increasing strip length. However, reducing the strip width will increase the loss resistance and reduce the radiation efficiency of antenna. The inductance in μH of a straight thin metal film as shown in figure 2.5 is given by

$$\mathrm{L} = 0.2l\left\{\ln\left(\frac{2l}{\mathrm{w+t}}\right) + 0.50049 + \frac{\mathrm{w+t}}{3l}\right\}\ , \tag{2.9}$$

where l is the length of conductor in m, t is the metal thickness in m, and w is the width of conducting strip in m. The loss resistance (or resistance due to ohmic loss) of the metal film shown in Figure 2.5 is given as

$$\mathrm{R} = \frac{l}{\sigma \mathrm{A_e}}, \tag{2.10}$$

where σ is the electrical conductivity in S/m and A_e is the cross-sectional area of conducting strip. The effective cross-sectional area of a conducting strip is

$$A_e = \begin{cases} w \times t & \text{for } t \leq \delta \\ w \times \delta & \text{for } t > \delta \end{cases}, \tag{2.11}$$

where δ is the skin depth of the conducting material. The thickness of the metal film does not affect the inductance when $t \ll w$. However, it will affect the resistance. This shows that geometry has to be adjusted to bring the input impedance of the antenna in to the working range for an RFID tag chip that gives maximum power transfer from the antenna to the RFID chip circuit.

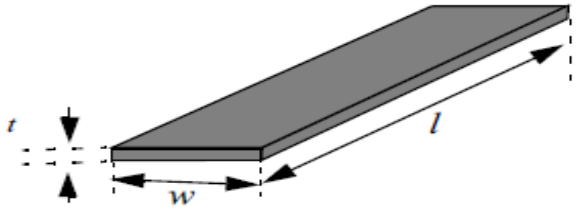

Figure 2.5: Thin metal conducting film

2.3 Source modeling in antenna structure:

There are various ways to model an antenna feed in a computational electromagnetic model, such as a voltage gap generator, a current probe excitation or a waveguide feed. In this work, current probe excitation [8], [12] is used on the antenna gap as shown in figure 2.6. Current I is impressed at the port of the folded dipole antenna along the line directed along the x-axis located at (y_1, z_1). The excitation current density can be modeled as

$$J_{imp}(x, y, z) = \hat{x} I_0 \delta(y - y_1, z - z_1), \; x \in L, \tag{2.12}$$

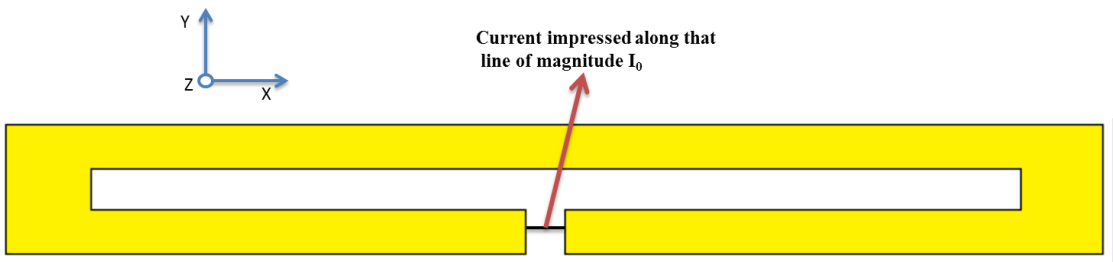

Figure 2.6: Excitation of antenna structure by impressed current

where I_0 is the current flowing into the antenna and L is the length of the probe. Using this current excitation, the electric field is computed everywhere in the computational domain using the COMSOL package. The probe voltage is then found by integrating the electric field along the length of probe:

$$V = -\int \hat{x}.\, E(y_1, z_1)\, dx \quad , \tag{2.13}$$

The input impedance of the antenna is then; $Z_{in} = \frac{V}{I}$.

CHAPTER 3

FINITE ELEMENT METHOD

The finite element method is a numerical procedure for approximating the solution of a boundary value problem. It transforms a boundary value problem described by a differential equation into sparse linear system that can be solved using linear algebra techniques. The general form of the equation to be solved by the finite element method is $\mathrm{Lu} = \mathrm{f}$, where u is unknown term, f is the source term and L is the differential operator. For time harmonic electromagnetic fields, the wave equation takes the form [8]:

$$\nabla \times (\mu_r{}^{-1} \nabla \times \mathrm{E}) - \mathrm{k_0}^2 \left(\varepsilon_r - \frac{\mathrm{j}\sigma}{\omega \varepsilon_0}\right) \mathrm{E} = -\mathrm{k_0 Z_0 J_{imp}} \tag{3.1}$$

The media are non-magnetic, so μ_r is equal to 1. ε_r and σ are the relative permittivity and conductivity of a medium respectively, k_0 is the free space wave number, and Z_0 is intrinsic impedance in free space. The FEM-based commercial software package COMSOL Multiphysics version 4.2 RF module (electromagnetic waves physics interface) [13] is chosen to analyze the antenna radiation characteristics. There are various boundary conditions associated with the simulation of the antenna, now summarized.

3.1 Boundary conditions

Following are the boundary conditions used in COMSOL for computing the electric field when a monopole antenna strip is radiating in free space.

3.1.1 Perfect electric conductor

This boundary condition is applied on the perfect electric interfaces of antenna being modeled and also to represent perfect electric ground conductor. It enforces the tangential component of electric field to being zero. It is written as

$$\hat{n} \times \mathbf{E} = 0 \,, \tag{3.2}$$

where $\hat{n}$ is the unit vector normal to that surface. It is used to represent a boundary with infinite conductivity. The figure 3.1 shows the COMSOL interface where the monopole antenna strip and ground plane are modeled as perfect electric conductor.

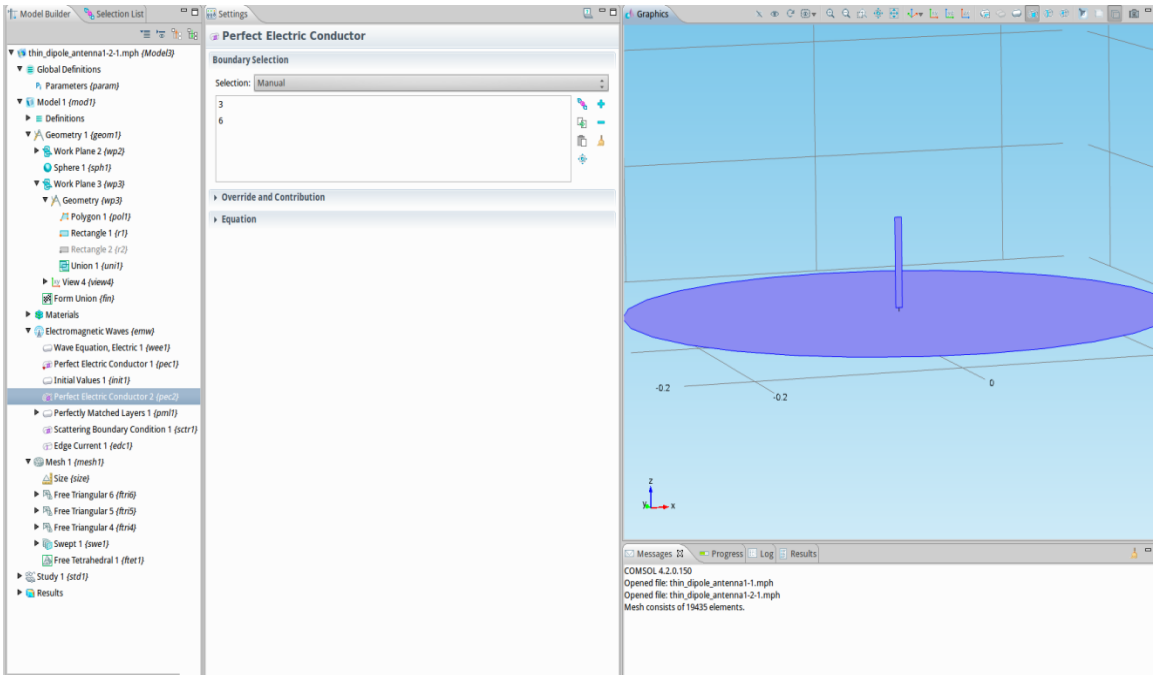

Figure 3.1: Ground plane and monopole modeled as perfect electric conductor in COMSOL

3.1.2 Edge current (or line feed)

For feeding the antenna port, an edge current (similar to current probe excitation discussed in section 2.3 [8], [12]) can be modeled by inserting a line segment that connects the perfectly conducting (PEC) ground plane to a monopole antenna structure, as shown in figure 3.2. The electric field distribution is computed everywhere in computational domain with a 1A excitation current on that edge. Once the electric field is found, the voltage drop between the monopole

probe and the PEC ground plane is found by integration of the electric field along the line that connect the PEC and monopole probe (This is the same technique as discussed in section 2.3).

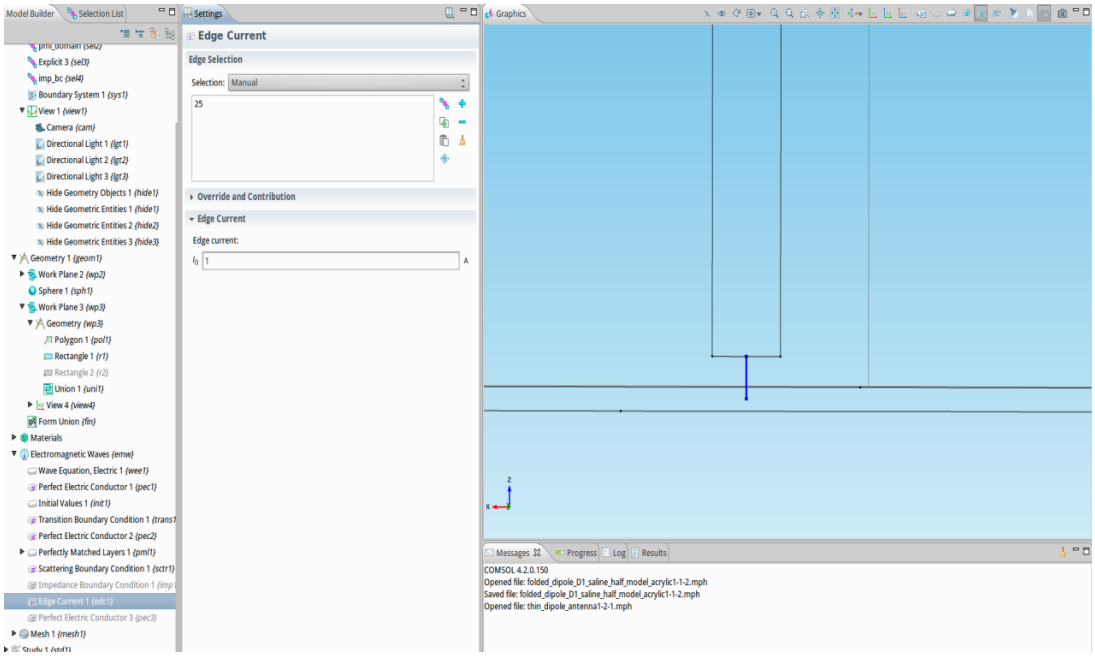

Figure 3.2: Line feed excitation using COMSOL

3.1.3 Lumped port Excitation:

The lumped port excitation is available in COMSOL to find the input impedance directly at an antenna port. A uniform port type is selected, meaning the input applied is a sinusoidal varying voltage difference between the antenna terminals. Figure 3.3 shows that the input voltage V_{in} and the characteristic impedance $\mathrm{Z_{ref}}$ is given to provide the wave excitation at this port. Figure 3.4 shows the COMSOL snapshot when using lumped port excitation. COMSOL allows this excitation technique when the surfaces of antenna structure are modeled as perfect electric conductors or as impedance boundaries [13], However, COMSOL does not allow the use of this excitation technique when the antenna surfaces are modeled as transition boundaries.

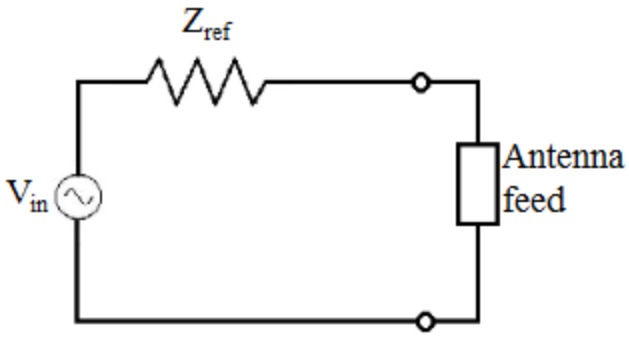

Figure 3.3: Antenna feeding technique using lumped port excitation in COMSOL

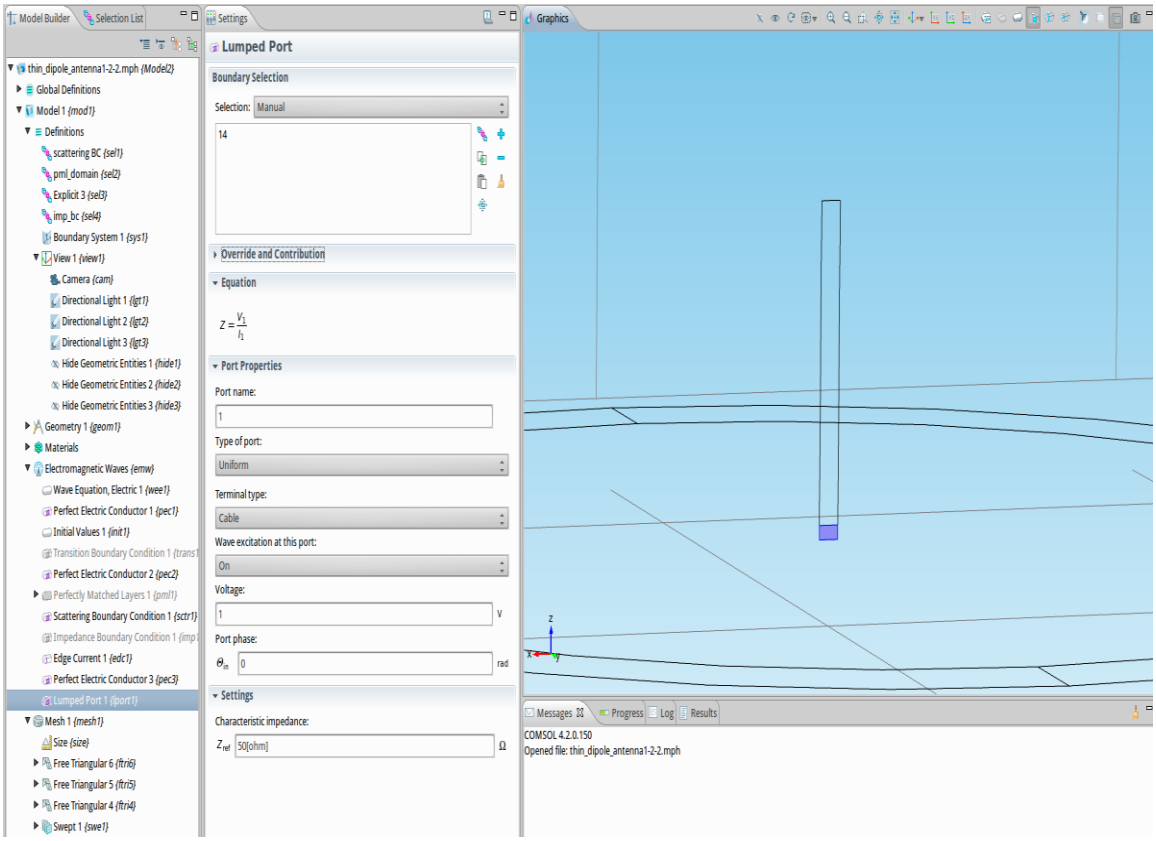

Figure 3.4: COMSOL snapshot for lumped port feeding technique.

3.1.4 Scattering boundary condition:

The scattering boundary condition is applied at the outer boundary of the computational domain in order to truncate the open region. With this boundary condition, the truncation interface is

transparent to incident or scattered fields that are normally incident, but partially reflects some of any non-normally incident fields. The minimum distance at which this boundary should be placed away from the radiating structure is one-half wavelength. In this work, both the plane wave and spherical wave boundary has been used, given by

$$\hat{n} \times (\nabla \times \mathbf{E}) - jk\hat{n} \times (\mathbf{E} \times \hat{n}) = 0 \tag{3.4}$$

for a plane wave and

$$\hat{n} \times (\nabla \times \mathbf{E}) - \left(jk + \frac{1}{r}\right) \hat{n} \times (\mathbf{E} \times \hat{n}) = 0 \tag{3.5}$$

for a spherical wave,

where k is the wave number of the medium. This boundary condition is equivalent to the first order absorbing boundary condition [8]. Figure 3.5 shows a COMSOL snapshot with the spherical type scattering boundary condition enabled. When the computational domain is chosen as a sphere, it is better to use spherical-wave type boundary condition since the wave front generated by the antenna will be incident almost normally on outer boundary.

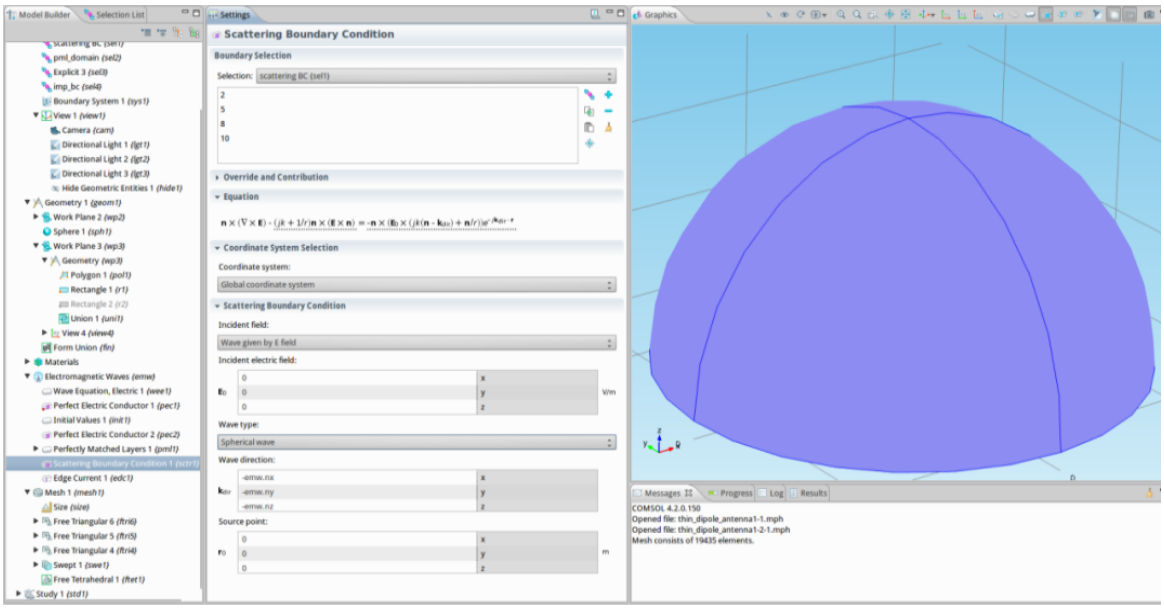

Figure 3.5: Scattering boundary condition applied at outer surface of computational model

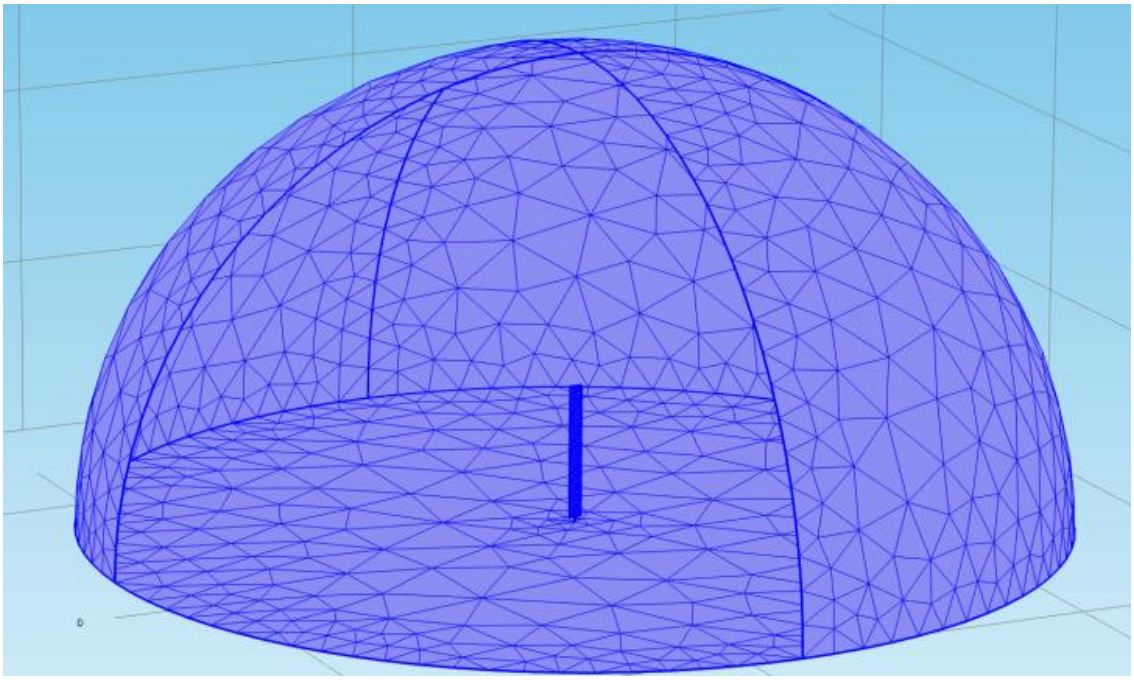

Figure 3.6: Discretization of the computational domain with tetrahedral elements

3.2 Problem formulation:

In an actual FEM solution, the computational model is divided into small finite elements such as triangles, tetrahedrals, prisms, hexahedrals or pyramids. Figure 3.6 shows the discretization of the computational domain using tetrahedral elements. The maximum element size depends on the wavelength of the medium. The maximum element size mentioned according to [22] should be smaller than one-fifth of the wavelength. Once the entire space (including the antenna and surrounding medium) is discretized, the unknown function to be found, the electric field E, is expanded as a weighted sum of basis functions. COMSOL uses vector-quadratic elements [14] for the interpolation of mesh elements. The overall discretized problem can be written in the form [A] [E] = [b], where A is a symmetric and sparse matrix and E is unknown function which is electric field. In COMSOL, this matrix equation can be solved by choosing the direct solver which is available in [23] under advanced solver topics. This solver is used to solve the large sparse matrix.

3.3 Impedance boundary condition (or Transition boundary condition in COMSOL):

In reality, all the metals have finite, not ideal, conductivity. Also, the metal that is used for the antenna structure will have a non-zero thickness. The transition boundary condition [13] is used for modeling thin metal sheets and dielectrics. This boundary condition is applied on the surface of the conductor or dielectric. This introduces a discontinuity in the tangential electric field at the surface of conductor due to the surface current at surface of conductor. This boundary condition does not require meshing the thickness of geometry and reduce the number of mesh elements considerably by large amount. This boundary condition is valid for modeling thin structure when thickness d is less than or comparable to the skin depth of the metal [25], [26]. Figure 3.7 shows the COMSOL snapshot with transition boundary condition used on metal structure.

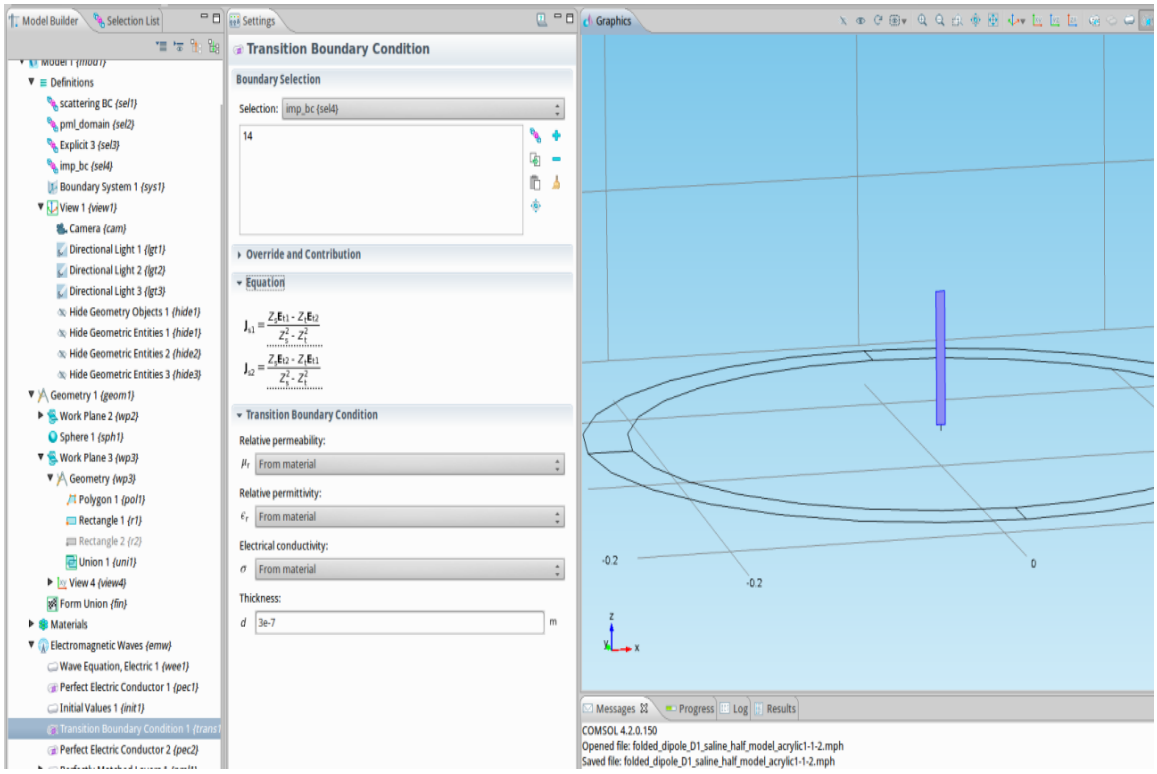

Figure 3.7: COMSOL snapshot for transition boundary condition

3.4 Perfectly matched layers:

One of the challenges in the finite element method is modeling the open boundary for antenna radiation problems. Since the scattering boundary condition must be placed at least one-half wavelength away from the radiating structure, this will lead to an increase in number of mesh elements and increase the computational time for the simulation. An alternative is to include another region which acts as an artificial absorber. PML of order 1 and 2 are implemented using COMSOL.. The material properties such as relative permittivity and electrical conductivity of a PML region should be same as that of the medium which the PML surrounds [19].

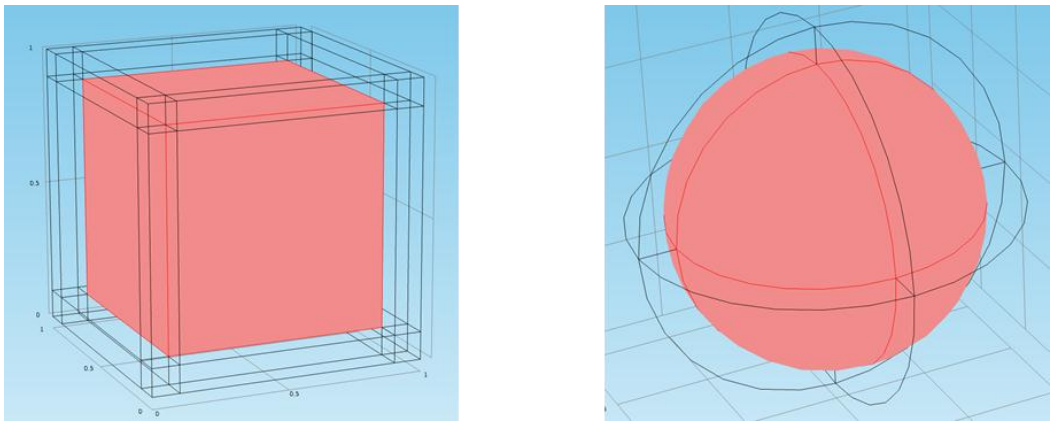

Figure 3.8: Snapshot of (a) Cube surrounded by Cartesian PML and (b) Sphere surrounded by Spherical PML

The performance of a PML is determined by the layer thickness. Thicker layers absorb more of the incident field and reduce reflection. However, increasing the thickness also increases the number of mesh elements, and increasing the computational time. Performance is improved by backing the PML with a scattering boundary condition or a first order absorbing boundary condition [9]. The PML should be sufficiently far from the radiating structure that it has negligible effects on radiated fields. In [8], it is mentioned that PML should be placed at distance of $\lambda/4$ distance from the scatterer. For meshing in the PML region, COMSOL recommends using its swept meshing feature [13], [18] which generates prism and hexahedral elements. The types of PML used in COMSOL are Cartesian and spherical, whose snapshots are shown in Figure 3.8.

Figure 3.9 shows a COMSOL snapshot for perfectly matched layers of spherical type surrounding the computational domain. Figure 3.10 shows the COMSOL snapshot with 6 layers of meshed PML elements, with one of the regions of the PML hidden to show the internal structure of PML mesh.

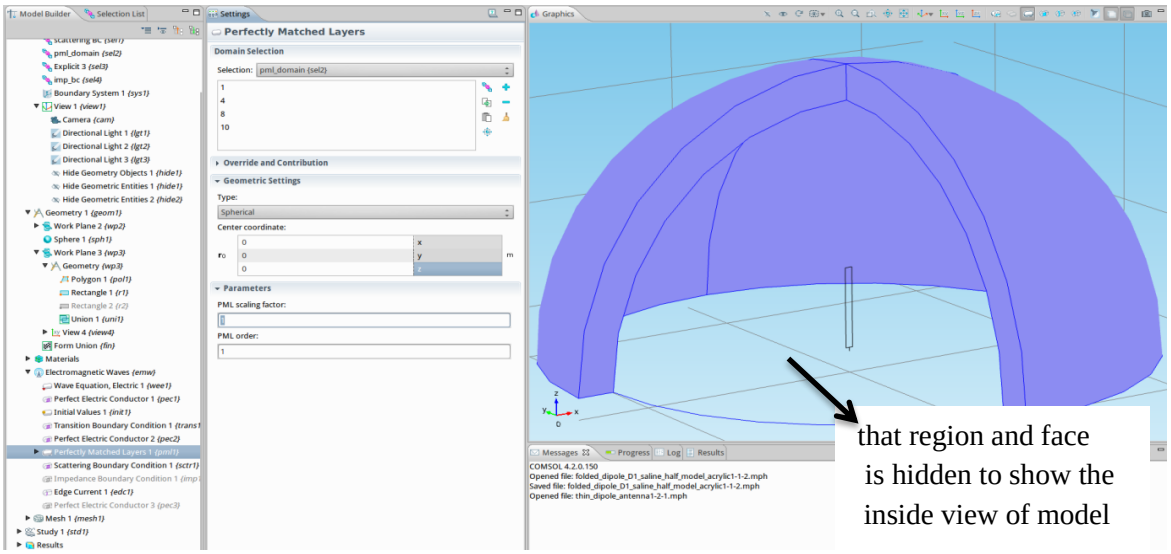

Figure 3.9: Spherical PML region modeled in COMSOL

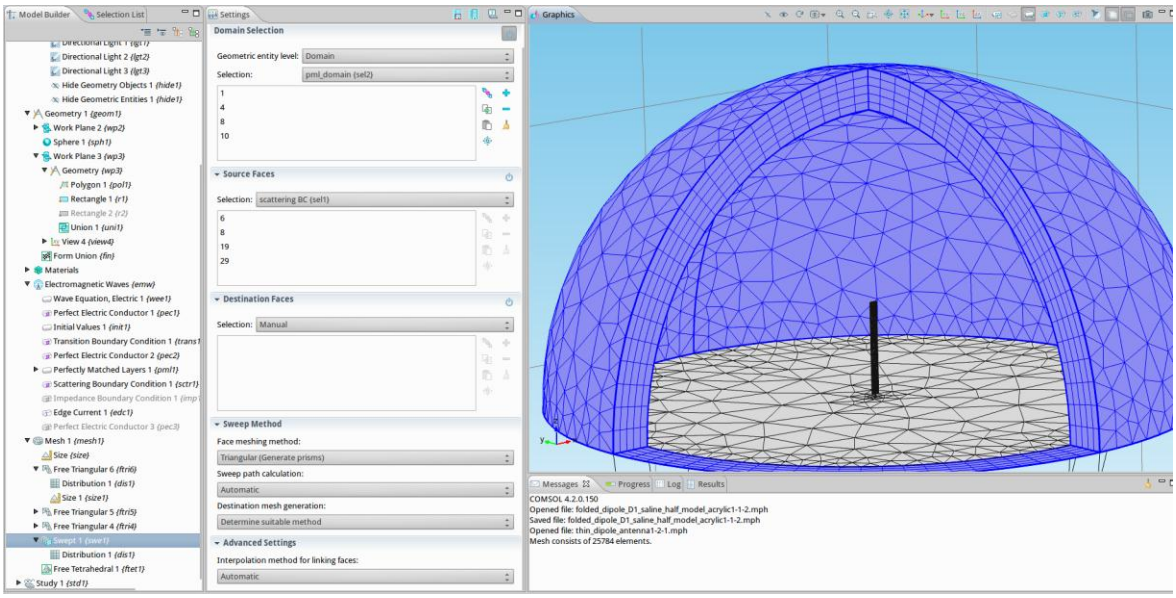

Figure 3.10: Mesh structure in PML region using prism element

3.5 Commercial software package based on MOM

The method of moments (MOM) is another computational tool that can find approximate solutions to electromagnetic problems. This requires the discretization of metal surface of the antenna only and does not require discretizing of the surrounding radiating medium. The Sommerfield radiation boundary condition eliminates the need to discretize the medium surrounding the radiating structure. Like FEM, this tool also converts the boundary value problem into linear matrix equations.

The commercial software package FEKO [30], based on MOM, is used for verifying the COSMOL simulation model. The electric field integral equation (EFIE) is used since open structures are modeled [38]. It forces the electric field boundary conditions to be met at the antenna surface. FEKO uses Rao-Wilton-Glisson (RWG) basis functions to discretize for the surface current on triangle surface elements and linear basis functions on wire segments [36], [37]. FEKO specifies that the maximum segment length in a wire element mesh should not be more than $\lambda/10$ and that the ratio of a segment length to its radius should be at least 4. When meshing with triangular elements on a surface, the area of the mesh element should not be more than $\lambda^2/70$. With nearly equilateral triangle elements, the maximum edge length should not be more than $\lambda/6$ where λ is the wavelength of the radiating medium.

CHAPTER 4

ANALYSIS OF MONOPOLE ANTENNA

In this chapter, a monopole antenna over a ground plane radiating in free space is modeled using both the COMSOL and FEKO simulation tools. FEKO does not require a truncation of the open boundary being modeled, so is expected to be more accurate. The accuracy of COMSOL depends upon the placement of the truncation boundary. First, the monopole antenna strip is modeled using both COMSOL and FEKO. Table 4.1 shows the dimensions of the monopole strip antenna modeled in COMSOL and FEKO. The simulation results from both are compared. Then a cylindrical monopole with radius one-fourth times the width of monopole strip with same length (an equivalent to the monopole strip) [20] is modeled using both COMSOL and FEKO. Their simulation results are also compared. Table 4.2 shows the dimensions of the cylindrical monopole antenna. The frequency of operation is set at 900 MHz.

4.1 Monopole antenna modeled using COMSOL:

Figure 4.1 shows a slice of the 3-dimensional computational domain containing the monopole antenna structure used in COMSOL. The monopole is fed with a line feed. It is radiating in free space, which is truncated by using the combination of a perfectly matched layer and the scattering boundary condition. An order 2 spherical PML of thickness 0.1 λ is used, placed 0.465 λ from the monopole. Additional calculations showed that this distance is sufficiently large to not affect the calculated antenna impedance. The antenna strip was modeled using both a perfect electric conductor and a gold conductor with finite conductivity. The transition boundary condition

was used to model thin gold conductor. Two types of excitations were used for calculation of the input impedance: line feed and lumped port excitation. The line feed length was 0.01 λ, which is equal to gap between the antenna and ground plane. The excitation current was 1A. Lumped port excitation can be modeled in COMSOL by inserting a rectangle of dimension 0.01 λ × 0.02 λ at the gap between the antenna and ground plane, as shown in Figure 4.2. Figure 4.3 shows the COMSOL mesh structure when the monopole antenna is excited using a line feed and Figure 4.4 shows the lumped port excitation at the gap between the monopole and ground plane. Table 4.3 and 4.4 shows the mesh settings for COMSOL when the monopole is excited using a line feed and a lumped port at the gap of monopole and ground plane, respectively. A monopole antenna with cylindrical geometry modeled as perfect electric conductor are also excited by the lumped port with dimension of 0.01 λ x 0.01 λ has also been simulated using COMSOL. Table 4.5 shows the mesh settings used for the simulation of cylindrical monopole antenna and Figure 4.5 shows the mesh structure. At least two triangle mesh elements are needed in the 90^0 arc to model the curved geometry. Figure 4.5 shows three mesh triangle elements per 90^0 arc.

Monopole antenna strip dimensions	
Width of monopole strip	0.02 λ
Monopole strip thickness	300 nm
Gap between the monopole strip and ground plane	0.01 λ
Height of monopole strip taken from ground plane	0.235 λ

Table 4.1: monopole antenna strip dimension

Cylindrical monopole antenna dimensions	
Radius of cylindrical monopole	0.005 λ
Monopole strip thickness	300 nm
Gap between the cylindrical monopole and ground plane	0.01 λ
Height of cylindrical monopole	0.235 λ

Table 4.2: Cylindrical monopole antenna dimension

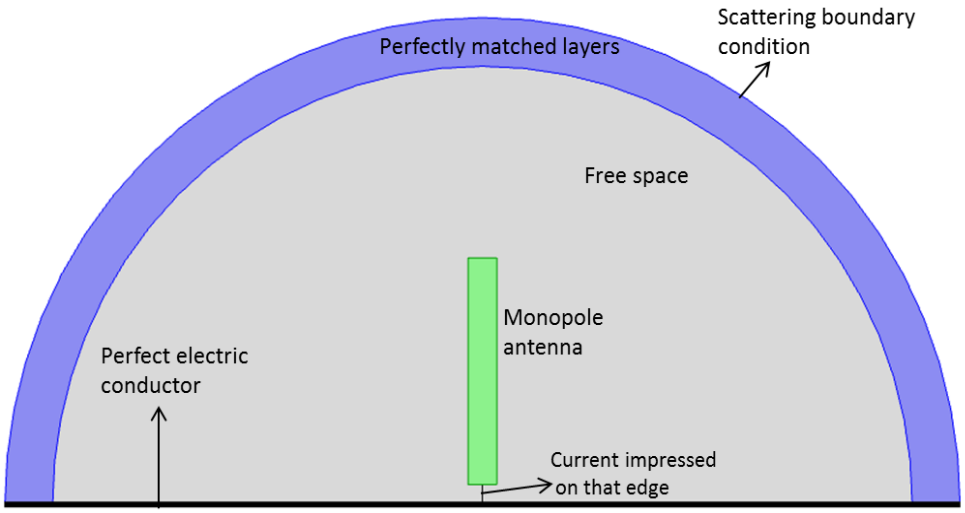

Figure 4.1: Monopole antenna over a perfect electric conducting ground plane in COMSOL using line feed excitation

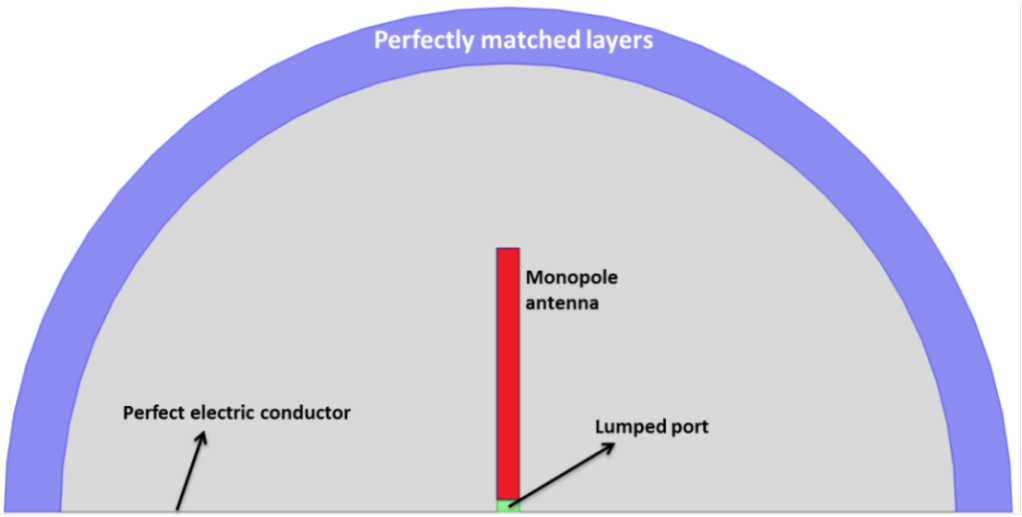

Figure 4.2: Monopole antenna over a perfect electric conducting ground plane in COMSOL using lumped port excitation

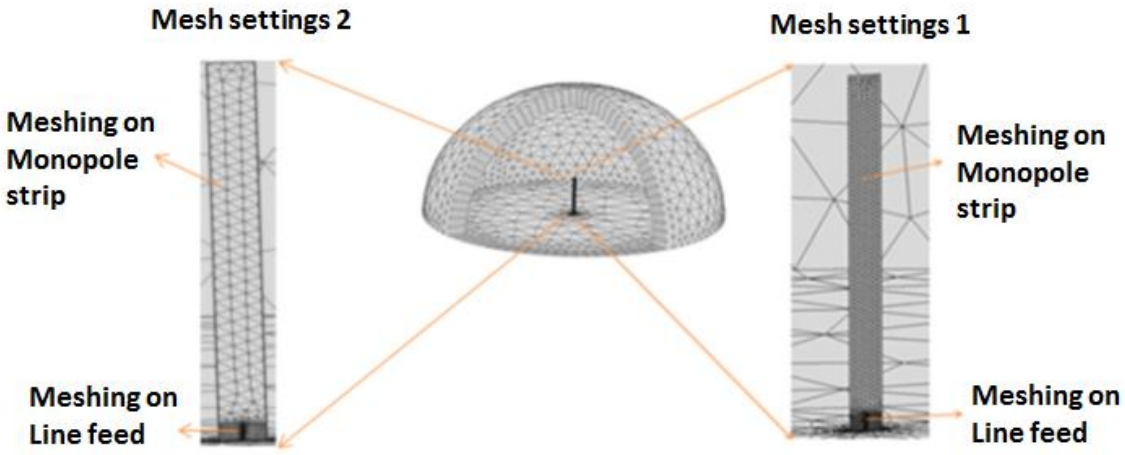

Figure 4.3: Mesh structure for monopole strip with line feed

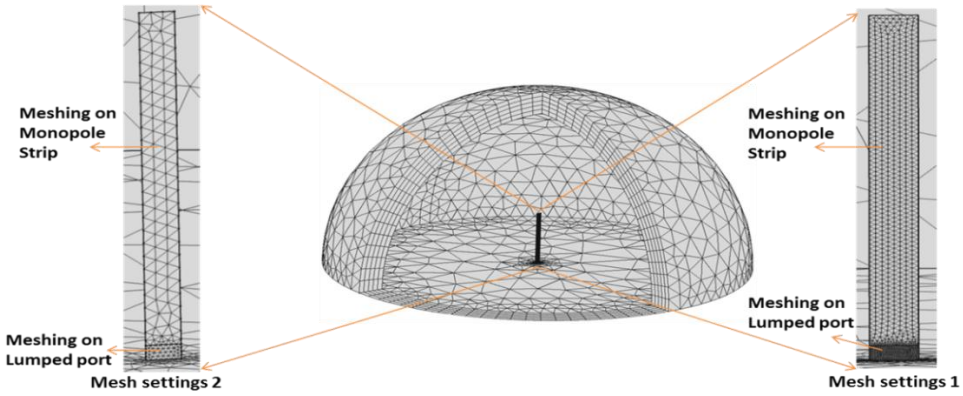

Figure 4.4 Mesh structure for monopole strip with lumped port

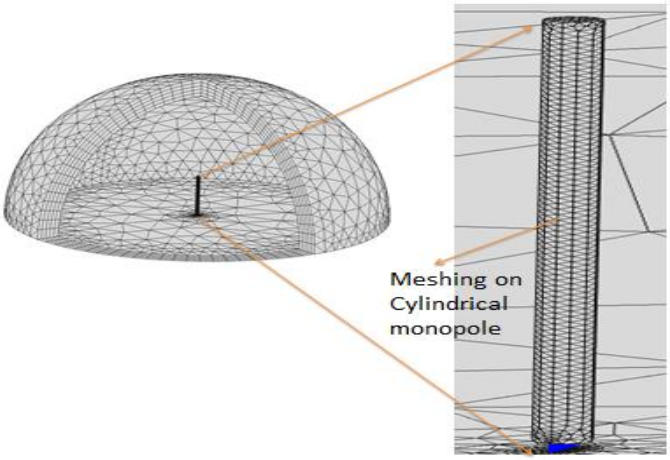

Figure 4.5: Mesh structure for cylindrical monopole antenna with lumped port

	Mesh settings 1	Mesh settings 2
Maximum mesh settings in free space	0.166 λ	0.166 λ
Maximum mesh size in antenna strip	1 mm (0.003 λ)	2.5 mm (0.0075 λ)
Number of triangle elements in conductor	1287	265
Line feed length	0.01 λ	0.01 λ
Distribution in line feed	200	200
Total number of tetrahedral elements	36442	27276
Total number of prism elements	7420	7420
Total mesh elements in computational domain	43862	34696

Table 4.3: COMSOL mesh setting in monopole strip antenna using line feed

	Mesh settings 1	Mesh Settings 2
Maximum mesh settings in free space	0.166 λ	0.166 λ
Maximum mesh size in conductor	1 mm (0.003 λ)	3 mm (0.009 λ)
Number of triangle elements in conductor	1322	178
Maximum mesh size on lumped port	0.0009 λ	0.003 λ
Dimension of lumped port	0.02 λ x 0.01 λ	0.02 λ x 0.01 λ
Triangle mesh elements in lumped port	618	66
Total number of tetrahedral elements	24396	9363
Total number of prism elements	7420	7420
Total mesh elements in computational domain	31816	16783

Table 4.4: Mesh settings when monopole antenna strip excited using lumped port

Maximum mesh settings in free space	0.166 λ
Maximum mesh size in conductor	0.003 λ
Number of triangle elements in conductor	2042
Maximum size on lumped port	0.0009 λ
Total mesh elements in computational domain	28966
Total number of tetrahedral elements	19746
Total number of prism elements	9220

Table 4.5: Mesh settings when cylindrical monopole antenna excited using lumped port

4.2 Monopole antenna modeled using FEKO:

The monopole antenna has also been simulated using FEKO. The dimensions of the monopole antenna geometry used are shown in Table 4.1 and Table 4.2. The monopole antenna was modeled as a thin strip, made of both a perfectly conducting material and gold. The strip of width 0.02 λ is modeled equivalent to wire of radius 0.005 λ. In FEKO, wire port excitation and edge port excitation are considered. In wire port excitation, a wire is connected between the monopole antenna and ground plane as shown in Figure 4.6. This can be viewed as infinitesimal dipole connected between antenna terminals. The radius of the wire in the excitation port is chosen 100 nm, which is less than one-quarter the length, as required. The wire port is discretized to 122 segments. In edge port modeling, antenna structure is excited by connecting a voltage source at its terminal as shown in Figure 4.7. The edge of the monopole strip which coincides with the perfectly conducting ground is chosen as the excitation port, as shown in Figure 4.7. Table 4.6 shows the mesh setting s for the wire port and the edge port excitations of the monopole antenna. The cylindrical monopole antenna can also be modeled as a wire with a radius of 0.005 λ, as shown in Figure 4.8. 10 segments with minimum length of 0.02 λ and maximum length of 0.027 λ are used to model the wire. The source excitation details are given in Table 4.8 when the antenna structure is excited using the wire port and the edge port.

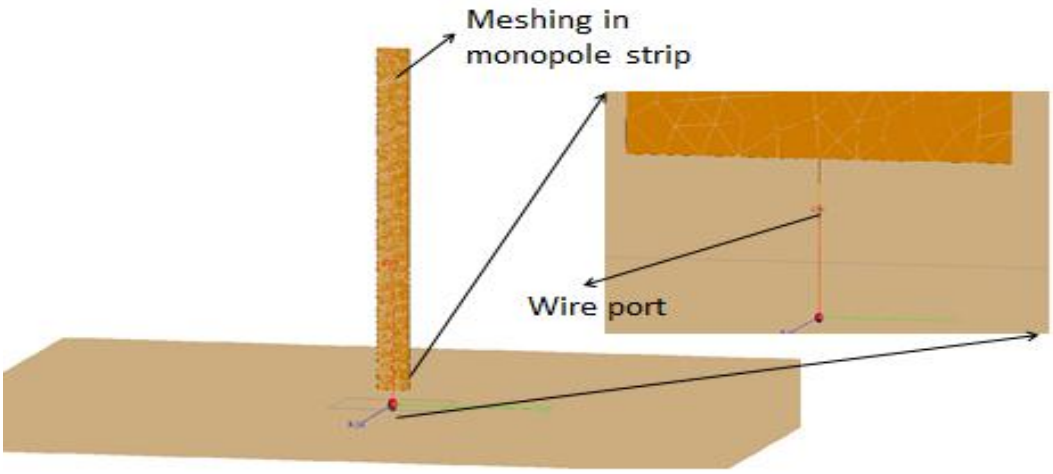

Figure 4.6: Monopole antenna strip modeled using wire port feeding technique

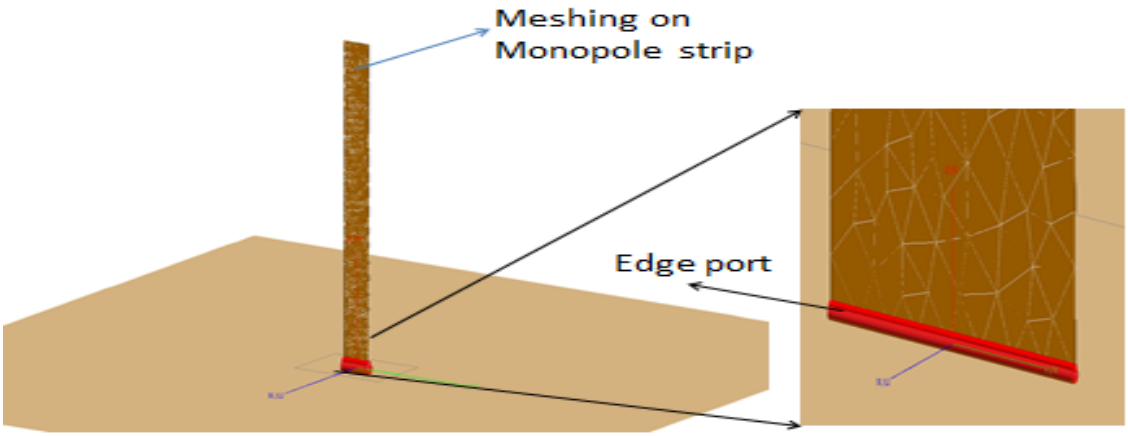

Figure 4.7: Monopole antenna strip excited using edge port feeding technique

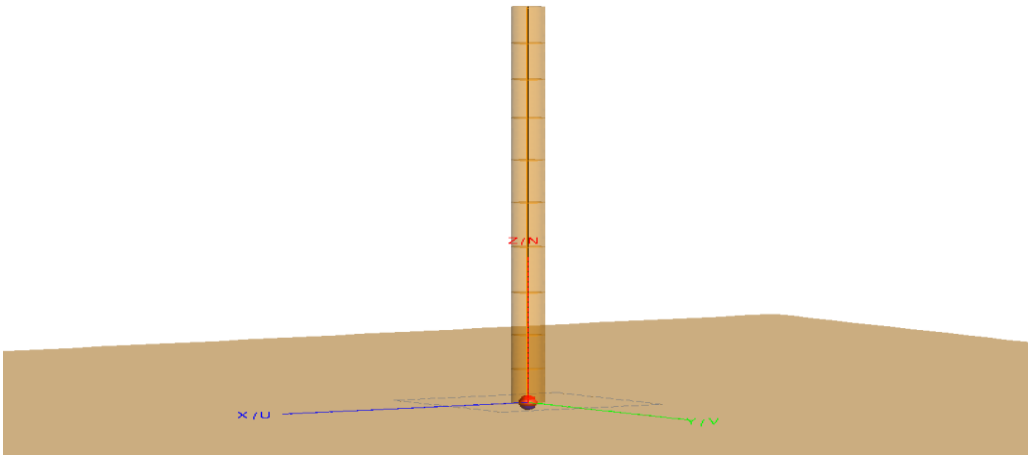

Figure 4.8 Monopole antenna modeled as wire that is divided into 10 segments

	Wire Port	Edge Port
Maximum mesh size on conducting surface	0.8 mm (0.0024 λ)	0.003 λ
Maximum segment length in wire port	0.00009 λ	N/A
Radius of wire port	100 nm	N/A
Total number of triangle elements	2496	1600
Number of segments in wire port	122	N/A

Table 4.6: FEKO mesh settings for monopole antenna strip

Maximum segment size:	0.027 λ
Total number of segments in wire	10
Wire radius	0.005 λ

Table 4.7: FEKO mesh settings for modeling a cylindrical monopole antenna

Source voltage	1 V
Source impedance	50 Ω

Table 4.8: Source excitation details for edge port and wire port

4.3 Discussion of results:

Table 4.9 shows the computed input impedance of the perfectly conducting, monopole strip antenna. The wire port feed in FEKO is analogous to the line feed in COMSOL, while the FEKO edge port and COMSOL lumped port are also similar. Different cell sizes on the monopole strip are analyzed in COMSOL, which has negligible effect on input impedance as shown in Table 4.9 and 4.11. The COMSOL and FEKO simulation results are in good agreement. Table 4.10 shows the input impedance when the monopole is modeled as a perfectly conducting cylinder. Good agreement is again achieved between COMSOL and FEKO. This also agrees with the strip monopole when the same excitation is used. The input impedance of cylindrical dipole antenna of length 0.47 λ will be twice the input impedance of cylindrical monopole of length 0.235 λ with

same radius. So, the input impedance of cylindrical dipole antenna modeled with perfect electric conductor are 78.22+19.4i Ω and 75.17+8.57i Ω using the COMSOL and FEKO simulation results, respectively. These values agree with [46]. Finally, the input impedance when the strip monopole made of gold is considered and fed with a wire port in FEKO and line feed in COMSOL which shows very little change when perfect electric conductor was considered. It is noted that the input reactance shows a significant difference when the strip monopole modeled with a perfect electric conductor is excited both by wire port and edge port in FEKO. In wire port excitation, the wire is connected between the monopole strip and the perfect electric conducting ground plane which gives an additional reactance due to the inductance of wire. Therefore, the input reactance in wire port excitation is more than with edge port excitation. Similarly, the input reactance with line feed excitation is higher than with lumped port excitation in COMSOL.

Input impedance of monopole strip with perfect electric conductor	
Wire port in FEKO	38.412+42.66i
Line feed in COMSOL	38.5422+34.9614i (using mesh settings 1) 39.2961+36.9801i (using mesh settings 2)
Edge port in FEKO	38.419+2.0385i
Lumped port excitation in COMSOL	38.5878+6.3094i (using mesh settings 1 of Table 5.3) 39.3265+8.272i (using mesh settings 2 of Table 5.3)

Table 4.9: Input impedance of monopole antenna strip with perfect electric conductor

Input impedance of cylindrical monopole with perfect electric conductor	
Edge port in FEKO	37.584+4.2843i
Lumped port in COMSOL	39.1122+9.7022i

Table 4.10: Input impedance of cylindrical monopole antenna with perfect electric conductor

Input impedance of monopole strip with gold conductor	
Wire port in FEKO	38.858+42.555i
Line feed in COMSOL	39.905+35.0198i (using mesh settings 1 of Table 5.4) 40.5846+36.9173i (using mesh settings 2 of Table 5.4)

Table 4.11: Input impedance of monopole antenna strip with gold conductor

CHAPTER 5

FOLDED DIPOLE STRIP ANTENNA

In this chapter, the input impedance of the proposed folded-dipole strip antenna is computed using both COMSOL and FEKO over the required operating band when it is radiated into a free space medium, a lossless dielectric medium, and a lossy dielectric medium. The results are also compared with a method of moment code written at Oklahoma State University. Once the simulation results are verified, the input impedance is computed at various frequencies for varying surrounding medium using COMSOL and FEKO. Figure 5.1 shows an antenna strip geometry that has been measured in the Mixed Signal VLSI Design Laboratory at Oklahoma State University. It is used in this chapter as the first test case for comparison between COMSOL and FEKO. As mention in Chapter 2, due to the requirement of higher inductive reactance at lower frequency, a planar loop antenna or folded dipole strip antenna is preferred. The strip thickness is 300 nm and the conducting material used is gold with an electrical conductivity of 45.6×10^6 S/m. Table 5.1 shows the dielectric constant and electrical conductivity of the media where the antenna is radiated. The lossy medium dielectric properties are close to dielectric properties of brain tissue (grey matter) [16] at 900 MHz. Table 5.2 shows the frequency range considered for different medium.

	Dielectric constant	Electrical conductivity in S/m
Free space medium	1	0
Lossless dielectric medium	50	0
Lossy dielectric medium	50	0.94

Table 5.1 Dielectric properties of homogenous medium considered

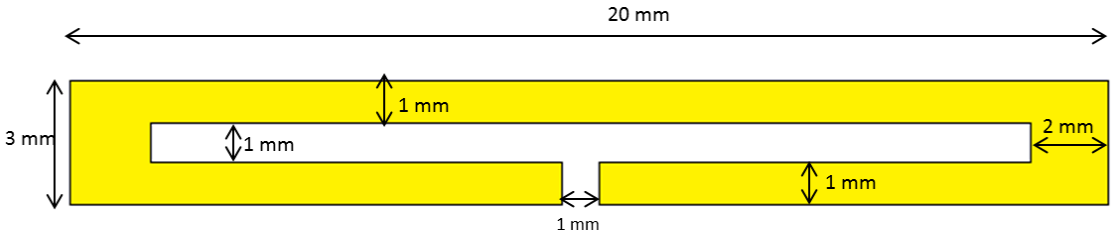

Figure 5.1: Folded dipole antenna strip geometry with strip thickness of 300 nm

	Frequency Range considered
Free space medium	0.9 GHz to 9.7 GHz
Lossless dielectric medium	0.85 GHz to 0.95 GHz
Brain tissue medium	0.75 GHz to 1.35 GHz

Table 5.2: Frequency range considered for different medium considered

5.1 Problem formulation using COMSOL:

Figure 5.2 shows that half of the symmetric geometry is modeled. This allows the computer memory required for the electromagnetic solution to be considerably reduced. A perfect electric conductor can be used as a boundary condition at the plane of symmetry giving an equivalent model of the full antenna through image theory [15]. The antenna is excited using a line feed in COMSOL. The input impedance obtained using the symmetric boundary condition is multiplied by 2 to get input impedance of the actual geometry.

The highest frequency analyzed was limited by the computational memory. In the dielectric medium, the wavelength reduces and so lowers the maximum frequency. The mesh settings need to be changed for each frequency of operation modeled. The maximum cell size was chosen based on the frequency being analyzed. The maximum cell size is fixed at 0.2 λ where λ is the wavelength, at the highest frequency of the analyzed band. As the frequency decreases, the cell size becomes smaller than 0.2 λ in terms of wavelength. The distance of the antenna structure to the PML was set to insure accuracy at the longest wavelength. Table 5.5 and 5.6 shows the

detail of the mesh PML region with a lossless dielectric medium and a lossy dielectric medium. The minimum distance of the PML from the antenna structure is 3.5 cm, which is 0.7 times the wavelength at 850 MHz in the lossless dielectric medium ($\varepsilon_r = 50$) and 0.64 times the wavelength at 750 MHz in the brain tissue medium. The maximum mesh size in the surrounding medium is 6 mm, corresponding to 0.134 times the wavelengths at 950 MHz in the lossless dielectric medium ($\varepsilon_r = 50$) and 0.19 times the wavelength at 1.35 GHz in the brain tissue medium. The maximum mesh size on the antenna structure is 0.15 mm, which is 0.0036 times the wavelengths at 950 MHz in lossless dielectric medium ($\varepsilon_r = 50$) and 0.0049 times the wavelengths at 1.35 GHz in the brain tissue medium. Figure 5.3 shows dielectric constant and electrical conductivity of brain tissue (grey matter) for the frequency range 750 MHz to 1350 MHz [16]. Figure 5.4 shows the mesh structure in COMSOL. Part of the face in the symmetric boundary condition is hidden in order to show the discretization of the antenna structure.

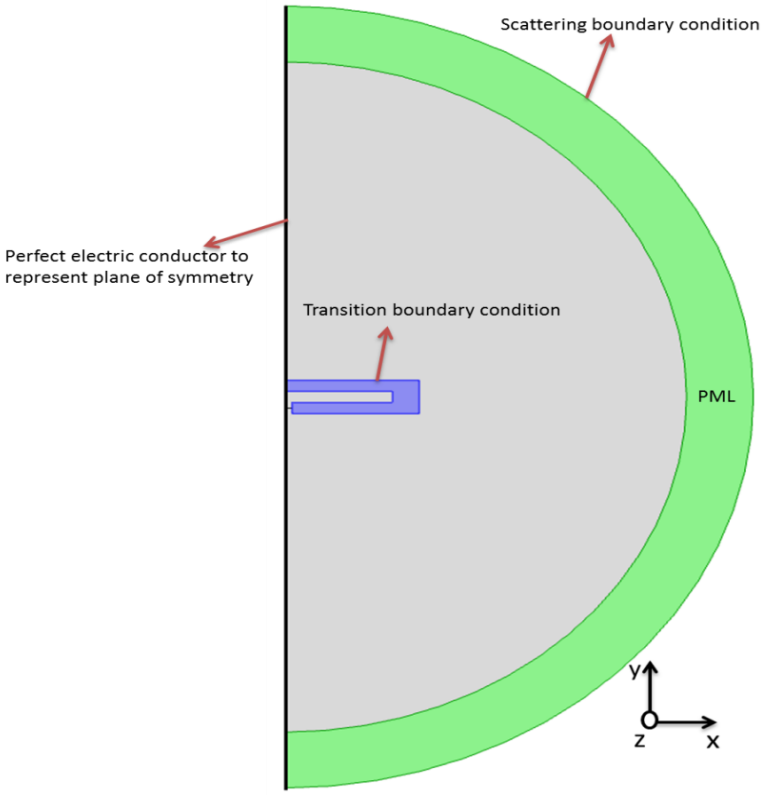

Figure 5.2: COMSOL model using symmetric boundary condition

Frequency range	0.9 GHz to 2 GHz	2.1 GHz to 5 GHz	5.1 GHz to 6 GHz	6.1 GHz to 9.7 GHz
PML type	Spherical	Spherical	Spherical	Spherical
PML thickness	10 cm	10 cm	2 cm	2 cm
Minimum distance of PML layer from the antenna	14 cm ($0.37\ \lambda_{large\ 1}$)	14 cm ($0.98\ \lambda_{large\ 2}$)	3 cm ($0.51\ \lambda_{large\ 3}$)	3 cm $0.61\ \lambda_{large\ 4}$)
PML order	1	1	1	1

Table 5.3: Details for PML region in free space medium for various frequencies; $\lambda_{large\ 1}$, $\lambda_{large\ 2}$, $\lambda_{large\ 3}$ and $\lambda_{large\ 4}$ are the wavelengths at 0.9 GHz, 2.1 GHz, 5.1 GHz and 6.1 GHz, respectively.

Frequency range	0.9 GHz to 2 GHz	2.1 GHz to 5 GHz	5.1 GHz to 6 GHz	6.1 GHz to 9.7 GHz
Maximum mesh size in free space	2.5 cm ($0.166\ \lambda_{short\ 1)}$	1 cm ($0.166\ \lambda_{short\ 2}$)	0.9 cm ($0.18\ \lambda_{short\ 3}$)	0.5 cm ($0.166\ \lambda_{short\ 4}$)
Distribution in line feed	50	60	60	50
Maximum mesh size in conductor	0.15 mm ($0.001\ \lambda_{short\ 1}$)	0.15 mm ($0.0025\ \lambda_{short\ 1}$)	0.15 mm ($0.003\ \lambda_{short\ 1}$)	0.15 mm ($0.005\ \lambda_{short\ 4}$)
Total mesh elements in computational domain	70595	78415	74547	79874

Table 5.4: Mesh settings in free space medium for various frequencies; $\lambda_{short\ 1}$, $\lambda_{short\ 2}$, $\lambda_{short\ 3}$ and $\lambda_{short\ 4}$ are the wavelengths at 2 GHz, 5 GHz, 6 GHz and 9.7 GHz, respectively.

PML type	Spherical
PML thickness	2 cm
Minimum distance of PML layer from the antenna	3.5 cm
PML order	1

Table 5.5: Details of PML region for lossy and lossless medium ($\varepsilon_r = 50$) for various frequencies

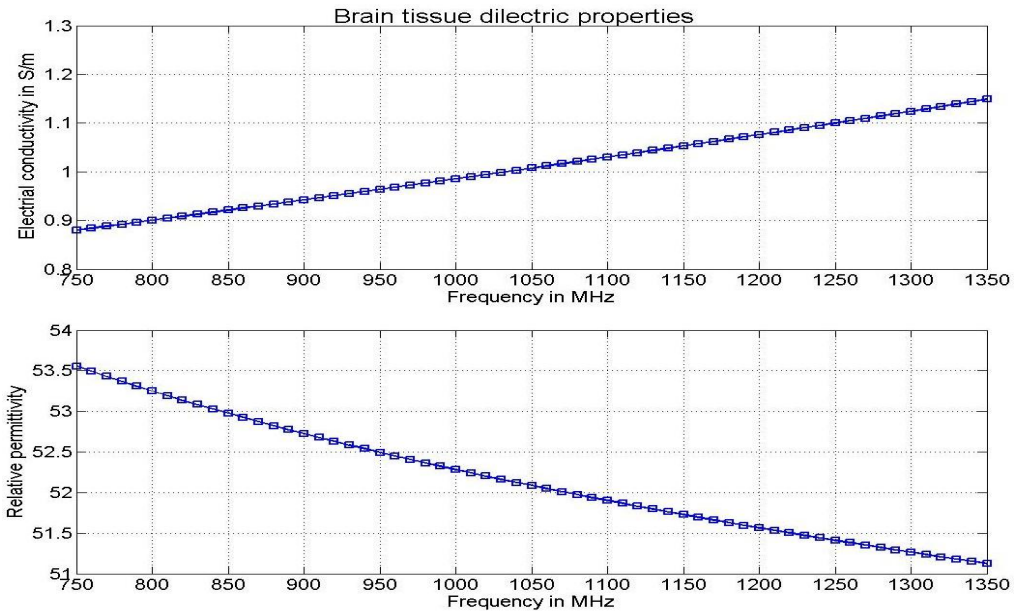

Figure 5.3: Brain tissue (grey matter) dielectric properties [16]

Maximum mesh size	6 mm
Distribution in line feed	100
Maximum mesh size in antenna structure	0.15 mm
Total mesh elements in computational domain	74074

Table 5.6: Mesh statistics in lossy and lossless medium for various frequencies

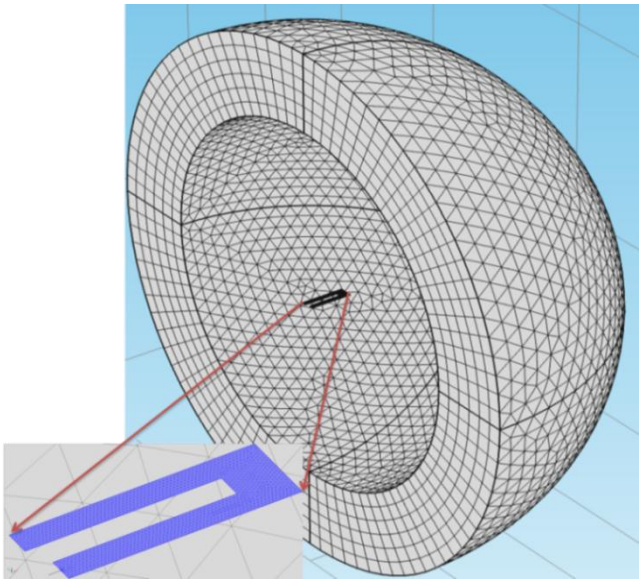

Figure 5.4: Mesh figure for folded dipole antenna strip surrounded by homogenous medium

5.2 Problem formulation using FEKO:

The folded dipole strip antenna has also been modeled in FEKO. The antenna was fed using the wire port technique. The modeled structure is shown in figure 5.5. As with COMSOL, only half the structure is simulated by taking the advantage of the plane of symmetry. The plane of symmetry is again chosen as a perfect electric conductor. The wire port radius used has no effect on the real part of the input impedance but has a minor influence on the imaginary part. Table 5.7 shows the mesh setting used in different homogenous radiating media in the FEKO simulation. The input impedance of the actual geometry in figure 5.1 will be twice that of the FEKO simulation obtained with the geometry of figure 5.5.

	Free space medium	Lossless dielectric medium with relative permittivity=50	Brain tissue medium
Frequency range	0.9 GHz to 9.7 GHz	850 MHz to 950 MHz	750 MHz to 1350 MHz
Maximum mesh size of triangle elements	0.2406 mm ($0.0078\ \lambda_{short}$)	0.2406 mm ($0.0055\ \lambda_{short}$)	0.2406 mm ($0.0078\ \lambda_{short}$)
Total number of triangle mesh elements	2934	2934	2934
Radius of wire port	1 μm	0.1 μm	0.05 μm
Maximum segment size	0.01 mm	0.01 mm	0.01 mm
Total number of segments in wire port	57	57	57

Table 5.7: FEKO mesh settings for folded dipole antenna strip; λ_{short} is the shortest wavelength in the frequency band

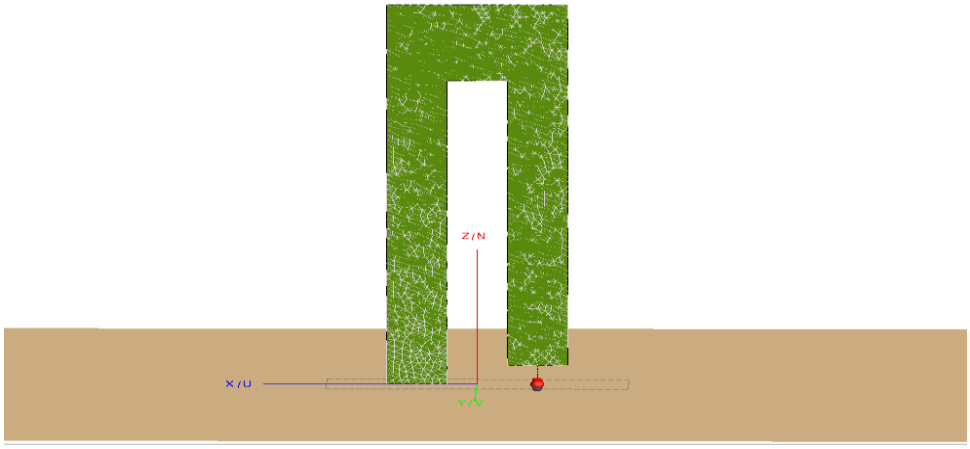

Figure 5.5: Mesh structure using wire port in FEKO

5.3 Discussion of results:

The input impedance of the test folded dipole strip computed with COMSOL and FEKO at 900 MHz are compared with that using a locally written MOM code in Table 5.8. COMSOL and FEKO are in good agreement. The MOM code gives good agreement in the real part of input impedance. The imaginary part has some difference, but it is highly sensitive to the antenna feed used. Figure 5.6 through 5.8 shows the calculated input impedance over a large frequency band for the free space, lossless dielectric, and brain tissue radiating media. COMSOL and FEKO show good agreement with each other. When radiating into free space, the antenna resonates at 4.4 GHz and 6.3 GHz. It is a parallel resonance at 4.4 GHz and a series resonance at 6.3 GHz [17]. Figure 5.7 shows the antenna is a series resonant circuit at around 880 MHz when radiating into the lossless dielectric. A parallel resonance appears at 1.3 GHz when radiating into brain tissue in Figure 5.8.

	Free space medium	Lossless dielectric medium (ε_r=50)	Lossy dielectric medium (ε_r=50, σ=0.94 S/m)
COMSOL	5.0292+88.7232i	38.8042+5.091i	54.429+16.7216i
FEKO	3.8488+89.206i	38.676+5.3274i	55.346+18.0034i
MOM code	2.98839+94.3839i	35.2103-11.7738i	53.9317-3.56391i

Table 5.8: Input impedance of folded dipole antenna strip in different homogenous medium at 900 MHz

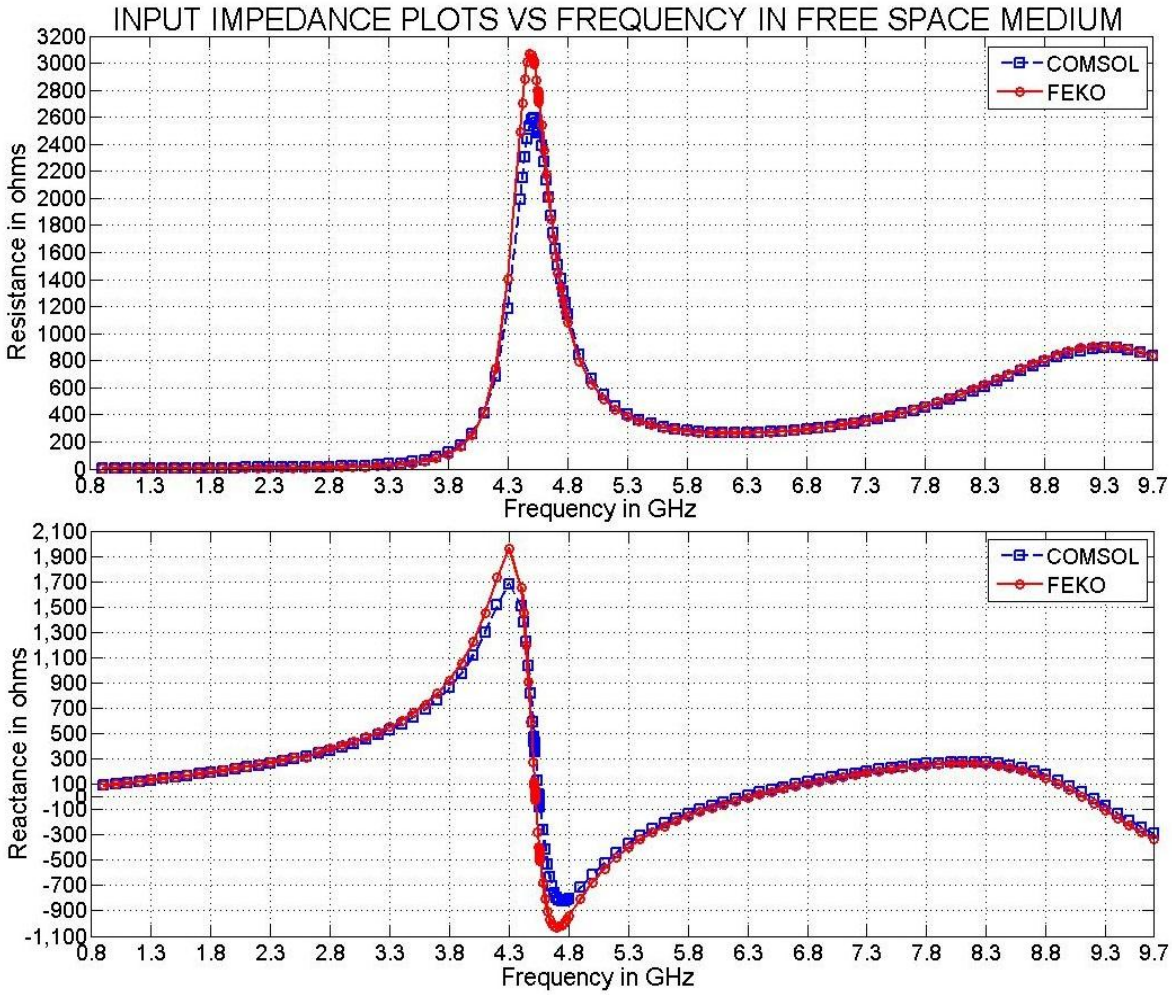

Figure 5.6: Input impedance of folded dipole antenna strip radiating in free space

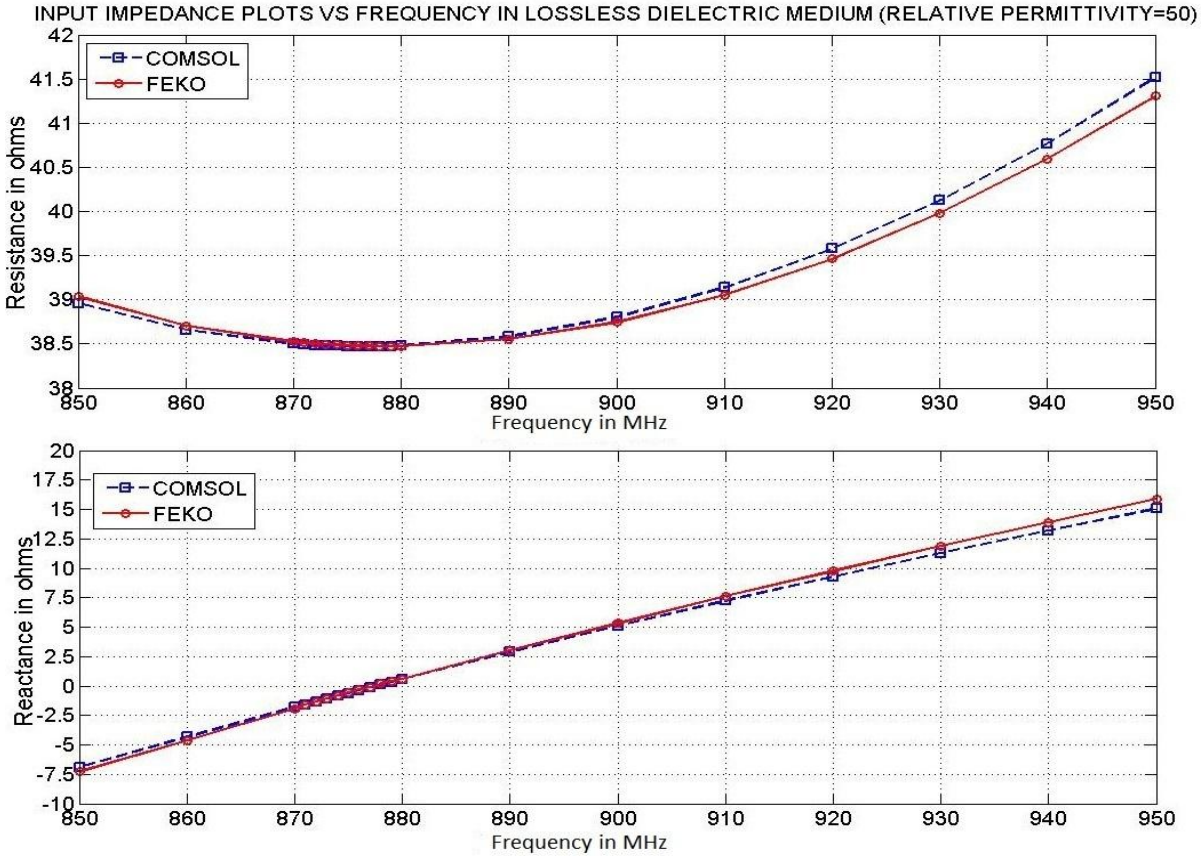

Figure 5.7: Input impedance of folded dipole strip antenna radiating in lossless dielectric medium

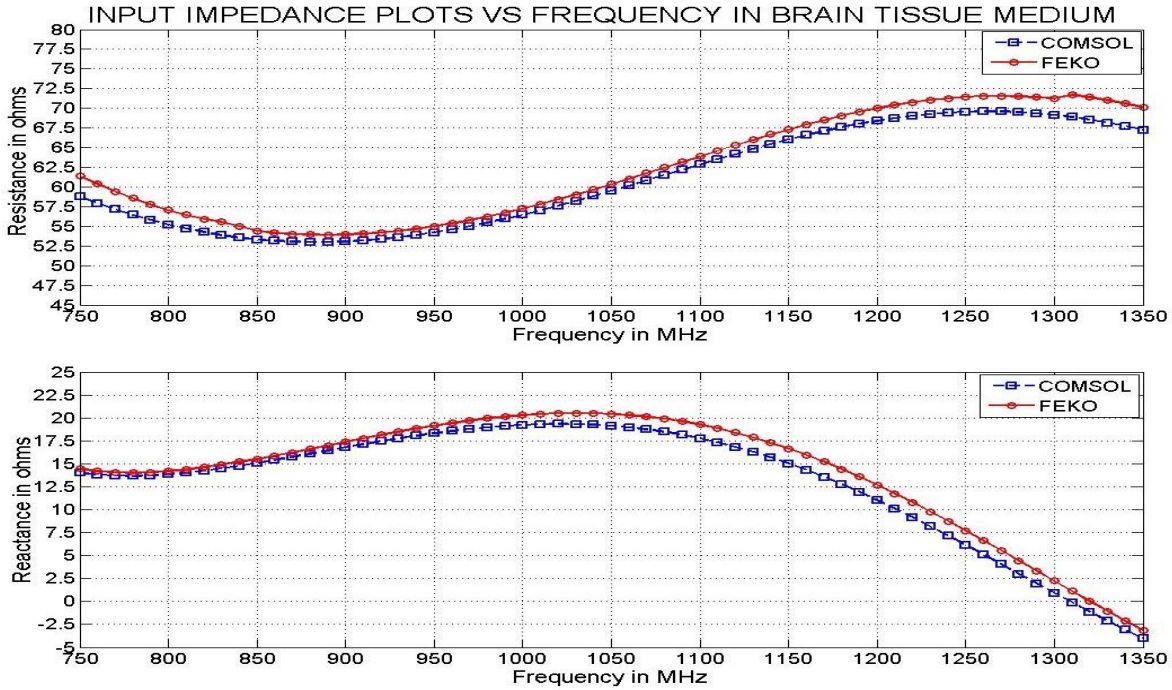

Figure 5.8: Input impedance of folded dipole antenna strip radiating in brain tissue medium

CHAPTER 6

COMSOL VALIDATION OF DESIGNED ANTENNA WITH FEKO

Up till now the COMSOL and FEKO simulation results were compared to varify the validity of the simulation models. Good agreement has been demonstrated. In this chapter, the four antenna geometries shown in Figure 6.1 are analyzed. The thickness of the gold conductor for each test antenna is shown in Table 6.1. Prototypes of these antennas were built at the University of Texas at Dallas. The numerical models of these antennas are again confirmed through a comparison of FEKO and COMSOL when radiating into homogeneous free space and saline media. COMSOL will then be applied to the antenna geometries shown in Figure 6.1 when printed on a substrate with an acrylic coating, as shown in Figure 7.1 in the next Chapter. This final configuration is suitable for implanting in living brain tissue.

Antenna geomtery type	Metal thickness
A	300 nm
B	300 nm
C	1 μm
D	300 nm

Table 6.1: Antenna geometry metal thickness

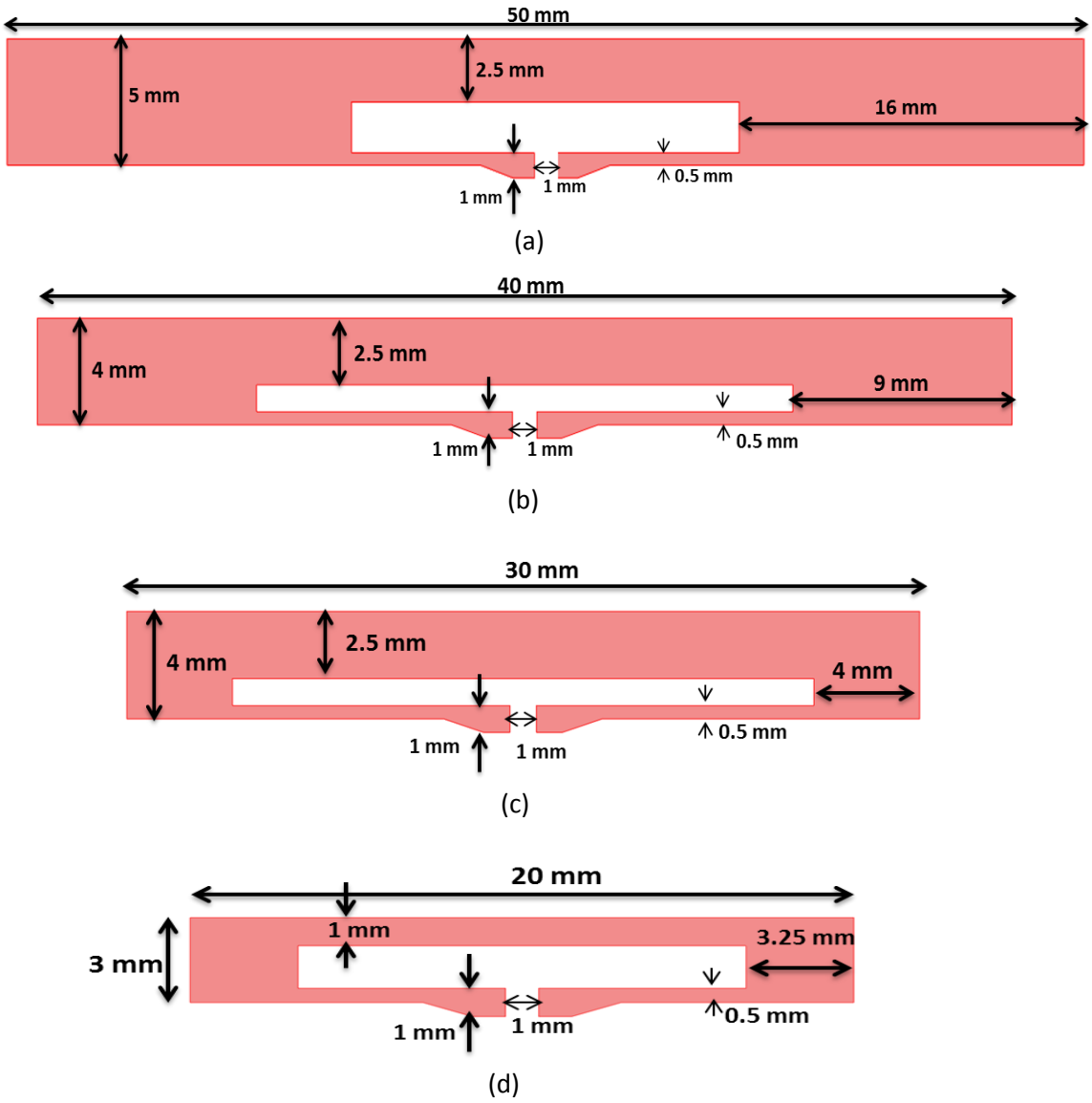

Figure 6.1: Antenna geometries (a) Antenna A (b) Antenna B (c) Antenna C (d) Antenna D

The complex relative permittivity of the 1% salt concentration saline solution is [31]

$$\varepsilon^*(\omega) = \varepsilon_\infty + \frac{(\varepsilon_s - \varepsilon_\infty)}{1+(j\omega\tau)^{1-\alpha}} - j\frac{\sigma}{\omega\varepsilon_0} \ , \tag{6.1}$$

where ω is the angular frequency of operation and the other parameters are given in Table 6.2. Equation (6.1) can be written in the form:

$$\varepsilon^*(\omega) = \varepsilon_r'(\omega) - j\varepsilon_r''(\omega) \ , \tag{6.2}$$

where $\varepsilon_r'(\omega)$ is the dielectric constant of the saline solution at angular frequeny ω. Similarly $\varepsilon_r''(\omega)$ can be expressed as follows:

$$\varepsilon_r''(\omega) = \frac{\sigma(\omega)}{\omega\varepsilon_0}. \tag{6.3}$$

More details regarding the complex permitivity of materials are given in [32]. Figure 6.2 shows the dielectric constant and effective electrical conductivity of saline medium as a function of frequency.

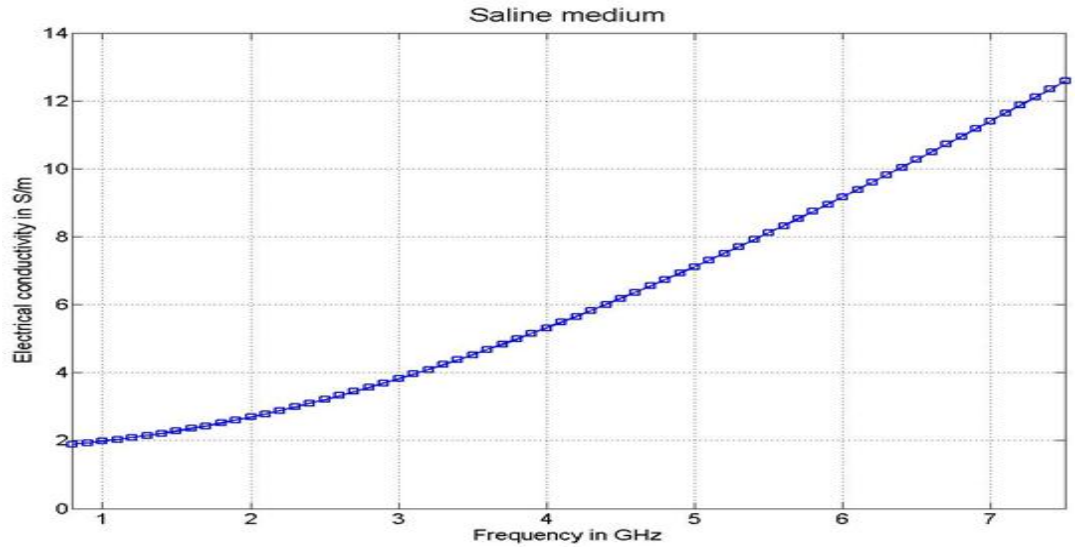

(a)

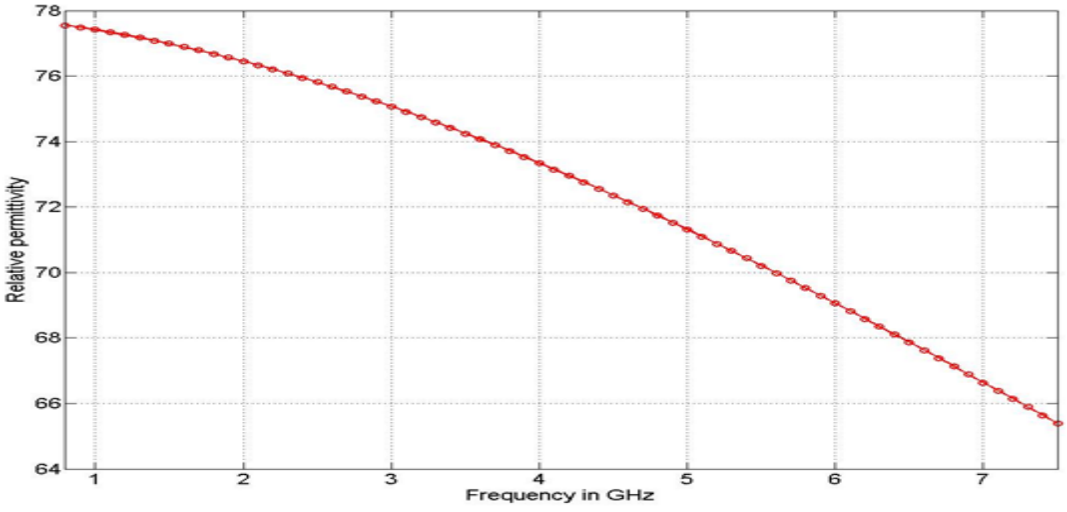

(b)

Figure 6.2 Dielectric properties of saline solution at salt concentration of 1% (a) electrical conductivity of saine soultion in S/m (b) dieltric constant of saline soultion.

Static permittivity (ε_s)	77.9
Optic permittivity (ε_∞)	4.15
Relaxation time (τ) in pecosecond	8.97
Conductivity in S/m (σ) at 20^0 C	1.73
Empirical Cole-Cole distribuition factor (α)	0.03

Table 6.2: Saline solution parameter readings from laboratory precise system [31]

6.1 Problem formulation using COMSOL

All antenna geometries shown in Figure 6.1 are symmetric and so can be analyzed using the half-geometry as shown in Figure 6.3. The antennas are again radiated into the free space and saline solution media. A perfectly conducting sheet is placed at the plane of symmetry in the simulations. A spherical PML is used when radiating into the free space medium and a Cartesian PML along with the scattering boundary condition is used with the saline solution medium for truncating the computational domain.

The Cartesian PML is used with the saline medium, since the wavelength will be very small in this region (down to 3 cm at 900 MHz), which makes the required mesh elements very small and leads to large number of mesh elements. Figure 6.3 shows that a spherical PML leads to large, empty areas that must be meshed. At one particular direction, the PML is very far from the structure. Hence, the Cartesian PML is appropriate for using with the saline medium, as shown in Figure 6.5. The current probe (or line feed) excitation technique is used to excite the antenna structure. Tables 6.3 and 6.4 shows the PML and mesh settings for all antenna geometries when radiating into both the free space and saline media. In Table 7.3, λ_{S_f} and λ_{L_f} are the wavelengths in free space corresponding to frequencies of 7.5 GHz and 0.8 GHz, respectively. In Table 7.4, λ_{S_S} and λ_{L_S} are the wavelengths in the saline medium at 7.5 GHz and 0.8 GHz, respectively. Figure 6.7 shows the COMSOL mesh structure of antenna radiating in to the free space and saline media.

Figure 6.4 and 6.6 shows the mesh of only the antenna structure for the free space and saline media, respectively. A large coarser mesh has been used on the antenna surface in the saline medium compared to one in free space. The cell size in free space is set at 0.0175 λ_{S_f}, 0.0075 λ_{S_f}, 0.00625 λ_{S_f} and 0.0045 λ_{S_f} for antenna A, B, C and D, respectively, where λ_{S_f} is the wavelengths in the free space at 7.5 GHz. Using that would require too much memory in the saline medium. So, the cell size in saline is set at 0.2 λ_{S_S}, 0.1 λ_{S_S}, 0.12 λ_{S_S}, and 0.1 λ_{S_S} for antenna A, B, C and D, respectively, where λ_{S_S} is the wavelengths in the saline media at 7.5 GHz. This meets the maximum cell size recommended by COMSOL.

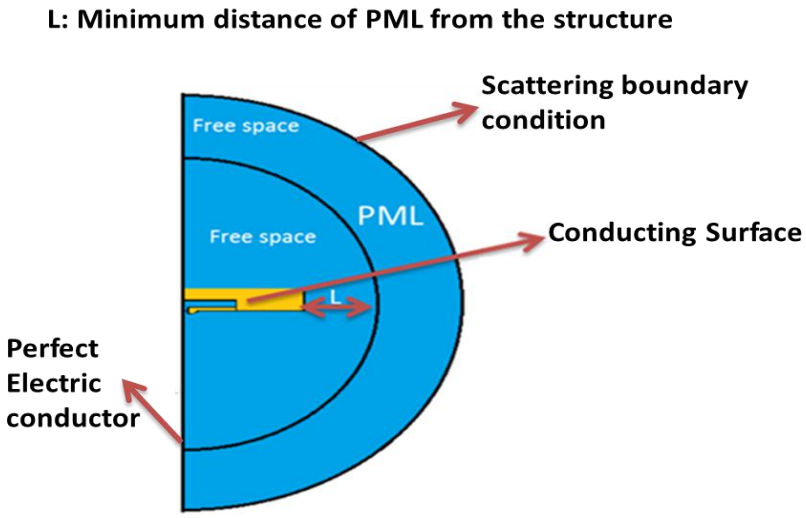

Figure 6.3 COMSOL sketch for problem formulation of antenna structure radiating in free space

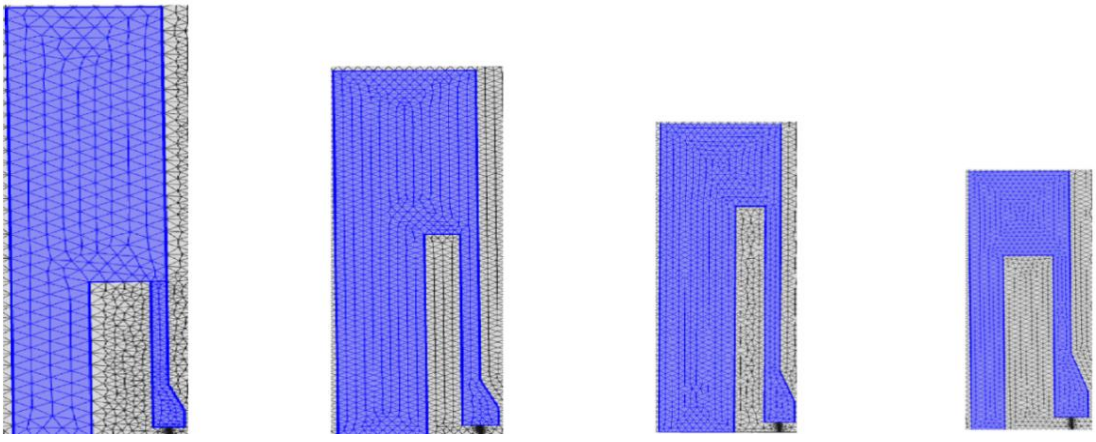

(a) (b) (c) (d)

Figure 6.4:COMSOL mesh structure for antenna geometries in free space medium for antenna geometries (a) Antenna A (b) Antenna B (c) Antenna C (d) Antenna D

Antenna	Antenna A	Antenna B	Antenna C	Antenna D
Maximum mesh size in free space	1 cm ($0.166\ \lambda_{S\_f}$)	0.7 cm ($0.175\ \lambda_{S\_f}$)	0.7 Cm ($0.175\ \lambda_{S\_f}$)	0.7 cm ($0.175\ \lambda_{S\_f}$)
Maximum mesh size on antenna structure	0.7 mm ($0.0175\ \lambda_{S\_f}$)	0.3 mm ($0.0075\ \lambda_{S\_f}$)	0.25 mm ($0.00625\ \lambda_{S\_f}$)	0.18 mm ($0.0045\ \lambda_{S\_f}$)
PML type	Spherical	Spherical	Spherical	Spherical
Order of PML	2	2	2	1
PML thickness	1 cm ($0.026\ \lambda_{L\_f}$)	0.5 cm ($0.013\ \lambda_{L\_f}$)	0.5 cm ($0.013\ \lambda_{L\_f}$)	0.5 cm ($0.013\ \lambda_{L\_f}$)
Minimum distance of PML from the antenna	3.5 cm ($0.093\ \lambda_{L\_f}$)	2.5 cm ($0.066\ \lambda_{L\_f}$)	2 cm ($0.0533\ \lambda_{L\_f}$)	2.5 cm ($0.066\ \lambda_{L\_f}$)
Total mesh elements in computational domain	46599	60127	54963	58626

Table 6.3: PML and mesh settings for antenna structure radiating in free space for COMSOL

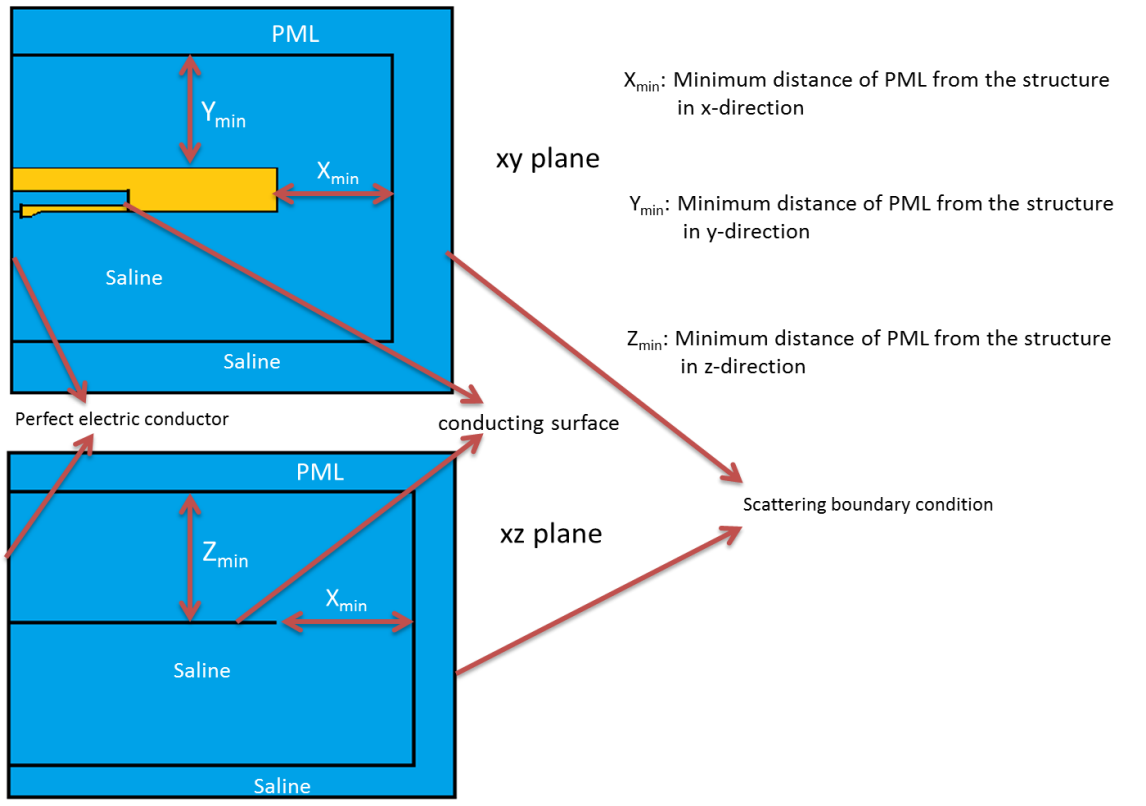

Figure 6.5 COMSOL sketch for problem formulation of antenna structure radiating in bulk saline solution medium

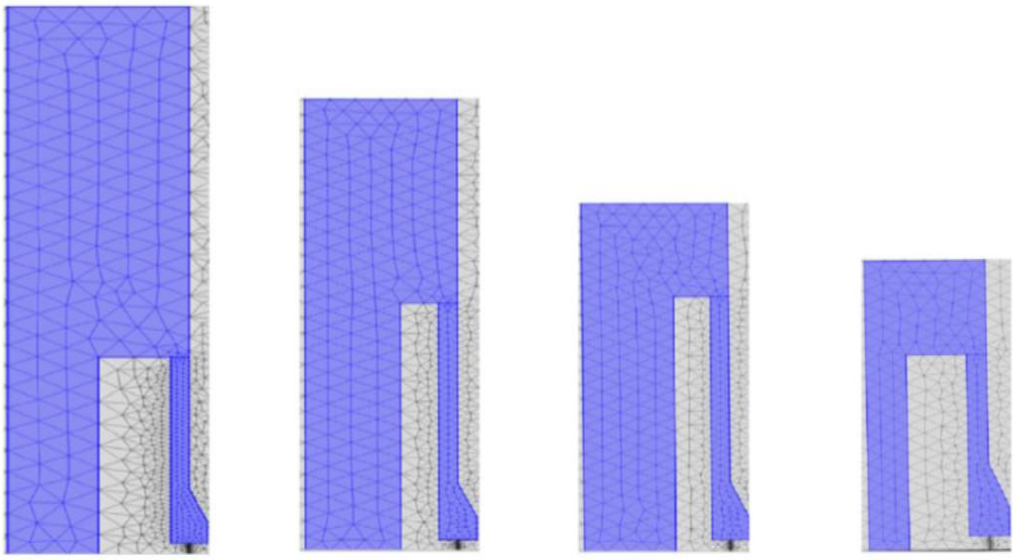

(a) (b) (c) (d)

Figure 6.6: COMSOL mesh structure of antenna geometries in saline medium for antenna geometries (a) Antenna A (b) Antenna B (c) Antenna C (d) Antenna D

	Antenna A	Antenna B	Antenna C	Antenna D
Maximum mesh size in saline	1 mm ($0.2\ \lambda_{S\_S}$)	0.98 mm ($0.199\ \lambda_{S\_S}$)	0.9 mm ($0.183\ \lambda_{S\_S}$)	0.9 mm ($0.183\ \lambda_{S\_S}$)
PML type	Cartesian	Cartesian	Cartesian	Cartesian
Order of PML	2	2	2	2
PML thickness	1 mm ($0.0234\lambda_{L\_S}$)	1 mm ($0.0234\lambda_{L\_S}$)	1 mm ($0.0234\lambda_{L\_S}$)	1 mm ($0.0234\ \lambda_{L\_S}$)
Maximum mesh size on antenna structure.	1 mm ($0.2\lambda_{S\_S}$)	0.5 mm ($0.1\lambda_{S\_S}$)	0.6 mm ($0.12\lambda_{S\_S}$)	0.5 mm ($0.1\lambda_{S\_S}$)
Minimum distance of PML from the radiating structure in x direction	4 mm ($0.0936\lambda_{L\_S}$)	4 mm ($0.0936\lambda_{L\_S}$)	4 mm ($0.0936\lambda_{L\_S}$)	6.5 mm ($0.152\lambda_{L\_S}$)
Minimum distance of PML from the radiating structure in y direction	3.5 mm ($0.082\lambda_{L\_S}$)	4 mm ($0.0936\lambda_{L\_S}$)	4 mm ($0.0936\lambda_{L\_S}$)	4.5 mm ($0.105\lambda_{L\_S}$)
Minimum distance of PML from the radiating structure in z direction	4 mm ($0.0936\lambda_{L\_S}$)	4 mm ($0.0936\lambda_{L\_S}$)	4 mm ($0.0936\lambda_{L\_S}$)	4 mm ($0.0936\lambda_{L\_S}$)
Total mesh elements in computational domain	78446	65063	64613	56421

Table 6.4: PML and mesh settings for antenna structure radiating in saline solution medium for COMSOL

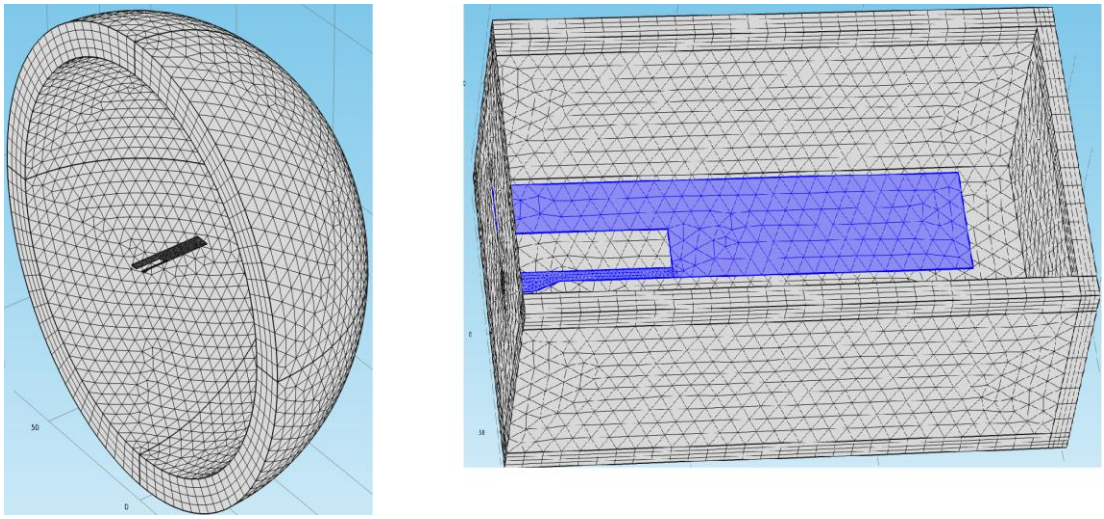

Figure 6.7 COMSOL mesh structure in (a) free space and (b) saline soultion medium

6.2 Problem formulation using FEKO:

The four test antennas were also modeled using FEKO. As with the COMSOL simulation, only half the structure is directly modeled with a perfect electric conducting (PEC) boundary condition used to represent the plane of symmetry. The antenna structure is excited by a wire port whose details are shown in Table 4.8. The input impedance obtained with this simulation again must be multiplied by two to get the actual input impedance. The antenna structures were analysed when surrounded by both the free space and saline solution media. Figure 6.8 shows the mesh generated for all geometries. The surface of the antennas are discritized into triangular patches. Table 6.5 shows the meshing parameters used in FEKO for the two different radiating media.

Antenna	A	B	C	D
Triangle edge length	0.35 mm	0.35 mm	0.25 mm	0.2 mm
wire segment length	0.01 mm	0.01 mm	0.01 mm	0.01 mm
wire radius	100 nm	100 nm	100 nm	100 nm
Number of segments in wire	57	57	57	57
Number of triangle elements	2697	1782	2452	1654

Table 6.5: Mesh settings in FEKO for antenna radiating in free space medium and saline medium

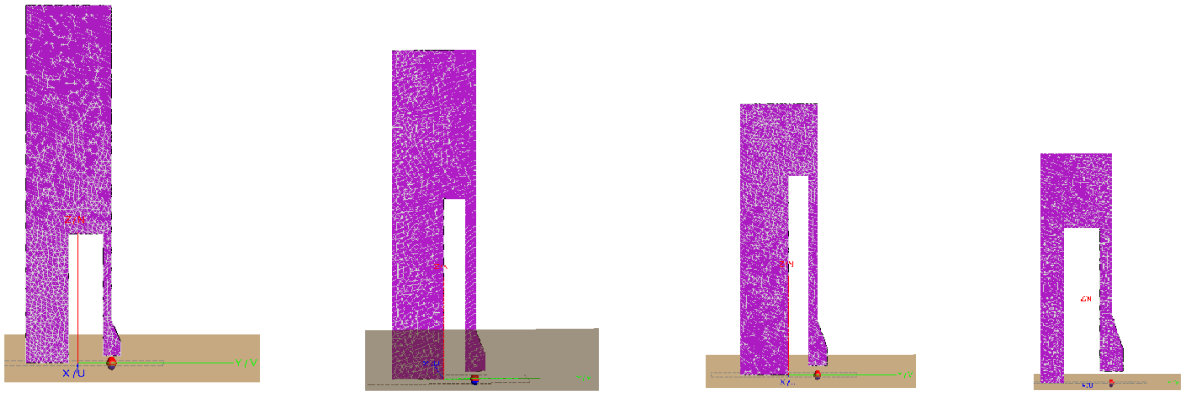

(a) (b) (c) (d)

Figure 6.8: Mesh structure in antenna for FEKO software tool (a) Antenna A (b) Antenna B (c) Antenna C (d) Antenna D

6.3 Formulation for computitng antenna radiation efficiency:

The radiation efficiency of the antenna structures when radiating into the saline medium has been found using both COMSOL and FEKO. FEKO computes the radiation efficiency directly, whereas COMSOL gives the surface integral of current density on the antenna surface directly. Using the computed surface integral of current density, total power dissipated by the antenna structure can be computed as [17]

$$P_{loss} = \frac{R_s}{2} \oint\oint |Js|^2 \, ds \ , \tag{6.4}$$

where R_s is the surface impedance [8], [17] and Js is the current density on the antenna surface. Loss resistance of antenna can be determined from power dissipated by the antenna using the relation

$$P_{loss} = \frac{1}{2} |I|^2 R_{loss} \ , \tag{6.5}$$

where R_{loss} is the loss resistance of antenna and I is the known current.

The radiation efficiency of the antenna can be computed using [15]

$$\epsilon = \frac{R_{in} - R_{loss}}{R_{in}} \ , \tag{6.6}$$

where R_{in} is the input resistance of the antenna.

6.4 Discussion of results:

Figures 6.9 through 6.16 show the input impedances of the four test antennas computed by COMSOL and FEKO. Impedances from COMSOL and FEKO are in good agreement in free space. For the saline medium, good agreement is achieved up to about 2 GHz, beyond which both the input resistance and reactance begin to diverge. When radiating in free space, the primary anti-resonant frequencies occur at around 5.7 GHz, 5.6 GHz, 6 GHz and 4.7 GHz for antennas A, B, C and D, respectively. There are secondary resonant frequencies at 2.4 GHz, 2.9 GHz and 3.8 GHz for antenna A, B and C respetively. Antenna D is randomly selected for additional analysis in the saline medium. The wavelength in saline media reduced to one-eighth times the wavelength in free space, this results in required cell size too small at higher frequencies and the computational limitations do not allow a sufficiently small cell size to be used. Therefore, the frequency range from 0.8 GHz to 2 GHz is considered for the computation of antenna radiation efficiency. The input resistance, loss resistance, radiation resistance, and radiation efficiency of antenna D are given in Figures 6.17 through 6.20. The radiation efficiency of antenna D is computed just to ensure that the COMSOL results agree with the FEKO results. As shown in Figure 6.20, the COMSOL and the FEKO simulation results demonstrate good agreement, giving additional confidence in the COMSOL results when the proposed antenna including the acrylic and the substrate surrounded by a saline medium is modeled in Chapter 8.

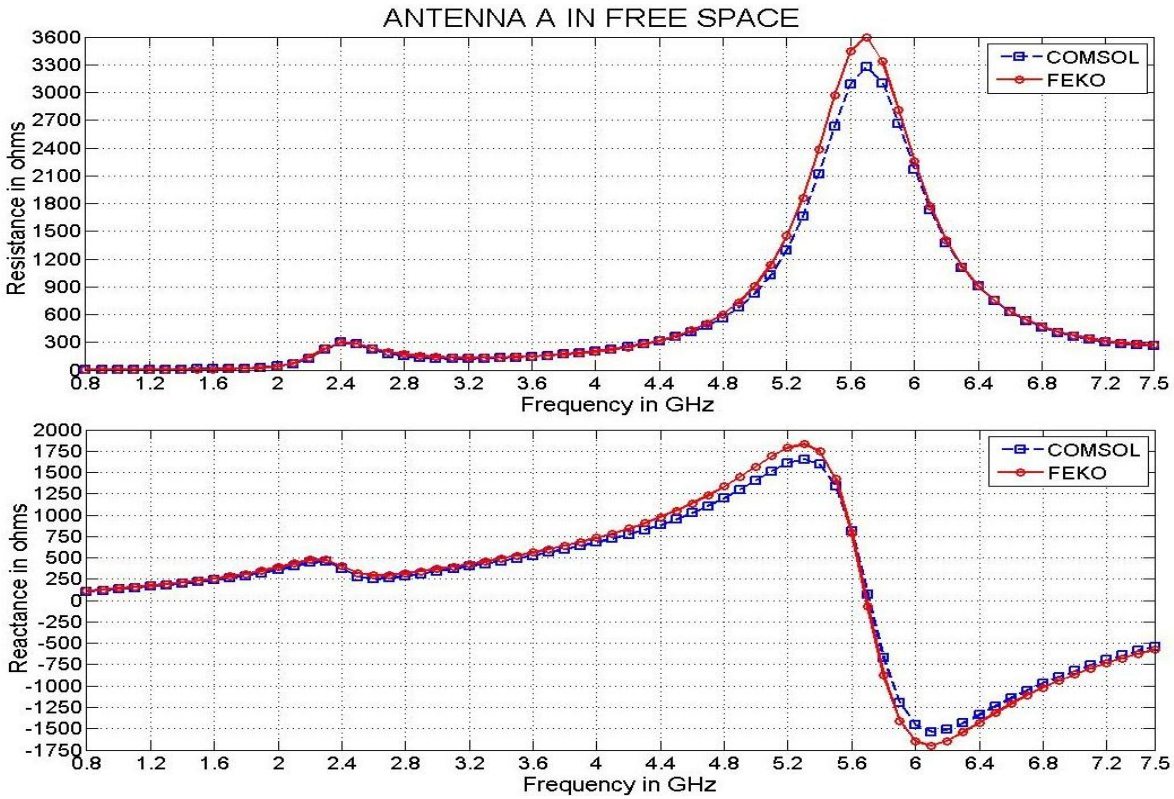

Figure 6.9: Input impedancce of antenna A radiating in free space

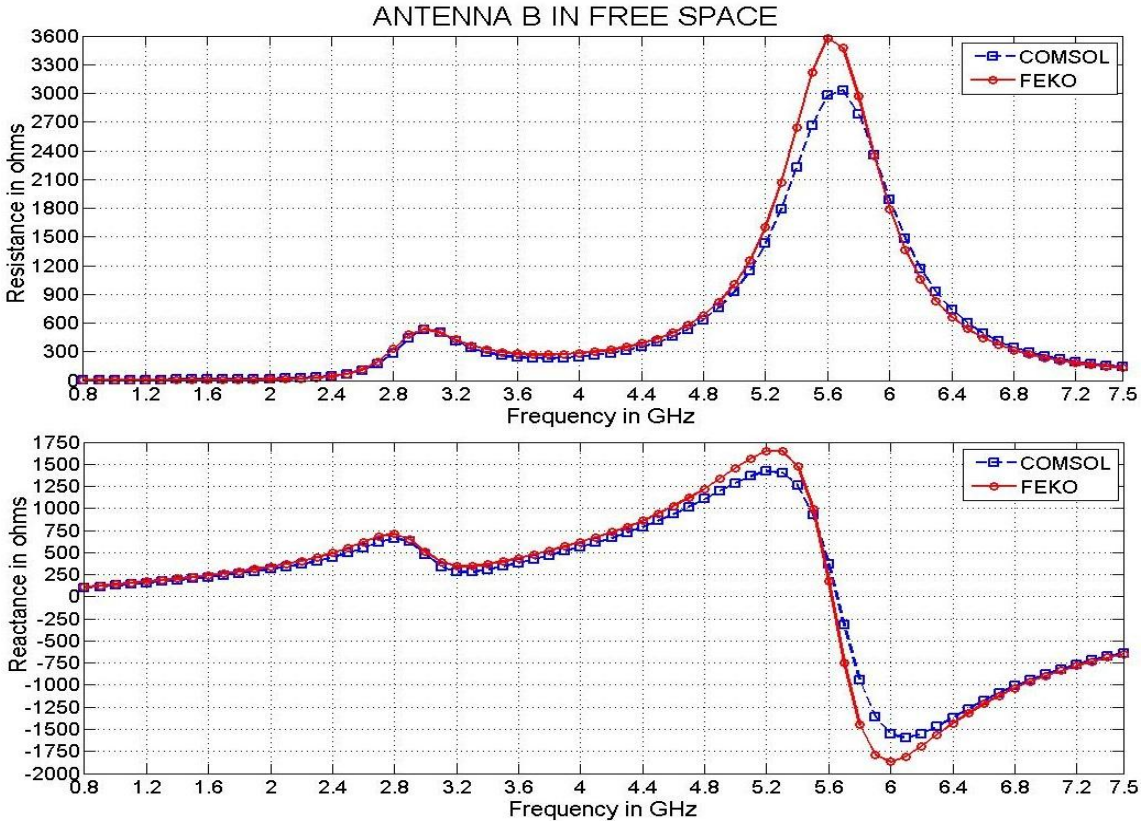

Figure 6.10: Input impedancce of antenna B radiating in free space

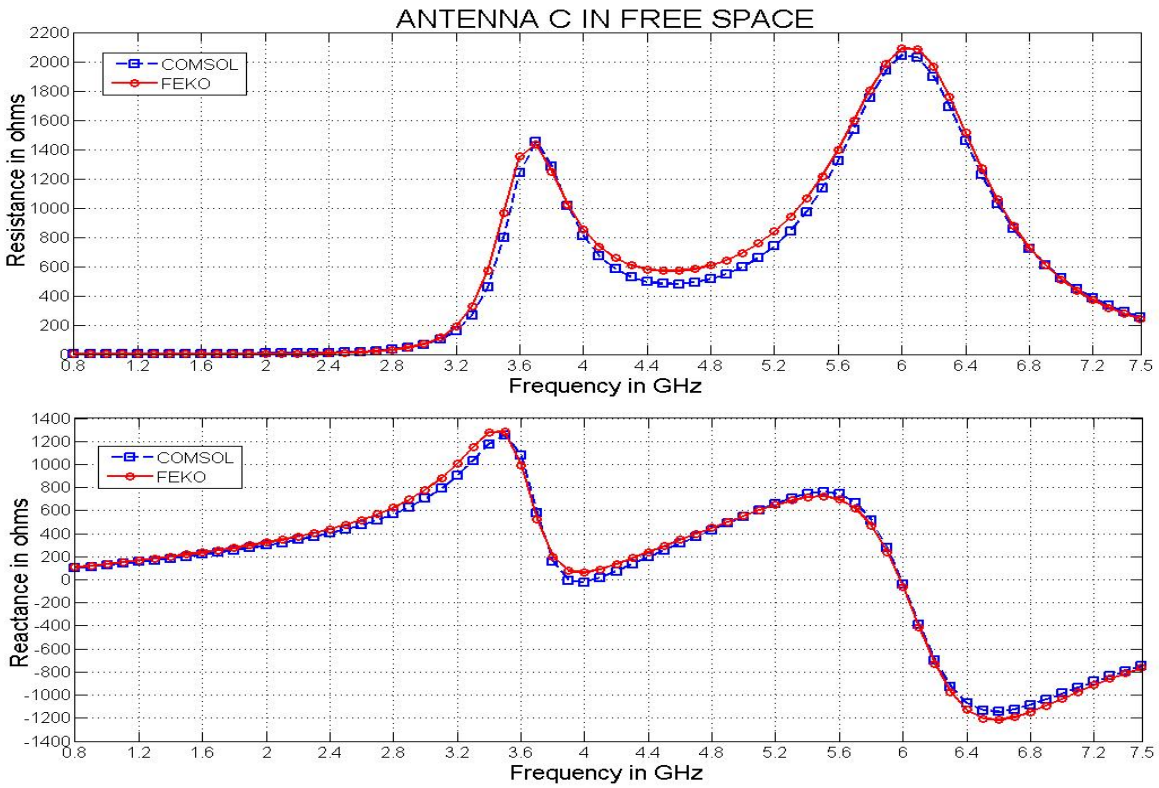

Figure 6.11: Input impedancce of antenna C radiating in free space

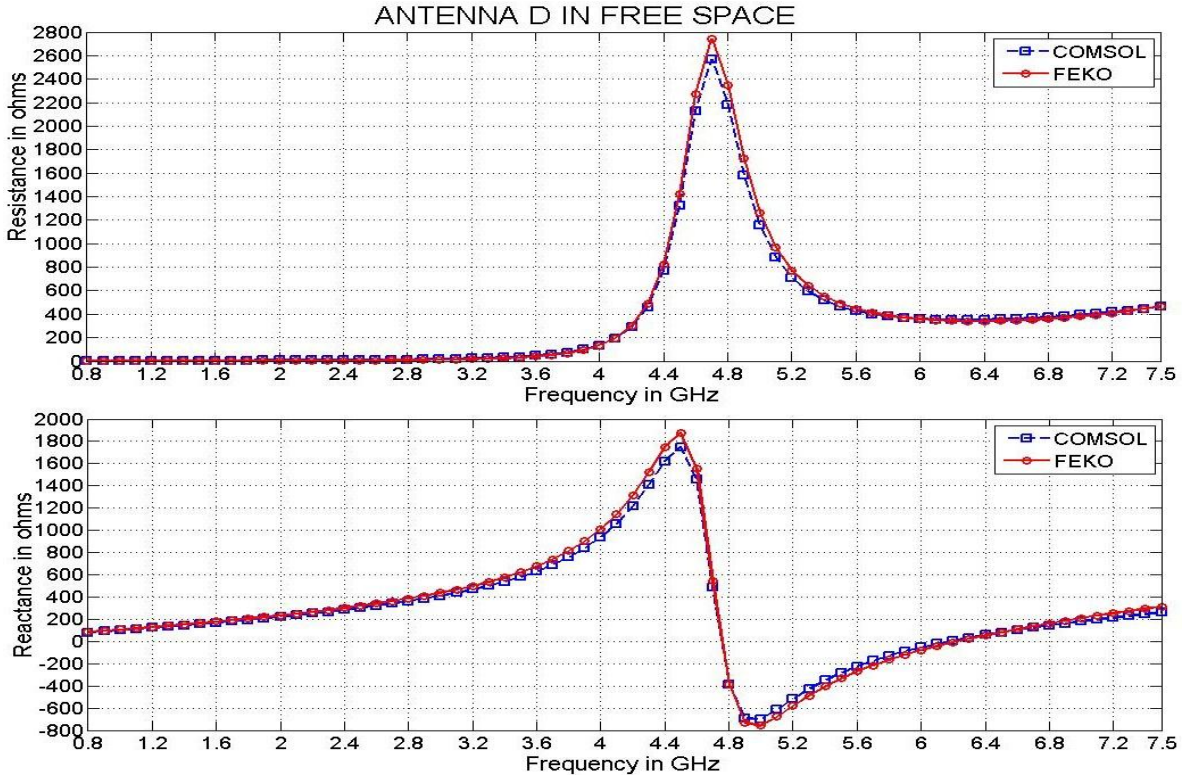

Figure 6.12: Input impedancce of antenna D radiating in free space

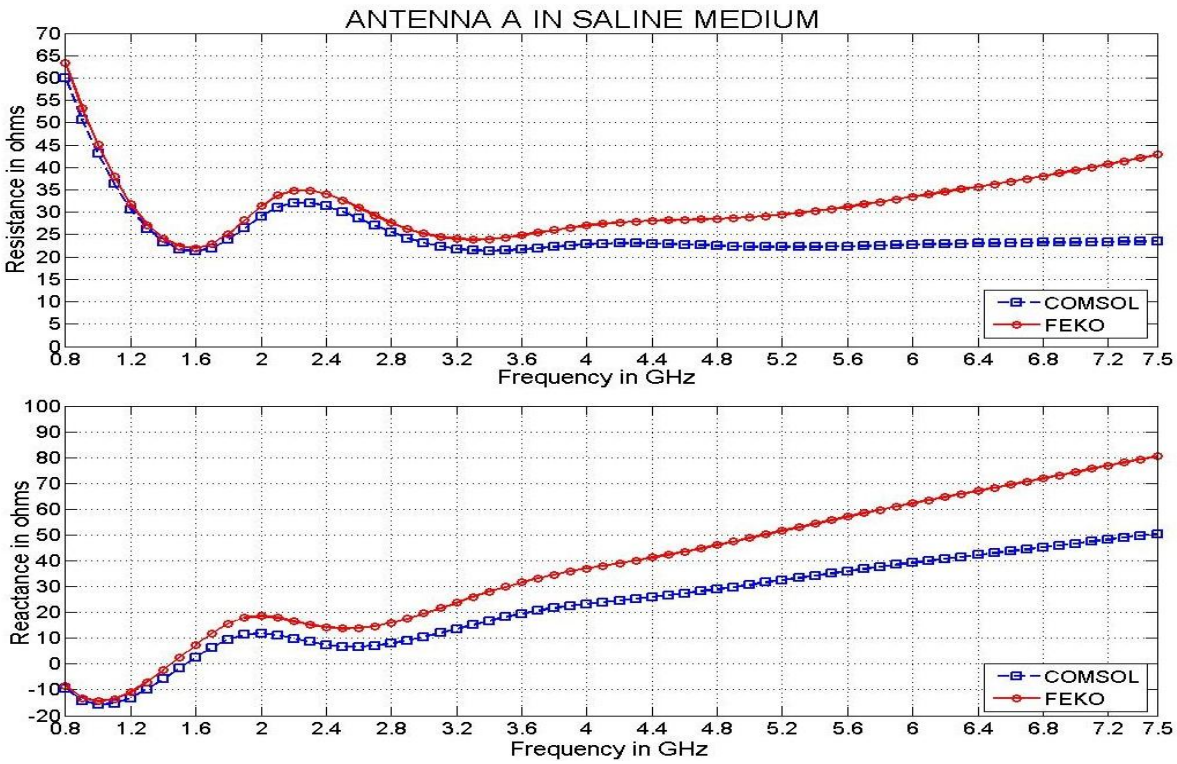

Figure 6.13: Input impedance of antenna A radiating in bulk saline medium

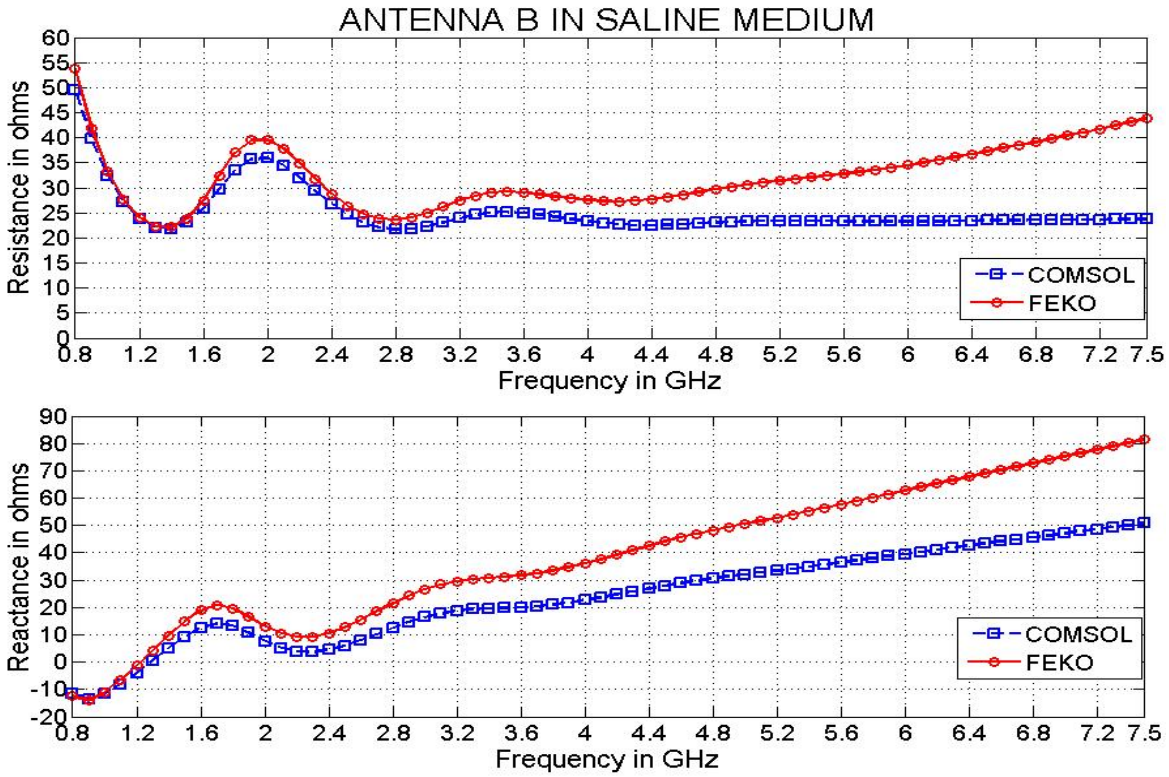

Figure 6.14: Input impedancce of antenna B radiating in bulk saline medium

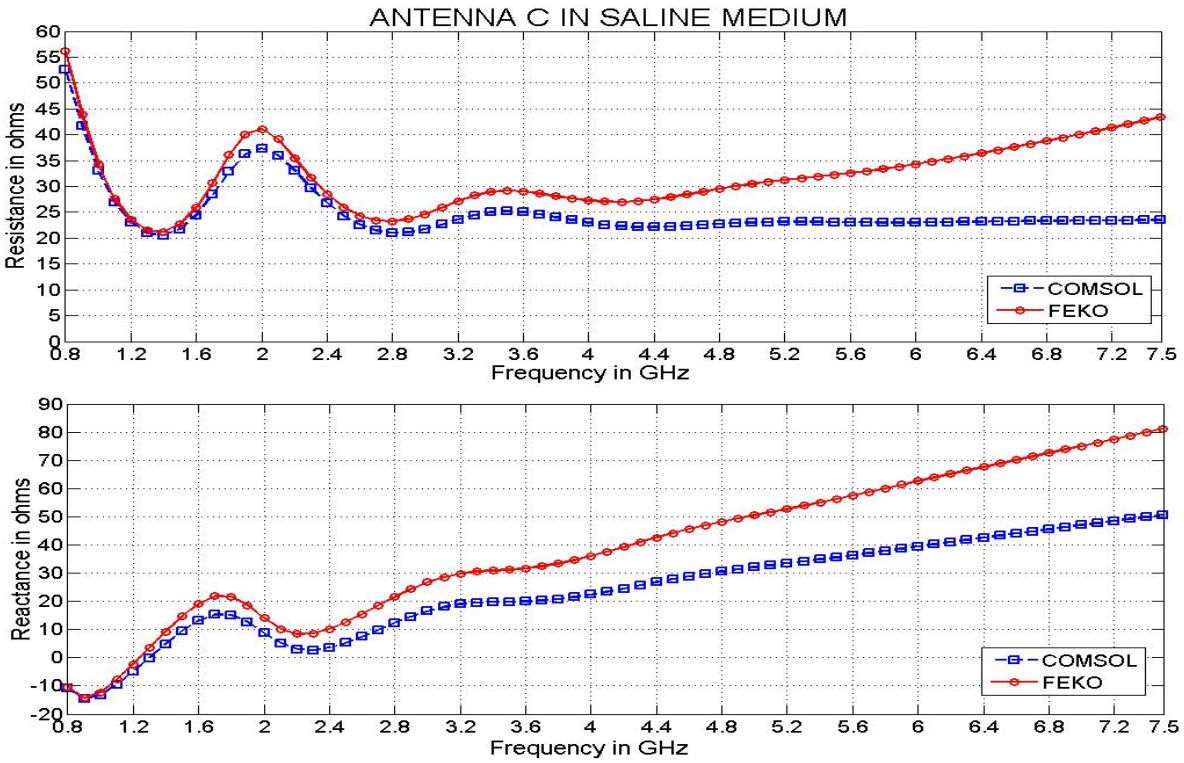

Figure 6.15: Input impedancce of antenna C radiating in bulk saline medium

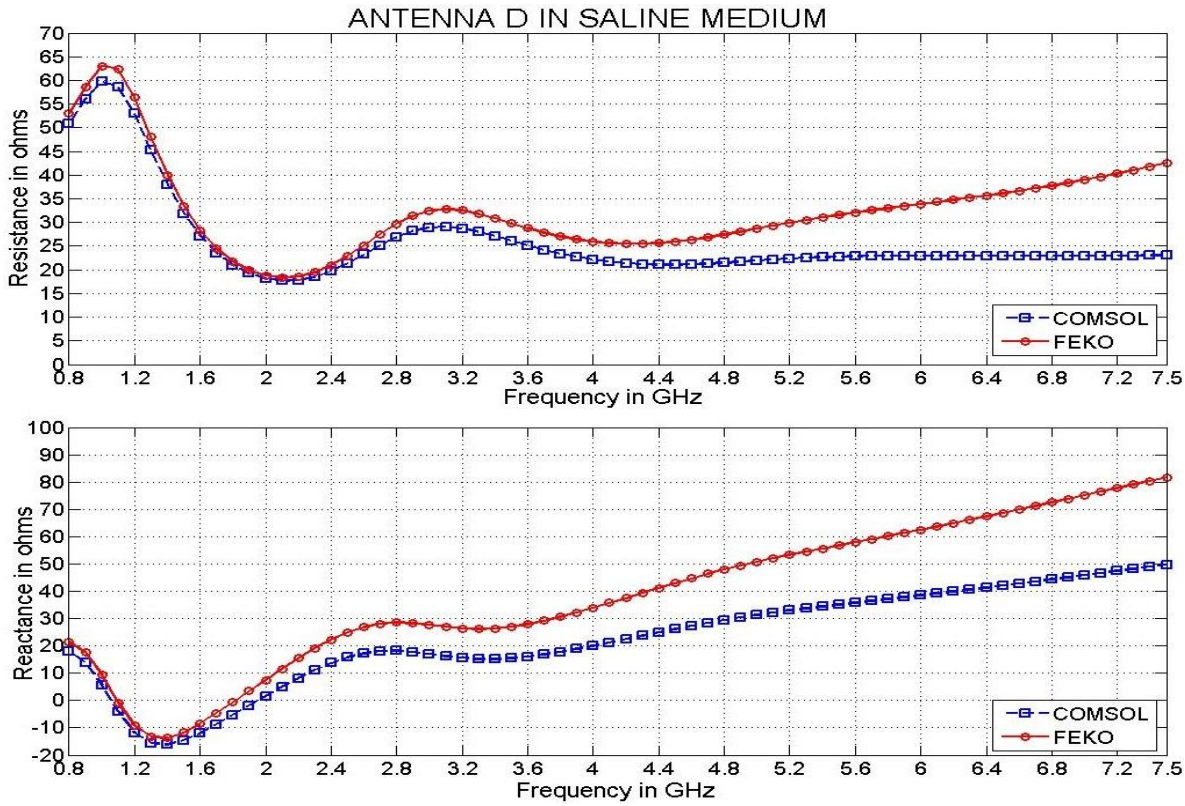

Figure 6.16: Input impedancce of antenna D radiating in bulk saline medium

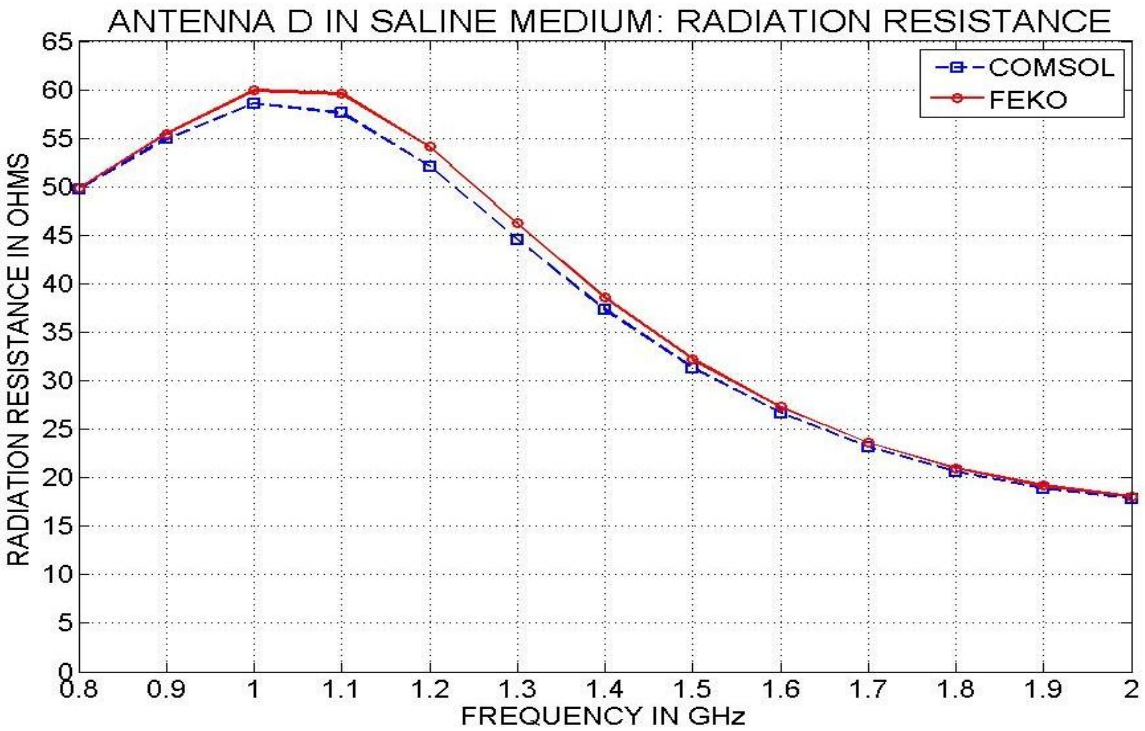

Figure 6.17: Radiation resistance of antenna D when radiating in saline medium

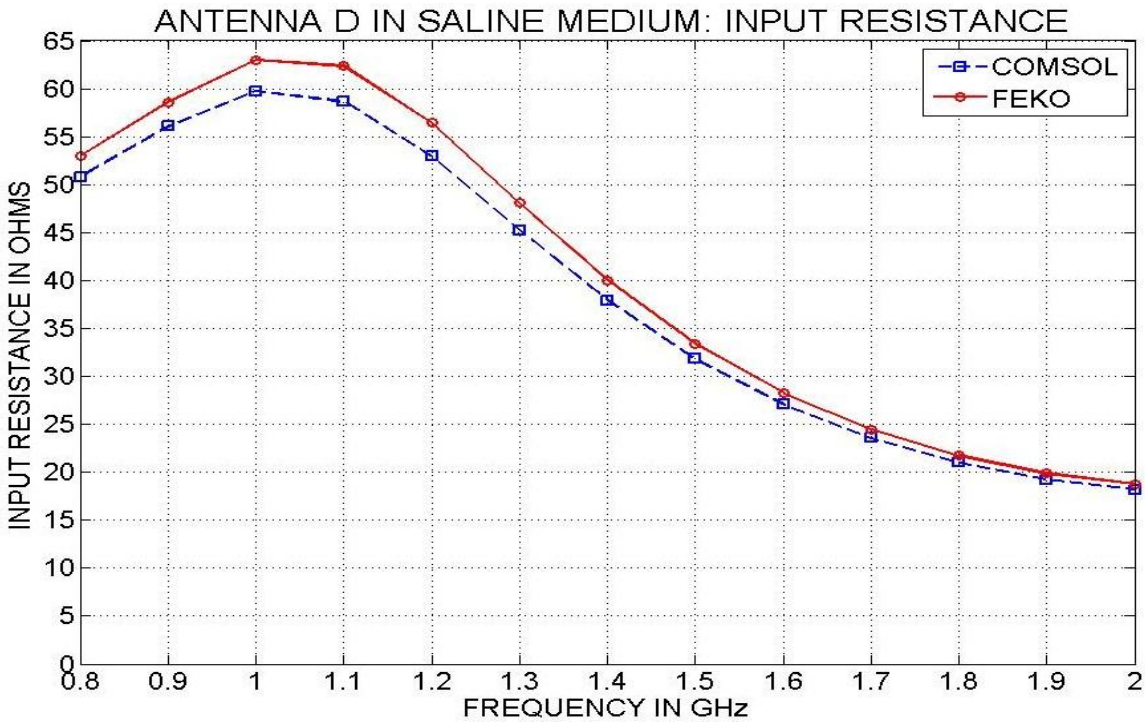

Figure 6.18: Input resistance of antenna D when radiating in saline medium

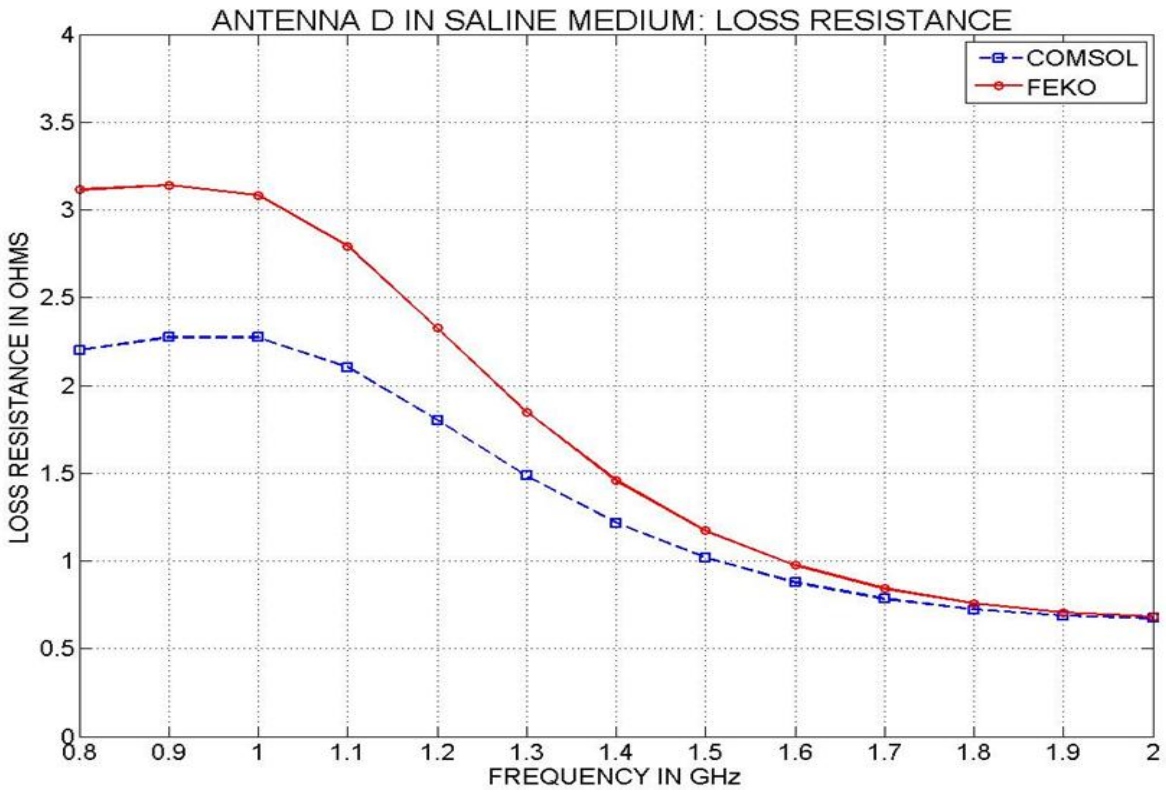

Figure 6.19: Ohmic loss resistance of antenna D when radiating in saline medium

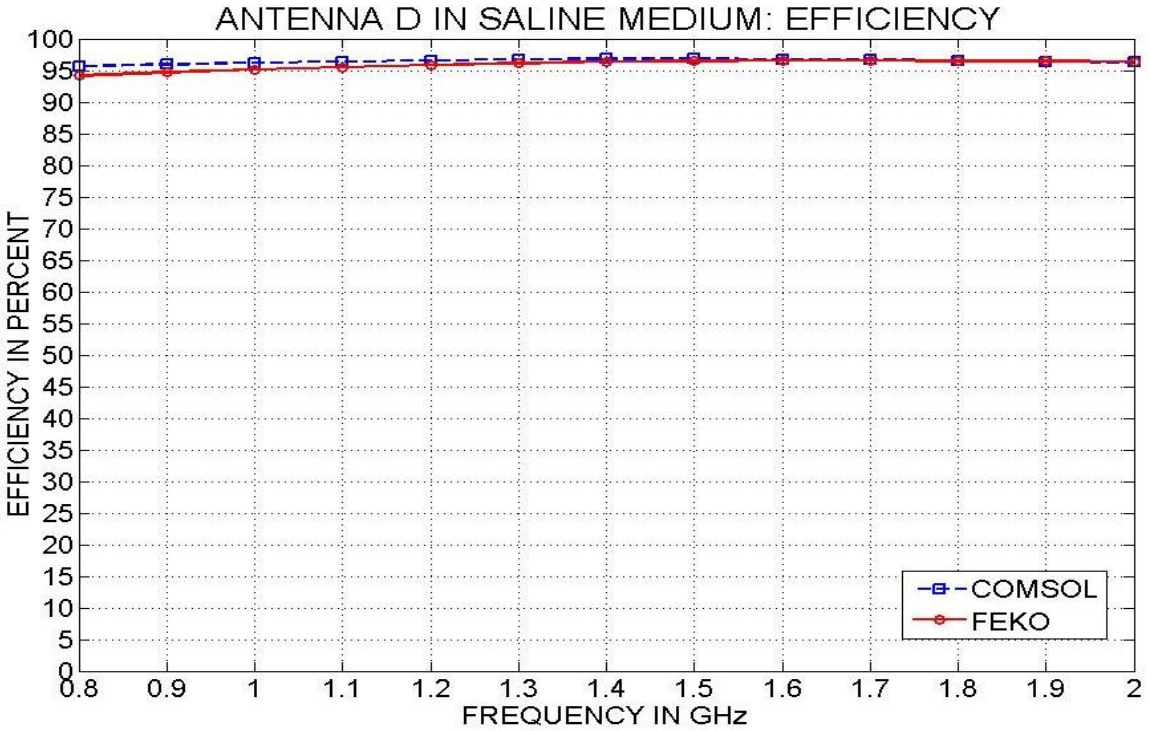

Figure 6.20: Radiation effiiciency of antenna D when radiating in saline medium

CHAPTER 7

VERIFICATION OF ANTENNA CONNECTED WITH FEED NETWORK

Thus far, all antennas considered have been analysed when radiating into a homogeneous medium so that FEKO may be used to verify the model in formulated COMSOL. Now an antenna that includes a dielectric substrate and an acrylic coating, as shown in Figure 7.1, is considered. FEKO cannot be used in this case since the radiating medium is inhomogeneous [8]. In this chapter, COMSOL is used to compute the input impedance of the full antenna structure including the dielectric substrate and acrylic coating. As before, both the free space and saline solution with a 1% salt concentration are considered as the surrounding media. The measurement of the same antenna structure including dielectric substrate and acrylic were performed in free space by the Mixed Signal VLSI Design Group at Oklahoma State University. They also performed the measurement when the full antenna including dielectric substrate and acrylic was sandwiched between two saline bags as shown in Figure 7.2. The saline bags were each of thickness 1.5 cm with 0.9% salt concentration. The simulation results obtained using COMSOL are compared with measured results under both free space and saline media.

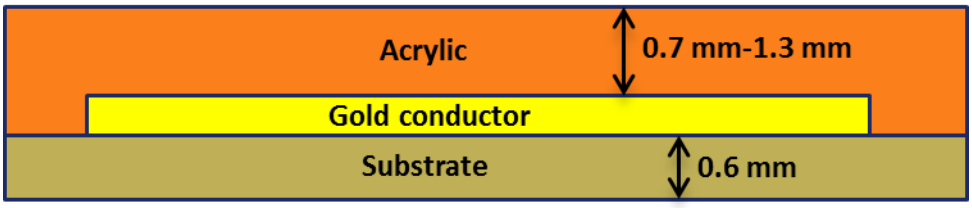

Figure 7.1: Antenna structure including substrate and acrylic

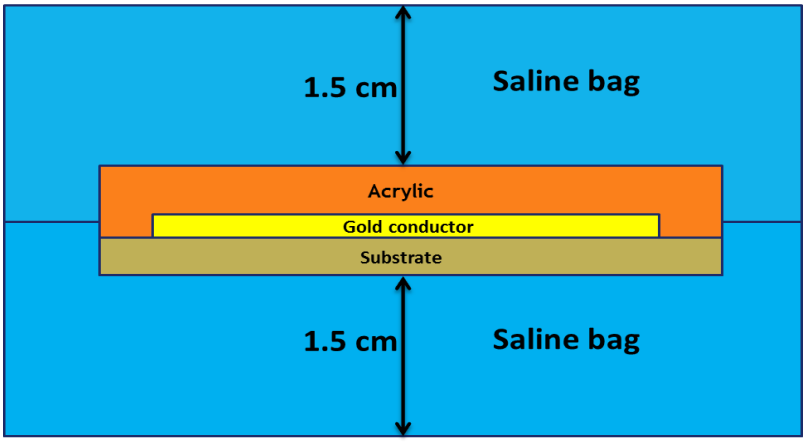

Figure 7.2: antenna printed on substrate with acrylic coating sandwitch between two saline bags done by Mixed signal VLSI group, Oklahoma state university.

7.1 Description of antenna structure and feed network

The antenna structure which includes a dielectric substrate and acrylic coating (shown in figure 7.1) were built at the University of Texas at Dallas. The antenna geometry and its metal thickness are shown in Figure 6.1 and Table 6.1, recspectively. The acrylic thickness varies from 0.7 mm to 1.3 mm and the substrate thickness is 0.6 mm. The Mixed Signal VLSI Design Group connected a feed network to the antenna as shown in Figure 7.3. The feed network was needed for the measurement with a vector network analyzer. The measurement was taken at the feed input as shown in Figure 7.3. (In actual use, the antenna will be excited directly by the RFID tag chip.) It is a "Bazooka" balun feed [15] which consists of a semi-rigid coaxial cable surrounded by a metal sleeve, shown in Figure 7.4. Also visible is the SMA feed connector.

Figure 7.3: Antenna C including dielectric substrate and acrylic connected to the feed network

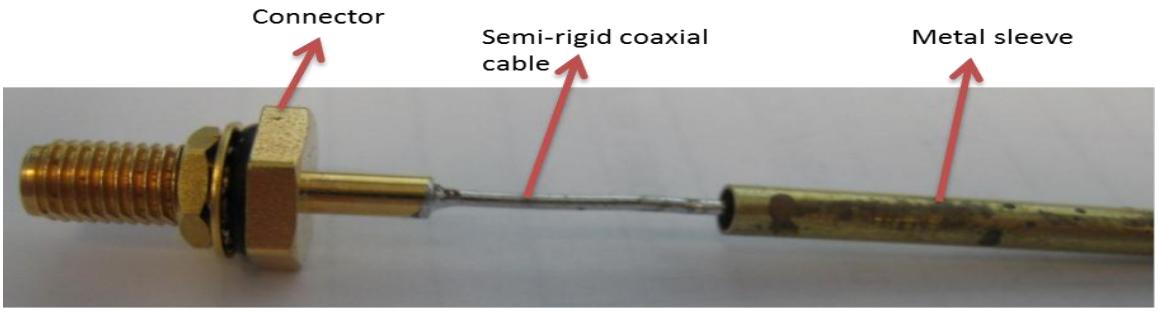

Figure 7.4: Structure of Bazooka balun feed

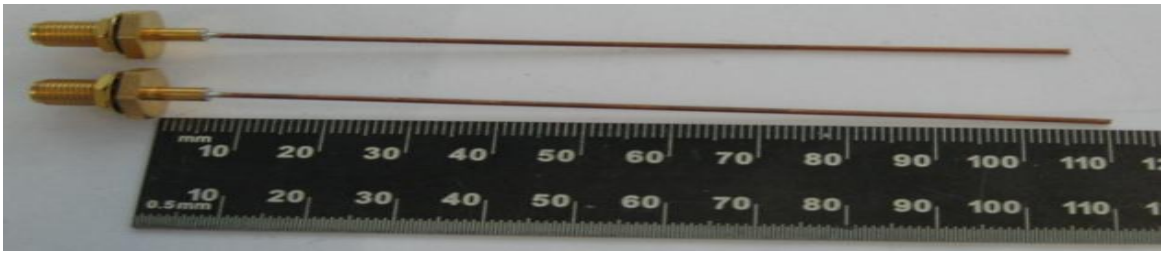
Figure 7.5: Semi-rigid coaxial cable dimension

The semirigid coaxial cable is 11 cm in length and the metal sleeve is 8 cm long, which is approximately a quarter wavelength in free space at 900 MHz. The total length of the balun is 12.1 cm, including the connector. When the coaxial cable is directly connected to an antenna, there is a net current flowing on outside conductor of the coaxial cable to the ground [15]. This leads to an unequal current on the two arms of antenna, resulting in an unbalanced system. So, the bazooka balun is used to balance the unbalanced coaxial cable. In a bazooka balun, the outer conductor of the coaxial cable is shorted with the metal sleeve at one end as shown in Figure 7.3. The metal sleeve must be a quarter-wavelength in length. This makes the input impedance at the open end of this short circuit transmission line very large or infinite, thus choking the return current flowing to the ground.

The transmission line used was made by Jyebao [45], part number .047AG-W-P-50 [33]. The manufacturer's specifications for this cable give an inner radius of 0.29 mm and an outer radius of 1.14 mm. The outer radius was physically measured to be 1.18 mm, which is in good

agreement with the specifications. The coaxial line is filled with polytetraflouro ethylene (PTFE), which has a dielectric constant of 2.1 [34]. The specified attenuation constant of the cable is shown in Table 7.1. A spline interpolation of these values gives an attenuation constant of 0.12 np/m at 900 MHz.

Frequency	Attenuation constant in dB/100 m	Attenuation constant in neper/m
0.5 GHz	78.7	0.0906
1 GHz	112.2	0.1291
5 GHz	285.5	0.3287
10 GHz	373.3	0.43
20 GHz	544.2	0.6265

Table 7.1: Attenuation constant for RF semirigid coaxial cable with part number .047AG-W-P-50 from [33]

7.2 Transmission line representation of balun:

Figure 7.6 shows the transmission line representation of the balun connected to the antenna. The antenna appears as the load impedance Z_A. The transmission line is filled with PTFE. The input impedance at the feed network input terminated with the antenna is [17]

$$Z_{in} = Z_0 \frac{Z_A + Z_0 \tanh(\gamma l)}{Z_0 + Z_A \tanh(\gamma l)}, \quad (7.1)$$

where Z_A is the input impedance of the antenna structure, Z_{in} is the input impedance at the feed network input, Z_0 is the characteristics impedance of the balun feed transmission line (50Ω), l is the length of transmission line and γ is the propagation constant of coaxial cable in the balun transmission line.

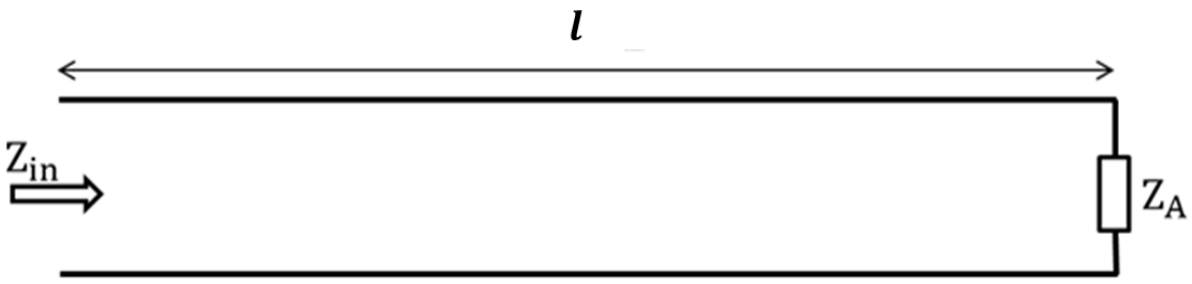

Figure 7.6: Transmission line representation of balun feed

The transmission line propagation constant can be expressed in terms of the attenuation constant and the phase constant as

$$\gamma = \alpha + j\beta \,, \tag{7.2}$$

where α is the attenuation constant in np/m and β is the phase constant in rad/m.

The propagation constant can also be found from the complex permittivity of the dielectric material. For a non-magnetic medium [32],

$$\gamma = j\frac{\omega}{c}\sqrt{\varepsilon_r' + \frac{\sigma}{j\omega\varepsilon_0}} = j\frac{\omega}{c}\sqrt{\varepsilon_r'}\sqrt{1 - j\frac{\varepsilon_r''}{\varepsilon_r'}}\,, \tag{7.3}$$

where σ is the effective electrical conductivity of the dielectric material, ε_0 is the permittivity of free space, and $\varepsilon_r'' = \frac{\sigma}{\omega\varepsilon_0}$ is the imaginary component of the complex relative permittivity.

The phase constant can be expressed for a low loss media ($\varepsilon_r' \gg \varepsilon_r''$) as

$$\beta = \frac{\omega}{c}\sqrt{\varepsilon_r'}\ , \tag{7.4}$$

where ω is the angular frequency, c is speed of light in vacuum, and ε_r' is the dielectric constant of the PTFE in semirigid coaxial cable. The dielectric loss tangent is

$$\tan(\delta) = \frac{\varepsilon_r''}{\varepsilon_r'}\,, \tag{7.5}$$

$\tan(\delta) \ll 1$ for low loss media.

Substituting β and tan(δ) into equation (7.3), gives

$$\gamma = j\beta\sqrt{1 - j\tan(\delta)}\ , \tag{7.6}$$

Using a first order Taylor series expansion, (7.6) is approximated as

$$\gamma = j\beta\left(1 - j\frac{\tan(\delta)}{2}\right) = \beta\frac{\tan(\delta)}{2} + j\beta \ , \tag{7.7}$$

Comparing equation (7.2) and (7.7), the dielectric loss tangent can be expressed as

$$\tan(\delta) = \frac{2\alpha}{\beta} = \frac{2\alpha}{\frac{\omega}{c}\sqrt{\varepsilon_r{}'}} \ , \tag{7.8}$$

7.3 Verification of feed network:

Figure 7.8 and 7.10 shows the measured input impedance of the feed network terminated with an open circuit and a short circuit, respectively. The length of the transmission line can be computed from the measured input impedances and compared with the length measured.

7.3.1 Open circuit analysis

Figure 7.7 shows transmission line terminated with an open circuit. The input impedance of the feed network at a distance l from the open circuit load can be obtained by using $Z_A = \infty$ in (7.1). This give

$$Z_{in\_oc} = Z_0\coth(\gamma l) \text{ for a lossy transmission line and}$$

$$Z_{in\_oc} = j * Z_0\cot(\beta l) \text{ for a lossless transmission line,}$$

where Z_{in_oc} is the input impedance at feed input. The effective length of the transmission line can be found from:

$$l = \frac{1}{\gamma}\coth^{-1}\left(\frac{Z_{in\_oc}}{Z_0}\right). \tag{7.9}$$

Using the identity, $\coth^{-1}(x) = \frac{1}{2}\ln\left(\frac{x+1}{x-1}\right)$, (8.9) can be written as

$$l = \frac{1}{2\gamma}\ln\left(\frac{\frac{Z_{in\_oc}}{Z_0}+1}{\frac{Z_{in\_oc}}{Z_0}-1}\right) = \frac{1}{2\gamma}\ln\left(\frac{Z_{in\_oc}+Z_0}{Z_{in\_oc}-Z_0}\right). \tag{7.10}$$

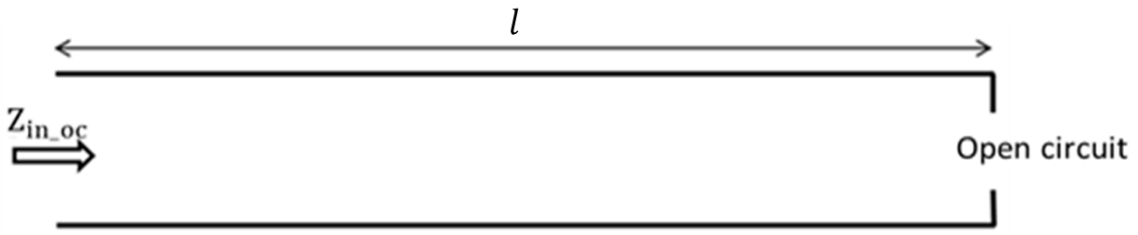

Figure 7.7: Transmission line representation of balun terminated with open circuit

Letting $Z_1 = \frac{Z_{in\_oc}+Z_0}{Z_{in\_oc}-Z_0} = |Z_1|e^{i\theta}e^{i2\pi k}$, where θ is phase angle of Z_1 and k is a non-negative integer, *l* can be written as

$$l = \frac{1}{2\gamma}[\ln|Z_1| + i(2\pi k + \theta)] \ , \tag{7.11}$$

Figure 7.8 shows the measured input impedance of the feed network terminated with an open circuit. The input impedance is very high over the frequency range 870 MHz to 930 MHz. The effective length of the transmission line computed from (7.11) over the frequency range of 870 MHz to 930 MHz was 11.4 cm for feed network 1 and 11.3 cm for feed network 2. The reactance in Figure 7.8 changes abruptly from 746 Ω at 902.5 MHz to -970 Ω at 917.5 MHz for feed network 1 and 729 Ω at 905 MHz to -1140 Ω at 920 MHz for feed network 2. This occurs with an open-circuited, lossless transmission line of a length that is a multiple of one-half wavelength [17]. The wavelength within the coaxial cable at 910 MHz is $\lambda = \frac{3\times10^8}{910\times10^6\times\sqrt{2.1}} = 22.75$ cm, where 2.1 is the dielectric constant of the semi-rigid coaxial cable dielectric. λ/2 therefore corresponds to 11.375 cm, which is in good agreement with the length obtained from (7.11).

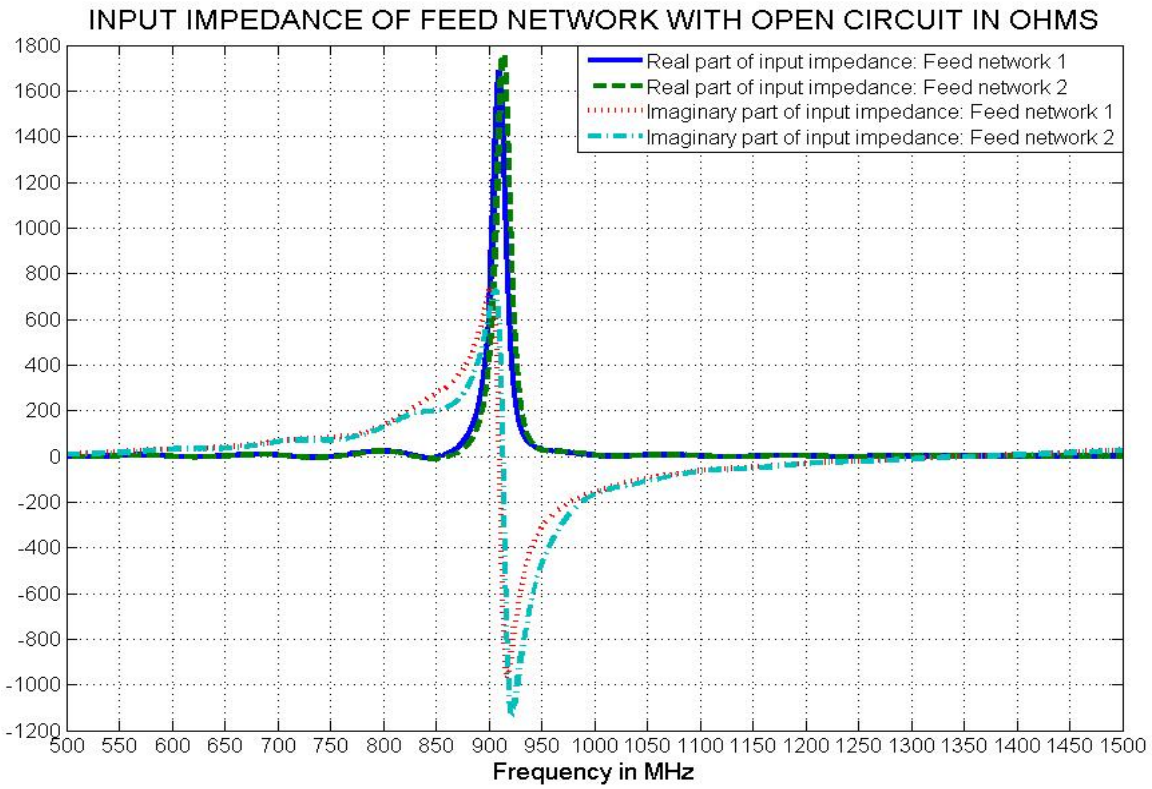

Figure 7.8: Input for two different feed network terminated with open circuit measured by Mixed Signal VLSI Design Group, Oklahoma State University

7.3.2 Short circuit analysis:

Figure 7.9 shows the transmission line terminated with a short circuit. The input impedane at the feed network input a distance l from the short circuit load can be obtained by using $Z_A = 0$ in equation (7.1). This leads to

$$Z_{in\_sc} = Z_0 \tanh(\gamma l) \text{ for lossy transmission line and}$$

$$Z_{in\_sc} = j * Z_0 \tan(\beta l) \text{ for lossless transmission line,}$$

where Z_{in_sc} is the input impedance of the feed network. The effective length of the transmission line can be found from

$$l = \frac{1}{\gamma} \tanh^{-1}\left(\frac{Z_{in\_sc}}{Z_0}\right), \tag{7.12}$$

Using the identity, $\tanh^{-1}(x) = \frac{1}{2}\ln\left(\frac{1+x}{1-x}\right)$, (8.12) can be written as

$$l = \frac{1}{2\gamma}\ln\left(\frac{1+\frac{Z_{in\_sc}}{Z_0}}{1-\frac{Z_{in\_sc}}{Z_0}}\right) = \frac{1}{2\gamma}\ln\left(\frac{Z_0+Z_{in\_sc}}{Z_0-Z_{in\_sc}}\right) \ , \tag{7.13}$$

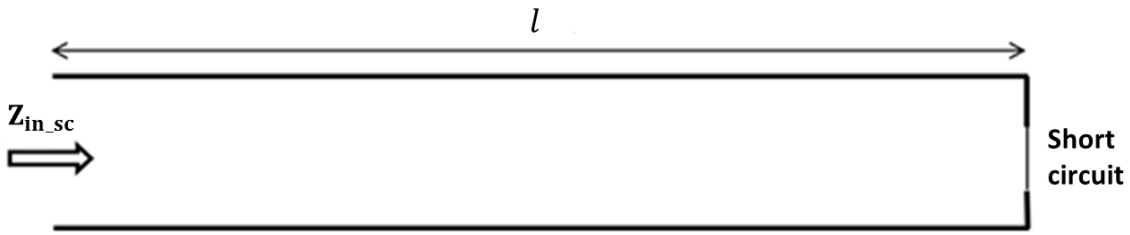

Figure 7.9: Transmission line representation of balun terminated with short circuit

Letting $Z_2 = \frac{Z_0+Z_{in\_sc}}{Z_0-Z_{in\_sc}} = |Z_2|e^{i\theta}e^{i2\pi k}$, where θ is phase angle of Z_2 and k is a non-negative integer, l can be expressed as

$$l = \frac{1}{2\gamma}[\ln|Z_2| + i(2\pi k + \theta)] \ , \tag{7.14}$$

Figure 7.10 shows the measured input impedance of the feed network terminated with a short circuit. The effective length of the transmission line computed from (7.14) over the frequency range of 870 MHz to 930 MHz was 12.43 cm. From Figure 7.10, the reactance is zero around 834 MHz. This behaviour is expected for a short-circuited lossless transmission line whose length is $0.25\lambda+n\frac{\lambda}{2}$ [17], where n is the non-zero integer. The wavelength within the coaxial cable at frequency 834 MHz is $\lambda = \frac{3\times10^8}{834\times10^6\times\sqrt{2.1}} = 24.8$ cm. λ/2 therefore corresponds to 12.4 cm, which is in good agreement with length obtained from (7.14).

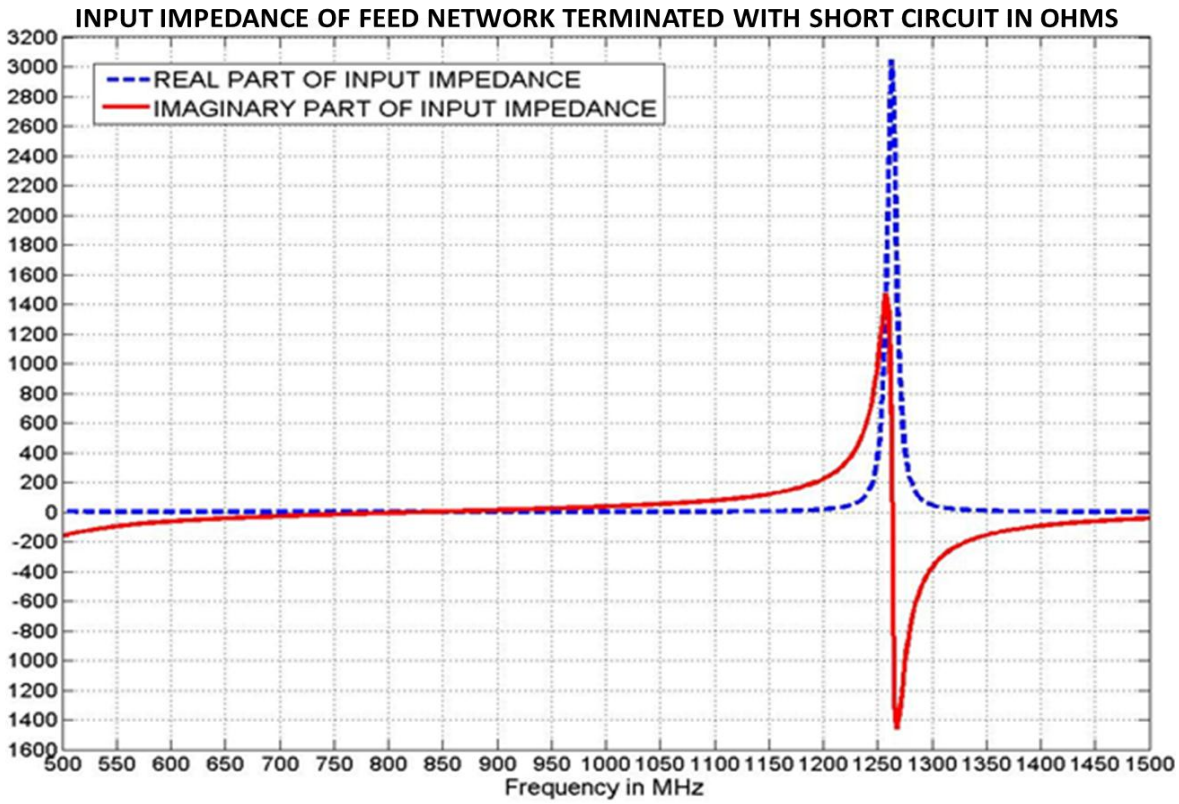

Figure 7.10 Input impedance of feed network terminated with short circuit measured by Mixed Signal VLSI Design Group, Oklahoma State University

The effective length of the transmission line terminated with both an open circuit and a short circuit have been computed. The effective length computed using the short cicuit analysis has better agreement with the measured length of 12.1 cm compared to the effective length found with the open circuit analysis. The short circuit analysis is used hereafter. Unintential radiation may occur from the wire tip in the open circuit case which can lead to errors.

7.4 Measurement of dielectric properties in Substrate:

Measurement of the dielectric constant and loss tangent of the substrate material used in the antenna was performed by the Mixed Signal VLSI Design Group at Oklahoma State University. The measurement technique used is described in [41] and [44]. Measurement of the dielectric constant is based on finding the resonant frequency of a dielectric loaded waveguide resonator as

shown in Figure 7.11. The loss tangent calculation is based on attenuation constant which can be computed by measuring S_{11} and S_{21} parameters [44]. Table 7.2 shows the initially measured dielectric constant and loss tangent of the substrate for 4 different samples. The dielectric waveguide resonator was then dipped in a saline solution for one day and the measurement was repeated. The results are shown in Table 7.3. The measured loss tangent and dielectric constant did not change significantly after being dipped in the saline. The dielectric constant of acrylic varies from 2.1 to 3.9 [28] and its loss tangent varies from 0.02 to 0.03 [43].

		Reading 1	**Reading 2**	**Reading 3**	**Reading 4**	**Average**
Sample #1	**Dielctric constant**	3.67	3.74	3.74	3.74	3.7225
	Loss tangent	0.026	0.0265	0.0256	0.0262	0.026075
	Q-factor					38.4
Sample #2	**Dielctric constant**	3.62	3.75	3.78	3.79	3.735
	Loss tangent	0.0254	0.025	0.0248	0.0234	0.02465
	Q-factor					40.6
Sample #3	**Dielctric constant**	3.62	3.61	3.64	3.61	3.62
	Loss tangent	0.0252	0.0259	0.0261	0.0256	0.0257
	Q-factor					39
Sample #4	**Dielctric constant**	3.68	3.77	3.76	3.78	3.7475
	Loss tangent	0.0256	0.0253	0.0267	0.0263	0.025975
	Q-factor					38

Table 7.2: Measurement of dielectric substrate before dielectric loaded waveguide resonator dipped in saline solution.

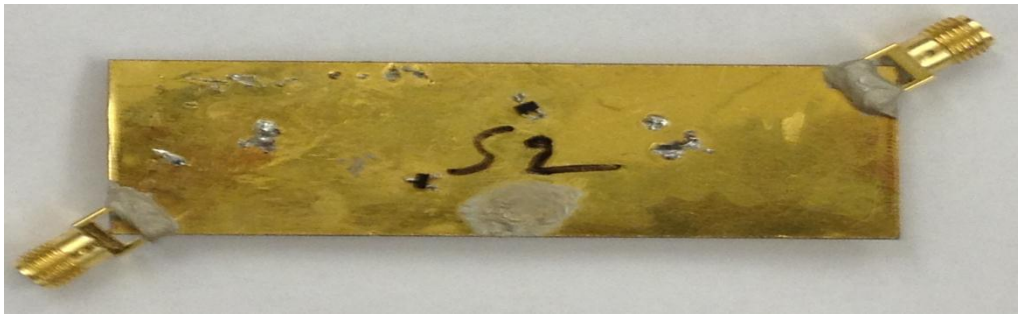

Figure 7.11 Dielectric loaded waveguide resonator used for measuring the dielectric properties of substrate

		Reading 1	Reading 2	Reading 3	Reading 4	Average
Sample #1	**Dielctric constant**	3.63	3.56	3.57	3.66	3.605
	Loss tangent	0.027	0.0262	0.0268	0.0265	0.026625
	Q-factor					37.6
Sample #2	**Dielctric constant**	3.55	3.68	3.63	3.57	3.6075
	Loss tangent	0.02770	0.02670	0.0273	0.0265	0.02705
	Q-factor					37
Sample #3	**Dielctric constant**	3.64	3.68	3.7	3.72	3.685
	Loss tangent	0.0272	0.027	0.0257	0.0262	0.02625
	Q-factor					37.7
Sample #4	**Dielctric constant**	3.7	3.65	3.74	3.67	3.69
	Loss tangent	0.0282	0.0275	0.027	0.0272	0.027475
	Q-factor					36

Table 7.3: Measurement of dielectric substrate after dielectric loaded waveguide resonator dipped in saline solution.

7.5 Problem formulation using COMSOL:

In the COMSOL simulation, the antenna geometries shown in figure 6.1 are considered including the acrylic and substrate. Figure 7.12 shows antenna D as used in COMSOL. The dielectric medium surrounding the antenna is modeled as extending to infinity. Figure 7.13 shows the antenna model embedded in the bulk saline medium with the PML and scattering boundary condition that simulates infinite extent. The antenna is symmetric, so symmetric boundary conditions are again used, as shown in Figure 7.13 and 7.15. A uniform thickness of 0.7 mm for the acrylic coating is used in the COMSOL simulation. Measurements showed that the acrylic thickness varies from 0.7-1.3 mm in the fabricated samples. However, errors in thickness less than 1 mm have a very small impact on the calculated input impedance. The dielectric constants of the acrylic and the substrate are both chosen to be equal, at a value 3.73. The loss tangent of acrylic and substrate are also chosen to be equal, at 0.026 based on the values in Table 7.2. The conducting material used in the antenna structure is gold with the thickness given in Table 6.1. The source of excitation is provided by impressing a current of 1A at the antenna terminal.

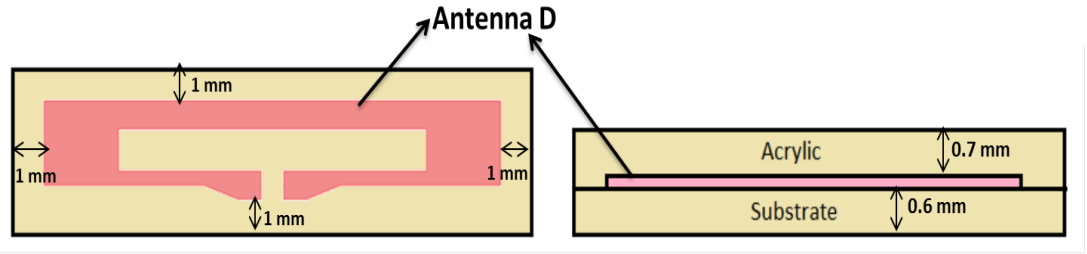

(a) Top view of antenna model (b) Side view of antenna model

Figure 7.12: Antenna D including acrylic and substrate modeled in COMSOL

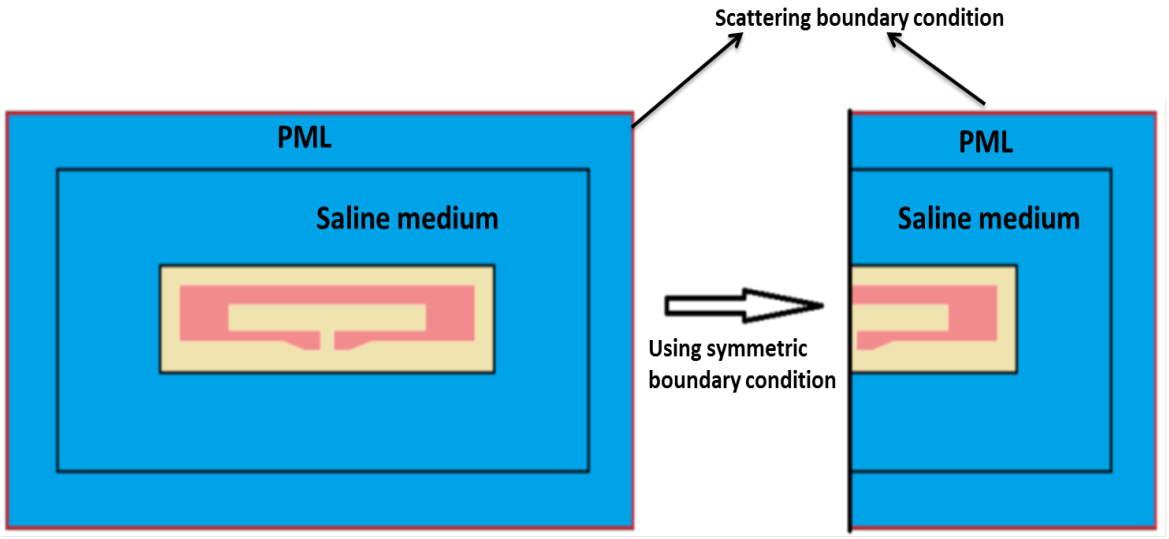

Figure 7.13: Antenna model embedded in bulk saline medium

The calculations were repeated for the antenna placed in a saline medium of thickness 1.5 cm above and below the antenna model, matching Figure 7.2. The difference between the calculated input impedance for infinite and finite-extent saline is negligible. Figure 7.14 shows the mesh structure used on the antenna surface when the surrounding medium is both free space and saline. Figure 7.15 shows the mesh structure of entire COMSOL model. Boundary layer meshing [18] was used to mesh the thin acrylic and substrate regions. Tables 7.4 and 7.5 shows the PML and mesh settings when the antenna is radiating into free space and the saline medium, respectively. λ_{short1} and λ_{short2} are the wavelengths corresponsing to a frequency of 930 MHz within in free space and the saline solution, respectively, and λ_{L_f} and λ_{L_S} are the wavelengths at 870 MHz in the two media.

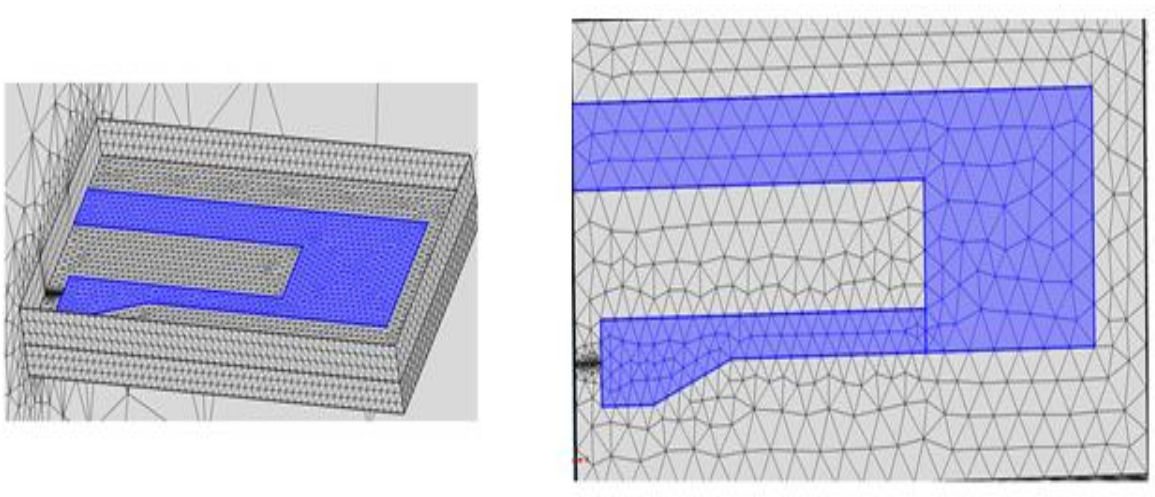

(a) (b)

Figure 7.14: Mesh structure of antenna model embedded in (a) free space and (b) saline media

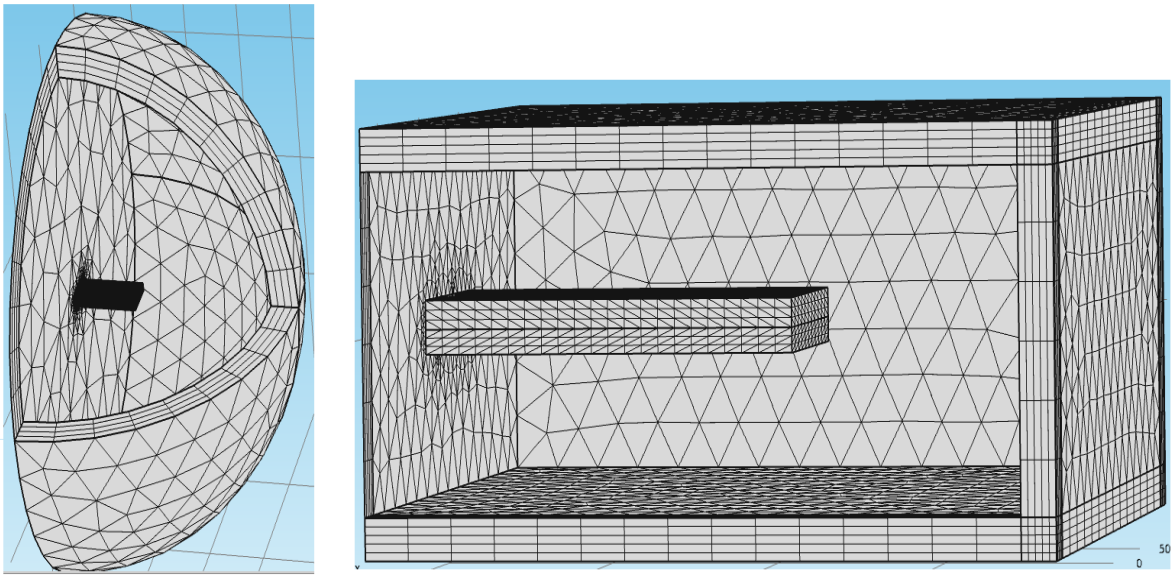

(a) (b)

Figure 7.15: COMSOL mesh structure of entire model when the surrounding medium is (a) free space and (b) saline medium

	Antenna A	Antenna B	Antenna C	Antenna D
Maximum mesh in free space	1 cm 0.031 λ_{short1}	1 cm 0.031 λ_{short1}	1 cm 0.031 λ_{short1}	1 cm 0.031 λ_{short1}
PML type	Spherical	Spherical	Spherical	Spherical
Order of PML	2	2	2	1
PML thickness	5 mm 0.0145 λ_{L_f}	5 mm 0.0145 λ_{L_f}	5 mm 0.0145 λ_{L_f}	5 mm 0.0145 λ_{L_f}
Minimum distance of PML layer from the antenna	3.4 cm 0.099 λ_{L_f}	2.3 cm 0.067 λ_{L_f}	2.9 cm 0.084 λ_{L_f}	2.4 cm 0.07 λ_{L_f}
Total mesh elements in computational domain	71473	91170	86735	75992

Table 7.4: PML and Mesh settings when antenna model is radiated in free space

	Antenna A	Antenna B	Antenna C	Antenna D
Maximum mesh in saline medium	1.3 mm 0.035 λ_{short2}	1.3 mm 0.035 λ_{short2}	1.1 mm 0.03 λ_{short2}	1.3 mm 0.035 λ_{short2}
PML type	Cartesian	Cartesian	Cartesian	Cartesian
Order of PML	2	2	2	2
PML thickness	1 mm 0.0255 λ_{L_S}	1 mm 0.0255 λ_{L_S}	1 mm 0.0255 λ_{L_S}	1 mm 0.0255 λ_{L_S}
Minimum distance of PML layer from antenna	4 mm 0.1 λ_{L_S}	4 mm 0.1 λ_{L_S}	4 mm 0.1 λ_{L_S}	9 mm 0.23 λ_{L_S}
Total mesh elements in computational domain	73940	64485	67615	45716

Table 7.5: PML and Mesh settings when antenna model is radiated in saline medium

7.6 Discussion of results:

The input impedance of antenna D was first considered when radiating into an infinite finite saline medium and the finite saline medium shown in figure 7.2. The acrylic coating and the dielectric substrate were included in the antenna model. The resulting input impedance at 900 MHz (the center of the desired operating band) is shown in Table 7.6.

	Input impedance at antenna terminal
Saline medium of infinite extent	14.4178+j107.585
Saline medium of finite extent	14.974+j108.928

Table 7.6: Impact on input impedance when saline medium are finite and infinite infinite extent

The truncation of the saline medium has only a small effect on the impedance. An infinite medium is therefore considered from now on in the comparison with the measured results. Two curves are plotted for each of the COMSOL simulations and measurements. Figure 7.16 through 7.23 compare the input impedance of the antenna found with COMSOL and that measured. The impedance is computed at antenna itself in COMSOL and then transformed to feed-network input using (7.1). The measured input impedance at feed-network input is then transformed back to give impedance at antenna itself using (7.1) and compared with COMSOL simulated antenna impedance.

Attenuation constant of balun transmission line used for frequency range from 870 MHz to 930 MHz is 0.12 np/m . The length of the transmission line was adjusted between 11.3 cm to 12.4 cm, the two lengths found for the balun feed in Section 7.3, to achieve a better match between the measured results and COMSOL simulation results. The best match was always obtained with lengths within 2 mm of 12 cm. Figure 7.16 thru 7.19 shows the transmission line effective length for antenna A, B, C, and D that demonstrates agreement between COMSOL and the measured results. The measured results depends on how the feed network was connected with the antenna terminal. The possible variation between the measured results and COMSOL simulation results in the impedance plot shows that the agreement is good.

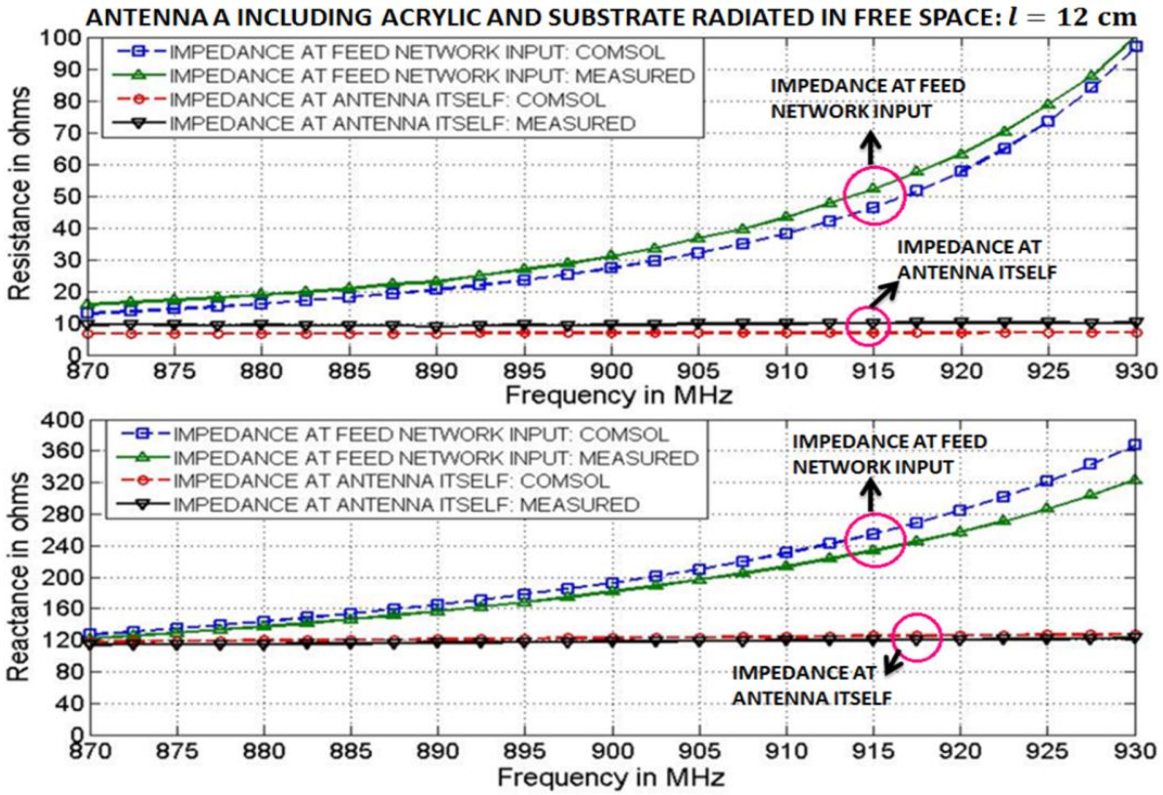

Figure 7.16: Input impedance plot when antenna type A radiating in free space with transmission line length of 12 cm.

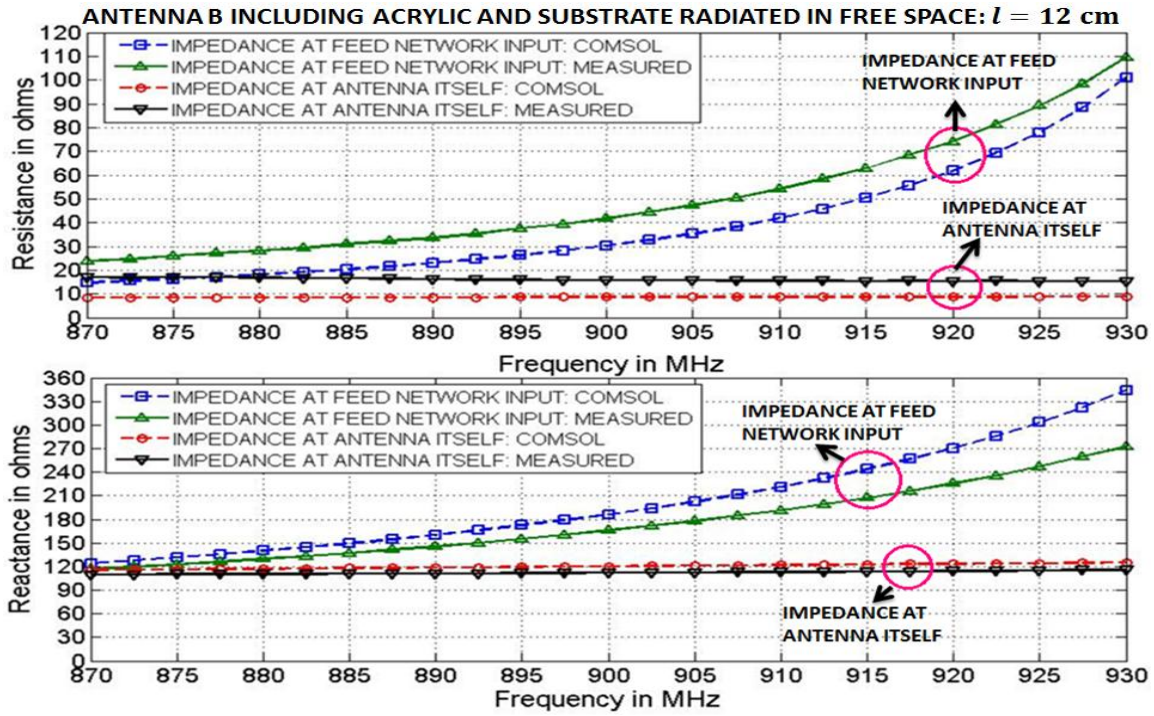

Figure 7.17: Input impedance plot when antenna type B radiating in free space with transmission line length of 12 cm.

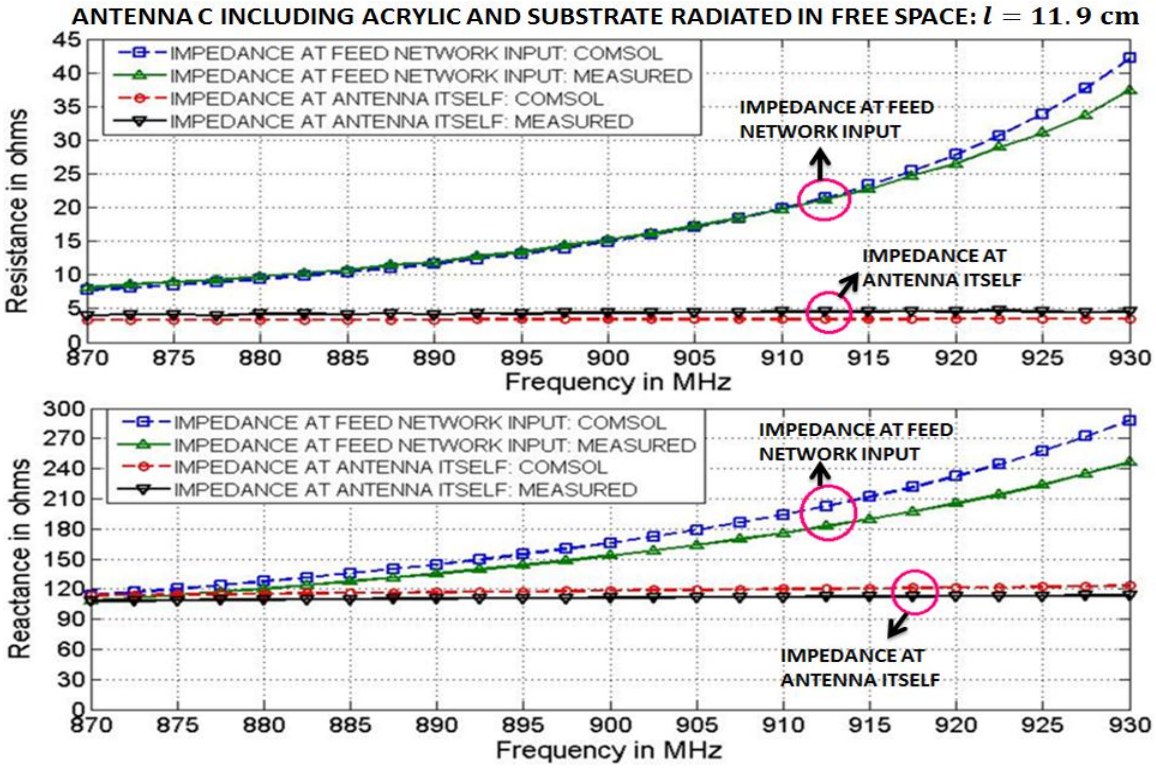

Figure 7.18: Input impedance plot when antenna type C radiating in free space with transmission line length of 11.9 cm.

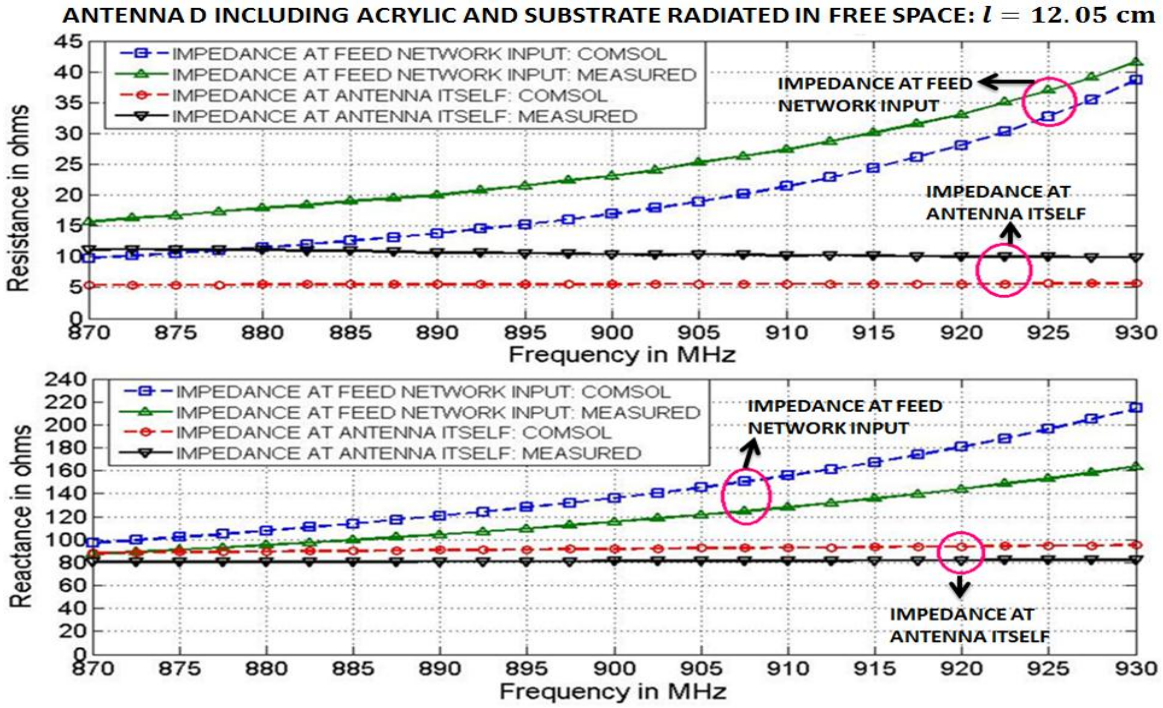

Figure 7.19: Input impedance plot when antenna type D radiating in free space with transmission line length of 12.05 cm.

Now, the computation of the impedance for four test antennas including a substrate and an acrylic are repeated using COMSOL when surrounded by a saline media. Figure 7.20 thru 7.23 compare the input impedance both at feed network input and the antenna impedance itself using COMSOL and measured results. Figure 7.20 thru 7.23 shows the transmission line effective length for antenna A, B, C, and D that demonstrates agreement between COMSOL and the measured results. There is a little variation in antenna impedance over the frequency range from 870 MHz to 930 MHz which shows that the antenna has low quality factor due to lossy saline medium. Like in free space analysis, the measured results still depends on how the feed network was connected to the antenna terminal when radiating in saline medium. It also depends on placement and thickness of the saline bags considered while the measurement was performed. The possible variation between measured results and the COMSOL simulation results shows that the agreement is good.

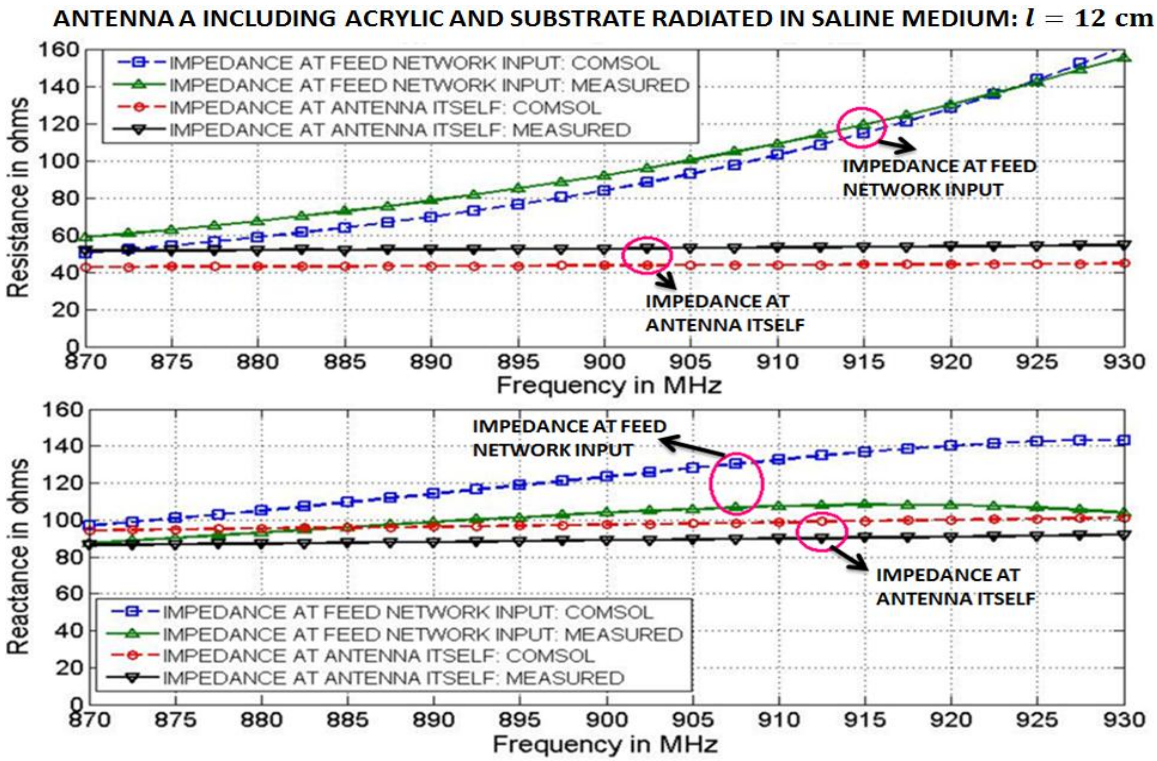

Figure 7.20: Input impedance plot when antenna type A radiating in bulk saline medium with transmission line length of 12 cm.

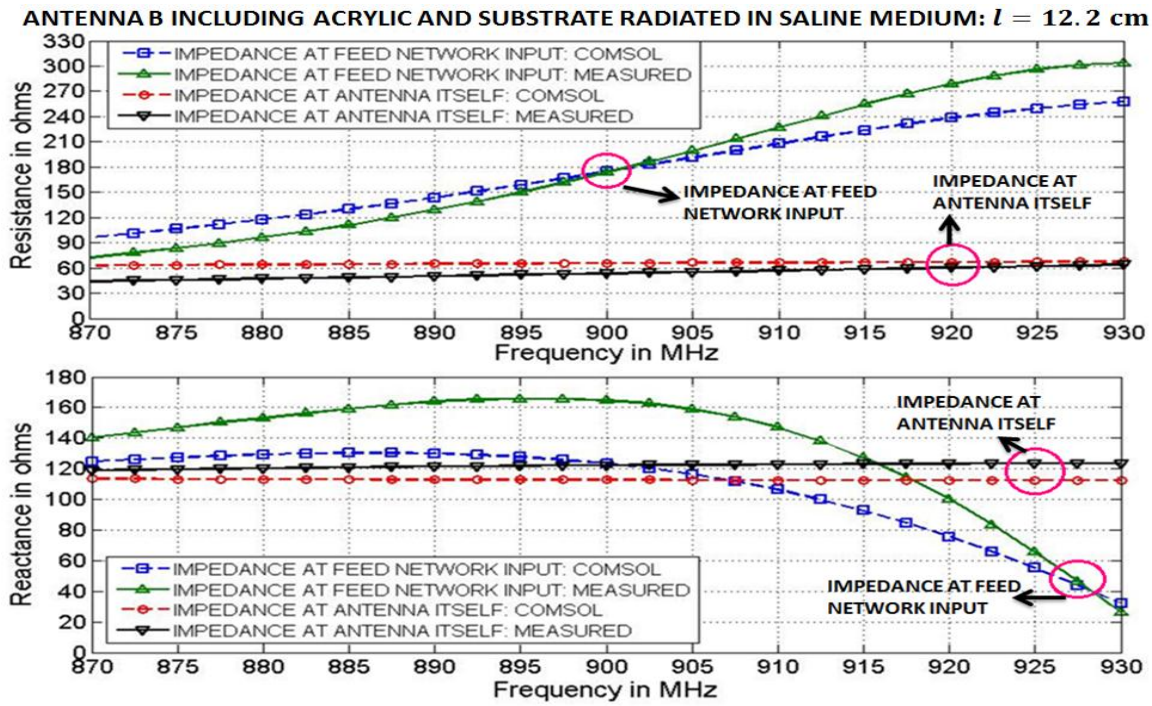

Figure 7.21: Input impedance plot when antenna type B radiating in bulk saline medium with transmission line length of 12.2 cm.

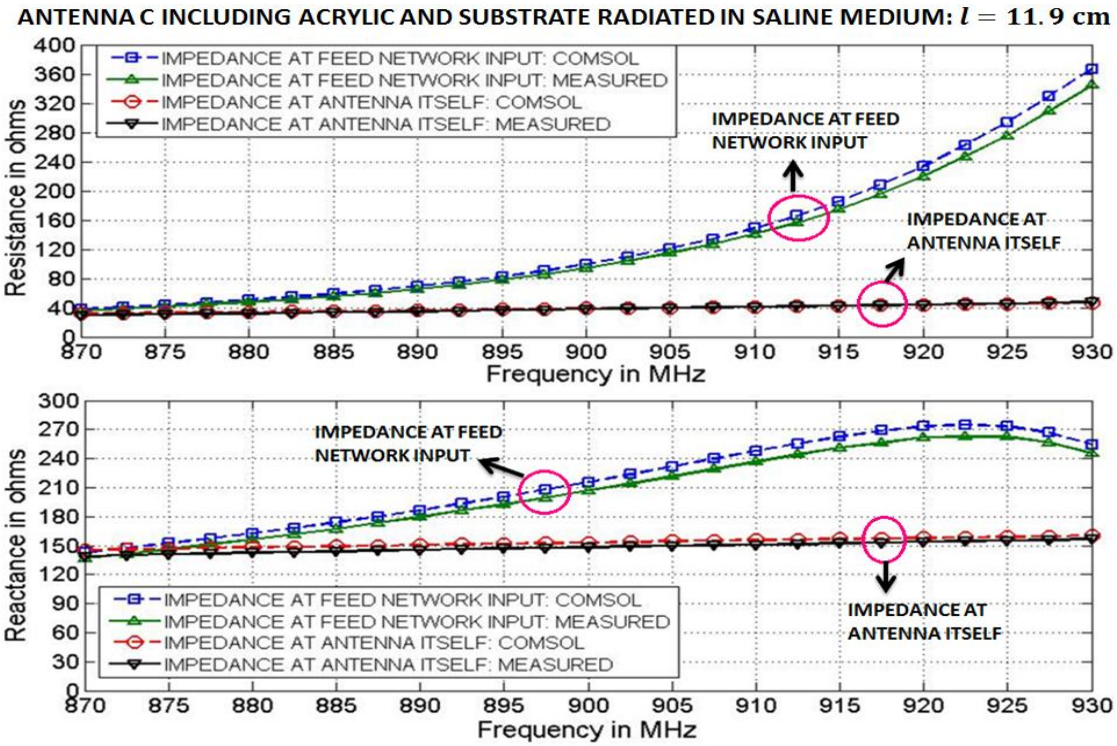

Figure 7.22: Input impedance plot when antenna type C radiating in bulk saline medium with transmission line length of 11.9 cm.

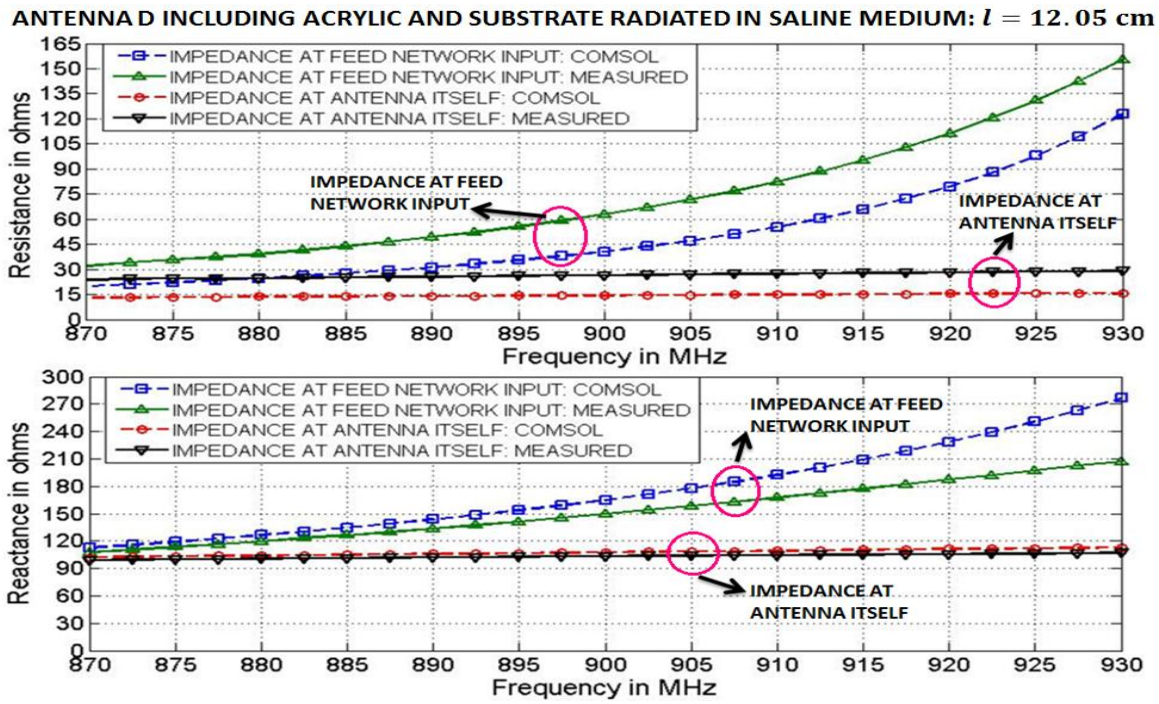

Figure 7.23: Input impedance plot when antenna type D radiating in bulk saline medium with transmission line length of 12.05 cm.

CHAPTER 8

PROPOSED ANTENNA DESIGN

The comparison between the COMSOL simulations and measured results was completed in the previous chapters. It showed the validity of the computed numerical results provided by COMSOL. In this chapter, an antenna geometry that is appropriate for use with the RFID tag device is introduced and analyzed. The equivalent circuit of the commercial RFID tag IC [7] is shown in Figure 2.3. Its input impedance over its operating frequency range from 870 MHz to 930 MHz is shown in Figure 8.1. The RFID tag IC impedance is 27.4-j200.9 Ω at the center frequency of 915 MHz.

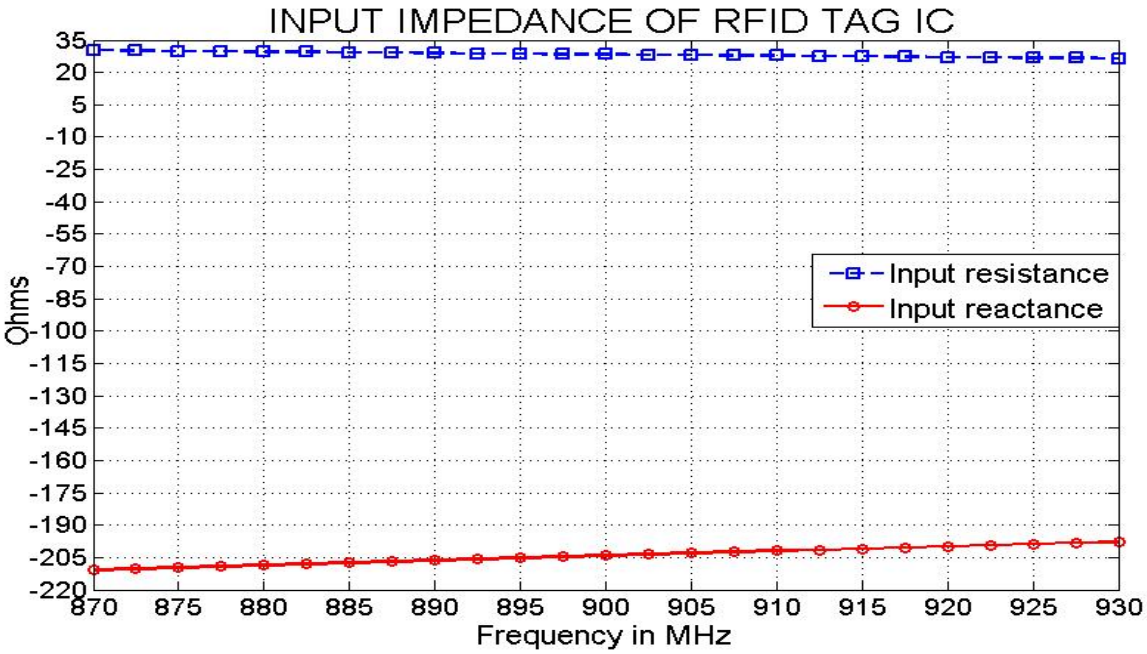

Figure 8.1: Input impedance of RFID tag IC [7]

Maximum power transfer from the antenna to the RFID tag therefore requires an antenna impedance of 27.4+j200.9 Ω. In the previous chapter, antenna C was shown to be the best candidate of all the antenna configurations considered. However, its impedance at 915 MHz is 42.586+j156.7526 Ω when radiating into the saline medium, which would give a sub-optimal match. A higher inductive reactance and a lower resistance is needed. The antenna geometry should be refined such that its impedance is closer to the complex conjugate of the RFID tag input impedance. The antenna reactance and loss resistance can be modified by changing its length and/or strip width according to (2.9) and (2.10), respectively. Loss resistance can also be controlled by the width of the antenna structure itself. As discussed in Chapter 2, the thickness of the metal film does not affect the inductance when the metal thickness is negligible compare to strip width. However, the loss resistance decreases with an increase in thickness. Taking all these factors into consideration, a proposed antenna geometry for use with the RFID tag is predicted is shown in Figure 8.2.

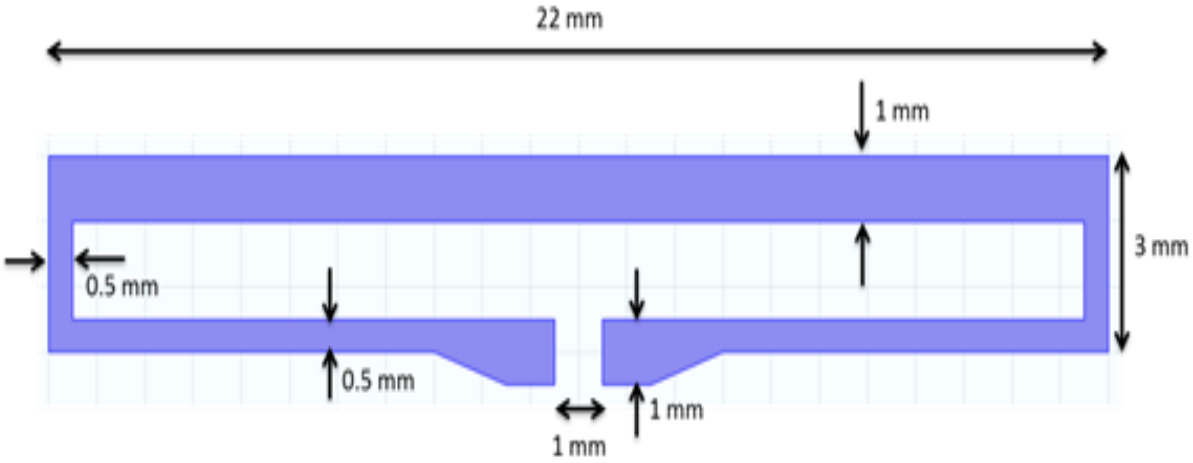

Figure 8.2: Proposed antenna geometry with gold conductor of 1μm thickness.

Figure 8.3 show the equivalent circuit of the implantable RFID tag device when it receives electromagnetic waves from RFID reader. In the figure, R_A is the real part of antenna impedance in ohms, X_A is the imaginary part of antenna reactance, R_{Chip} is the real part of RFID

tag chip impedance, X_{Chip} is the imaginary part of RFID tag IC impedance, and V_A is the induced voltage due to electromagnetic wave received at antenna terminal.

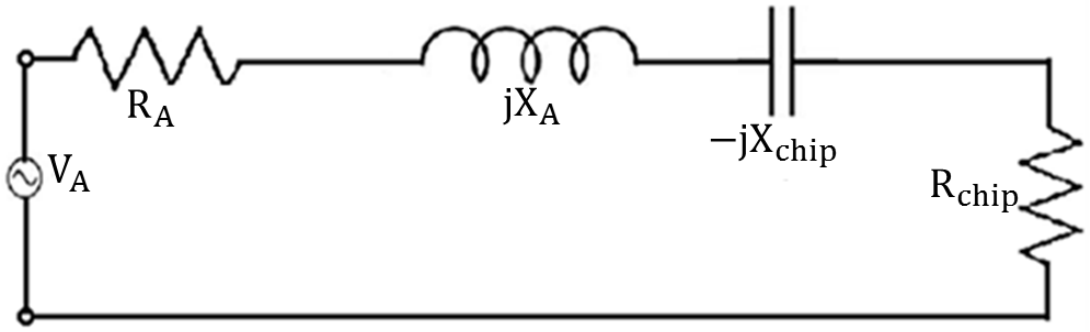

Figure 8.3: Equavalent circuit of implantable RFID tag in receiving mode

8.1 Problem formulation in COMSOL:

The proposed antenna structure including the substrate and acrylic is modeled using COMSOL. The same dielectric constant, loss tangent and thickness are used for both the acrylic and the substrate as discussed in the last chapter. It is embedded in the bulk saline medium as before. A Cartesian PML of order 2 and the scattering boundary condition are used that simulates the infinite extent of the radiation medium. The mesh settings used in COMSOL are shown in Table 8.1. Figure 8.4 shows the mesh structure in COMSOL used for this simulation. The antenna is symmetric, so symmetric boundary conditions are again used, as shown in Figure 8.4. The source of excitation is provided by impressing a current of 1A at the antenna terminal.

Maximum mesh size in saline medium	3 mm ($0.08\lambda_s$)
Maximum mesh size in antenna surface	0.25 mm ($0.0068\lambda_s$)
Total mesh elements	44988

Table 8.1: Mesh settings for discretizing the entire COMSOL model, λ_s is the wavelengths in saline medium at 930 MHz

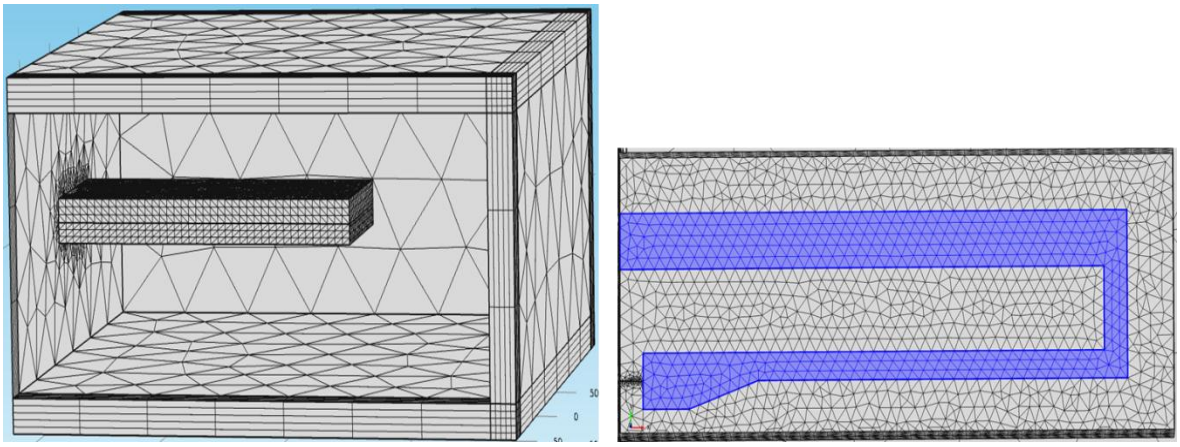

(a) (b)

Figure 8.4: Mesh structure in COMSOL for (a) Entire model (b) Antenna surface

8.2 Simulation results of proposed antenna

Simulated radiation characteristics of the proposed antenna are obtained using COMSOL and discussed in this section. The antenna impedance is shown in Figure 8.5. The input impedance is 28+j201.5 Ω at 915 MHz, which is close to the complex conjugate of RFID tag IC input impedance. Figure 8.6 shows the radiation resistance, loss resistance, and input resistance of the proposed antenna. This yields a radiation efficiency of 86.7% at 915 MHz. The radiation efficiency could be increased by increasing the strip width or metal thickness. However, increasing the strip width reduces the antenna inductive reactance which would give a poorer match. The only viable method to improve the efficiency is to increase the thickness of the gold. However, the thickness used in the proposed antenna is 1 μm, which is the maximum thickness that can be fabricated at the Mixed Signal VLSI Design Laboratory.

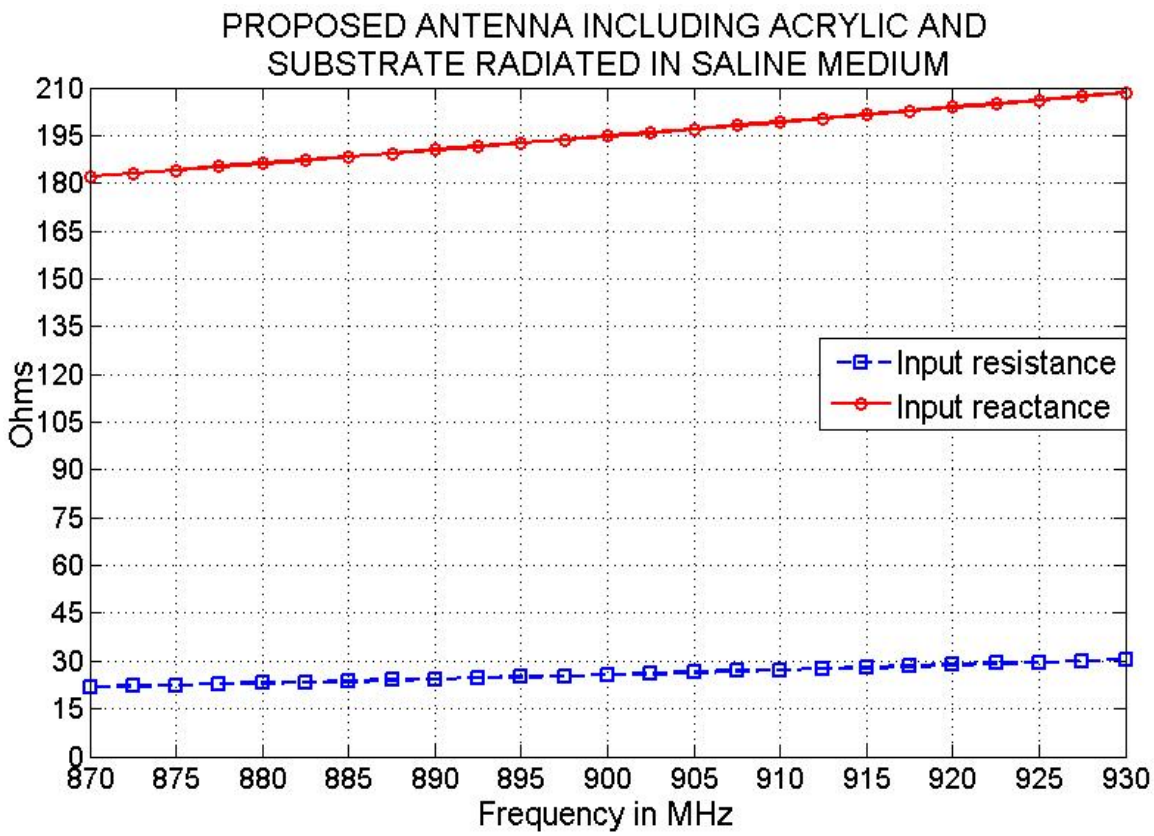

Figure 8.5: Input impedance plot of proposed antenna in saline medium

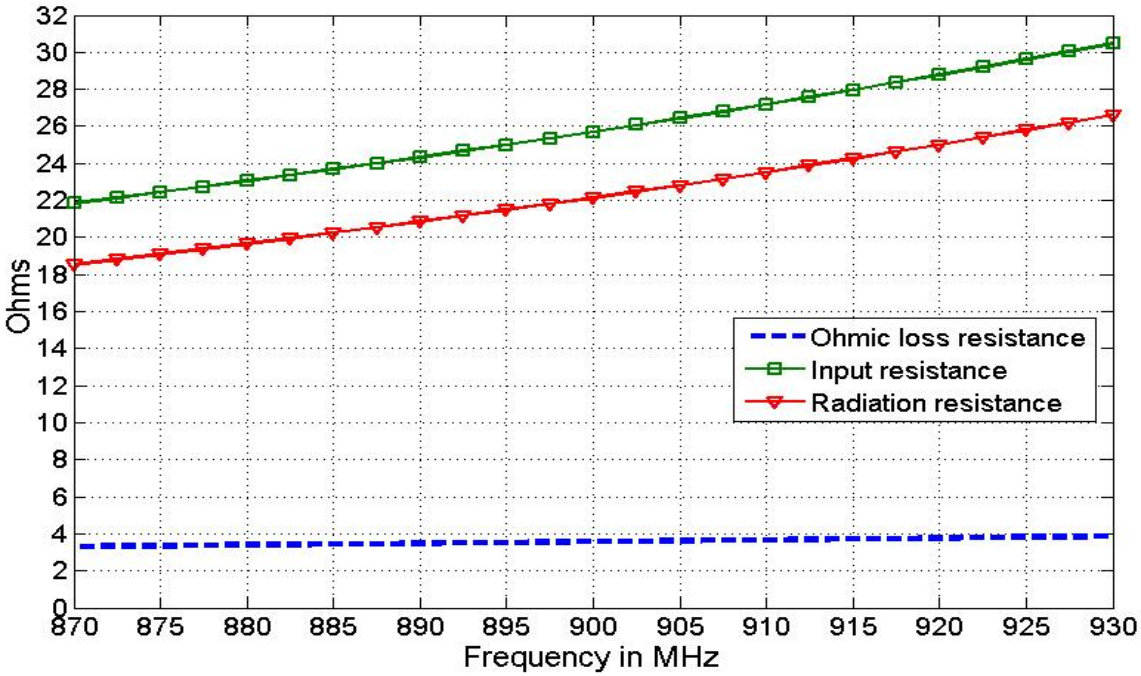

Figure 8.6: Proposed antenna radiating performance in saline medium

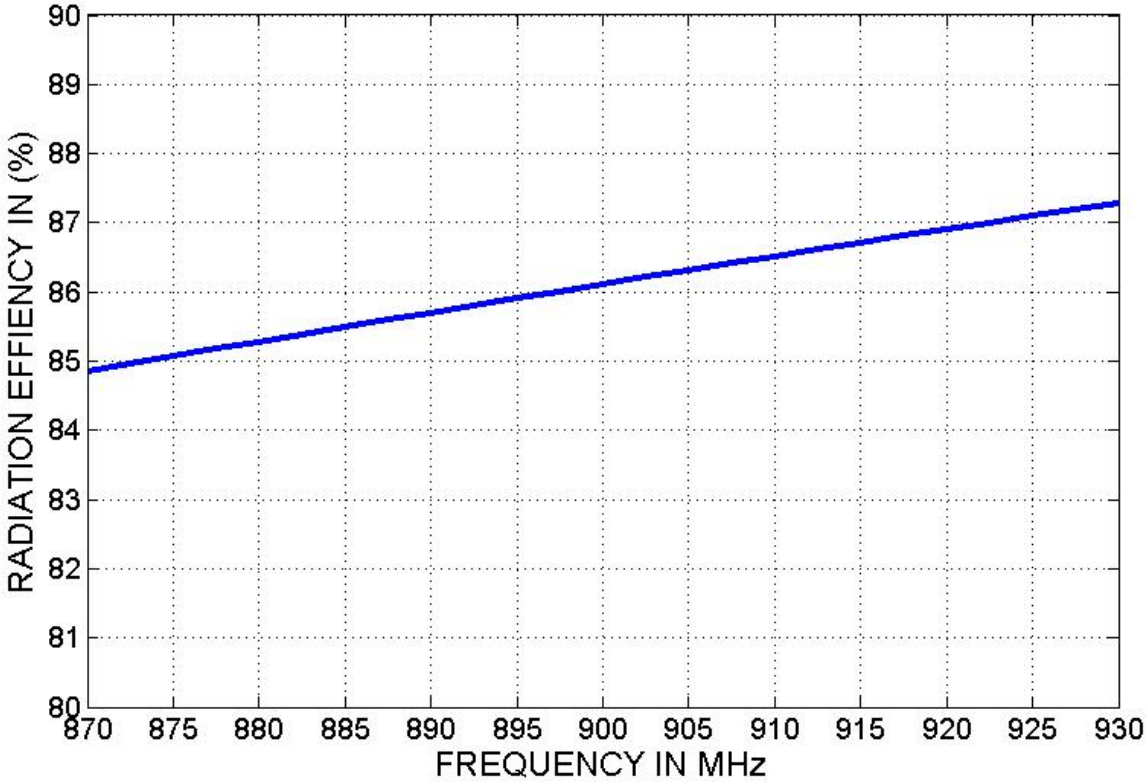

Figure 8.7: Proposed antenna radiation efficiency in saline medium

The quality factor (Q) for a resonating circuit (or unloaded Q) can be computed as:

$$Q = \frac{w_0}{2R_{A|w_0}} \left|\frac{dX_{net}}{dw}\right|_{w_0}, \tag{8.1}$$

where $X_{net} = X_A - X_{Chip}$ is the net reactance, $w_0 = 2\pi f_0$ is the angular resonant frequency, R_A is the input resistance of antenna, $R_{A|_{w_0}}$ is the input resistance of antenna at resonant frequency. Figure 8.8 shows the plot for net reactance versus frequency of operation. It is found that the resonance occurs between 912.5 MHz and 915 MHz. At 912.5 MHz frequency, X_{net} = -1.08075 and R_A=27.57 Ω while at 915 MHz frequency, X_{net} = 0.594255 and R_A=27.96 Ω. The resonant frequency is therefore $f_0 \approx$ 915 MHz with $R_{A|_{w_0}} \approx$ 27.96 Ω. The derivative of the net reactance can therefore be estimated from

$$\left|\frac{dX_{net}}{dw}\right|_{w_0} = \frac{0.594255 + 1.08075}{2\pi(915 - 912.5) \times 10^6}$$

giving

$$Q \approx \frac{2\pi \times 915 \times 10^6}{2 \times 27.96} \times \frac{0.594255 + 1.08075}{2\pi(915 - 912.5) \times 10^6} = 10.96\,.$$

A high Q-factor is essential in order to develop the high DC voltage required to turn on the diodes in RFID circuit. (In general, a Q factor of at least 10 is desirable to obtain the required voltage for RFID tag chip [42].)

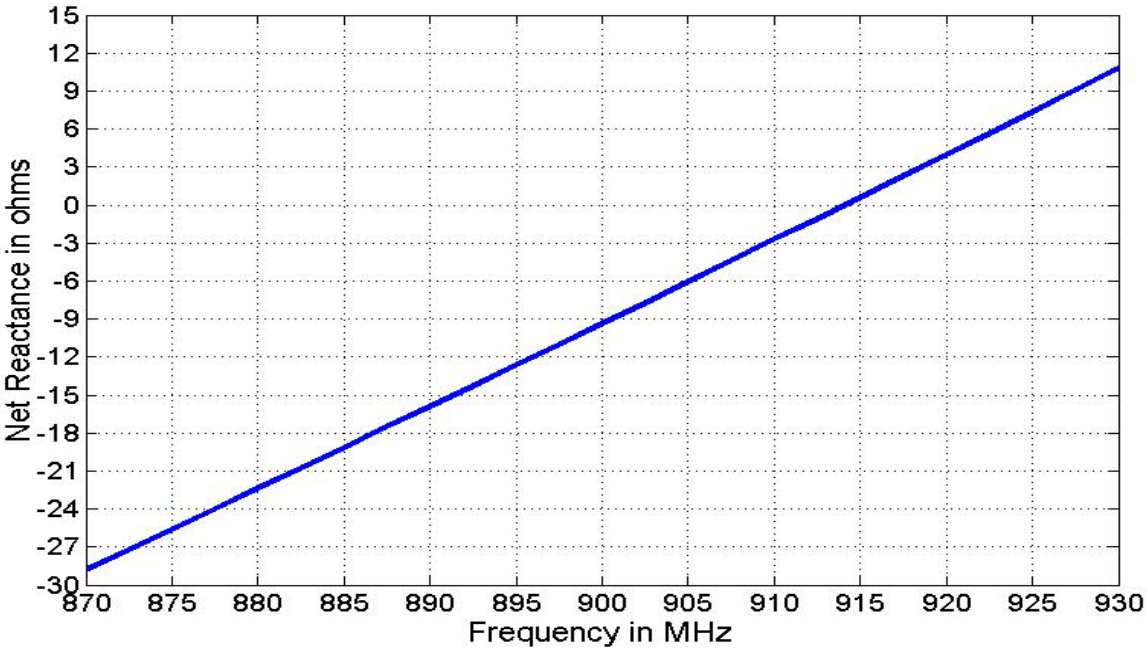

Figure 8.8: Net reactance vs. frequency

CHAPTER 9

CONCLUSION

In this work, the COMSOL computational electromagnetics package has been used to determine an appropriate geometry for an implantable antenna for used with an RFID tag. It is a unique far-field problem since antenna is radiated in a highly lossy medium. Several test antennas have been considered to confirm the validity of the COMSOL simulation modeling techniques used. The simulation results from COMSOL were first compared with FEKO when the antenna structure radiating into a bulk homogeneous medium. Good agreement between COMSOL and FEKO was demonstrated. Both COMSOL and FEKO also showed good agreement with a locally written method of moments code as well. The simulated characteristics of various test antennas that include the dielectric substrate and the acrylic coating needed with the implantable antennas were then generated using COMSOL and compared with measured results obtained at the Mixed Signal VLSI Design Laboratory at Oklahoma State University. Good agreement was again demonstrated. It was found that test configuration antenna C showed the best agreement among all the antenna configurations considered. Hence, it is concluded that the simulation results from the COMSOL package are valid.

However, antenna C cannot be used in RFID tag as its input resistance is too high and its reactance is too low for use with the RFID tag at 915 MHz. A proposed antenna design was obtained by refining antenna geometry C so as to bring its input impedance in the working range

that gives maximum power transfer when used with the RFID tag. The proposed antenna results in 86.7% radiation efficiency when it is embedded in a saline medium (or human tissue). A Q-factor of greater than 10 can be obtained when the proposed antenna is used in RFID tag chip. This allows the turn-on voltage of the RFID tag to be exceeded.

REFERENCES

[1] C E. Y. Chow, C. L. Yang, A. Chlebowski, S. Moon, W. J. Chappell, and P. P. Irazoqui, "Implantable Wireless Telemetry Boards for In Vivo Transocular Transmission," *Ieee Transactions on Microwave Theory and Techniques,* vol. 56, pp. 3200-3208, Dec 2008.

[2] An implantable antenna. Technology review published by MIT. http://staging.technologyreview.com/news/420276/an-implantable-antenna/?mod=related

[3] Battery free neural implantable sensors. Technology review Published by MIT http://www.technologyreview.com/news/416151/a-battery-free-implantable-neural-sensor/

[4] Radio frequency emissions. http://aboutus.verizonwireless.com/wirelessissues/radioEmmissions.html

[5] T. S. Ibrahim, D. Abraham, and R. L. Rennaker, "Electromagnetic power absorption and temperature changes due to brain machine interface operation," *Annals of Biomedical Engineering,* vol. 35, pp. 825-834, May 2007.

[6] RFID-Handbook – RFID-Frequencies. http://rfid-handbook.de/about-rfid/radio-regulation/19-frequency-ranges.html

[7] Higgs™ 3 EPC Class 1 Gen 2 RFID Tag IC http://www.alientechnology.com/docs/products/Alien-Technology-Higgs-3-ALC-360.pdf

[8] J.-M. Jin and D. J. Riley, *Finite element analysis of antennas and arrays*. Hoboken, N.J.: John Wiley & Sons: IEEE Press, 2009.

[9] J.-M. Jin, *The finite element method in electromagnetics*, 2nd ed. New York: John Wiley & Sons, 2002.

[10] M. N. O. Sadiku, *Numerical techniques in electromagnetics with MATLAB*, 3rd ed. Boca Raton, Fla.: CRC Press, 2009

[11] F. Gustrau and D. Manteuffel, *EM modeling of antennas and RF components for wireless communication systems*. Berlin; New York: Springer, 2006.

[12] C. A. Balanis, *Modern antenna handbook*. Hoboken, NJ: Wiley, 2008.

[13] Comsol multiphysics RF Module users guide: ver. 4.2 © 1998–2011 COMSOL

[14] Comsol multiphysics reference guide: ver. 3.5a © 1998–2008 COMSOL

[15] C. A. Balanis, *Antenna theory: analysis and design*, 3rd ed. Hoboken, NJ: John Wiley, 2005.

[16] Dielectric properties of biological tissue http://niremf.ifac.cnr.it/tissprop/

[17] D. M. Pozar, *Microwave engineering*, 2nd ed. New York: Wiley, 1997.

[18] Comsol multiphysics users guide: ver. 4.2 © 1998–2011 COMSOL

[19] Balanced patch antenna for 6 GHz. Solved with COMSOL Multiphysics version 4.2 copyright 2011. http://www.comsol.com/showroom/gallery/782/

[20] Modeling a Center-driven Dipole with FEKO. http://www.cvel.clemson.edu/modeling/software/feko_dipole.html

[21] A. Taflove, *Advances in computational electrodynamics: the finite-difference time-domain method*. Boston: Artech House, 1998.

[22] Frequency dependent meshing. COMSOL support knowledge base http://www.comsol.com/support/knowledgebase/1103/

[23] Comsol multiphysics reference guide: ver.4.1 © 1998–2010 COMSOL AB

[24] F D. M. Sullivan and IEEE Microwave Theory and Techniques Society., *Electromagnetic simulation using the FDTD method*. New York: IEEE Press, 2000.

[25] R. Horton, B. Easter, and A. Gopinath, "Variation of Microstrip Losses with Thickness of Strip," *Electronics Letters,* vol. 7, pp. 490-&, 1971.

[26] F. Alessandri, G. Baini, G. D'Inzeo and R. Sorrentino, "Conductor loss computation in multiconductor MIC's by transverse resonance technique and modified perturbational method," *Microwave and Guided Wave Letters, IEEE* , vol.2, no.6, pp.250-252, June 1992

[27] E. E. Altshuler, T. H. O'Donnell, S. R. Best, B. Kaanta, "A review of an electrically small antenna immersed in a dielectric," Air Force Research Laboratory, Electromagnetics technology division, Hanscom AFB, MA.

[28] http://www.engineeringtoolbox.com/liquid-dielectric-constants-d_1263.html

[29] R. Want, "An introduction to RFID technology," *Ieee Pervasive Computing,* vol. 5, pp. 25-33, Jan-Mar 2006

[30] FEKO, Suite 6.1.1, EM Software & Systems–S.A. (Pty) Ltd, Stellenbosch, South Africa, http://www.feko.info

[31] J. Hilland, "Simple sensor system for measuring the dielectric properties of saline solutions," *Measurement Science & Technology,* vol. 8, pp. 901-910, Aug 1997.

[32] C. A. Balanis, *Advanced engineering electromagnetics*. New York: Wiley, 1989

[33] RF CABLE *SEMI-RIGID COAXIAL CABLE:* *www.jyebao.com.tw/files%20download/**SEMI-RIGID**.pdf*

[34] http://en.wikipedia.org/wiki/Ptfe

[35] W. L. Stutzman and G. A. Thiele, *Antenna theory and design*, 2nd ed. New York: J. Wiley, 1998.

[36] D.B. Davidson, I.P. Theron, U. Jakobus, F.M. Landstorfer, F.J.C Meyer, J. Mostert and J.J. Van Tonder, "Recent progress on the antenna simulation program FEKO," *Communications and Signal Processing, 1998. COMSIG '98. Proceedings of the 1998 South African Symposium on* , vol., no., pp.427-430, 7-8 Sep 1998

[37] C. J. Reddy, "Advanced computational tool for antenna design and placement". http://rfalliance.org/Nov%2009%20Conference/Presentations/(3)%20CJReddy_RFAlliance_2009.pdf

[38] FEKO, Suite 6.1.1, EM Software & Systems, "User's manual", copyright 1998-2011.

[39] C. Hutchens, R. L. Rennaker, 2nd, S. Venkataraman, R. Ahmed, R. Liao, and T. Ibrahim, "Implantable radio frequency identification sensors: wireless power and communication," *Conf Proc IEEE Eng Med Biol Soc,* vol. 2011, pp. 2886-92, 2011.

[40] Y. Lee, "Antenna circuit design for RFID application," Microchip Technology Inc, 2003.

[41] L.S. Napoli and J.J. Hughes , "A Simple Technique for the Accurate Determination of the Microwave Dielectric Constant for Microwave Integrated Circuit Substrates (Correspondence)," *Microwave Theory and Techniques, IEEE Transactions on* , vol.19, no.7, pp. 664- 665, Jul 1971

[42] N. Tran, B. Lee and J.W. Lee, "Development of Long-Range UHF-band RFID Tag chip Using Schottky Diodes in Standard CMOS Technology," *Radio Frequency Integrated Circuits (RFIC) Symposium, 2007 IEEE* , vol., no., pp.281-284, 3-5 June 2007

[43] http://www2.dupont.com/Pyralux/en_US/assets/downloads/pdf/HighSpeedMaterialConsiderations.pdf

[44] H. P. Yue, K. L. Virga, and J. L. Prince, "Dielectric constant and loss tangent measurement using a stripline fixture," *Ieee Transactions on Components Packaging and Manufacturing Technology Part B-Advanced Packaging,* vol. 21, pp. 441-446, Nov 1998.

[45] http://www.jyebao.com.tw/company.htm

[46] C. A. Balanis, *Antenna theory: analysis and design*, 3rd ed. Hoboken, NJ: John Wiley, 2005, pp. 461.

VITA

Rahul Bakore

Candidate for the Degree of

Master of Science

Thesis: ANALYSIS AND VERIFICATION OF A PROPOSED ANTENNA DESIGN FOR AN IMPLANTABLE RFID TAG AT 915 MHz

Major Field: Electrical Engineering

Biographical:

Education:

Completed the requirements for the Master of Science in Electrical Engineering at Oklahoma State University, Stillwater, Oklahoma in December, 2012.

Bachelor of Engineering - Electronics and Communication Engineering, University of Rajasthan, Jaipur, Rajasthan, July 2008.

Experience:

Research Assistant in the Mixed Signal VLSI Design Group, Oklahoma State University, April 2012 to August 2012.